Changes in the macromolecular structure of a Type I kerogen (Unita Basin) during maturation /

INFORMATION TO USERS

This manuscript has been reproduced from the microfilm master. UMI films the text directly from the original or copy submitted. Thus, some thesis and dissertation copies are in typewriter face, while others may be from any type of computer printer.

The quality of this reproduction is dependent upon the quality of the copy submitted. Broken or indistinct print, colored or poor quality illustrations and photographs, print bleedthrough, substandard margins, and improper alignment can adversely affect reproduction.

In the unlikely event that the author did not send UMI a complete manuscript and there are missing pages, these will be noted. Also, if unauthorized copyright material had to be removed, a note will indicate the deletion.

Oversize materials (e.g., maps, drawings, charts) are reproduced by sectioning the original, beginning at the upper left-hand corner and continuing from left to right in equal sections with small overlaps. Each original is also photographed in one exposure and is included in reduced form at the back of the book.

Photographs included in the original manuscript have been reproduced xerographically in this copy. Higher quality 6" x 9" black and white photographic prints are available for any photographs or illustrations appearing in this copy for an additional charge. Contact UMI directly to order.

UMI

A Bell & Howell Information Company
300 North Zeeb Road, Ann Arbor MI 48106-1346 USA
313/761-4700 800/521-0600

Changes in the Macromolecular Structure of a Type I Kerogen (Uinta Basin) During Maturation

by

Shang Li

Presented to the Graduate and Research Committee
of Lehigh University
in Candidacy for the Degree of
Doctor of Philosophy
in
Polymer Science and Engineering

Lehigh University
December 20, 1996

Approved and recommended for acceptance as a dissertation in partial fulfillment of the requirements for the degree of Doctor of Philosophy.

_____
Date

Dissertation Director

2 January 1997
Accepted Date

Committee Members:

Dr. J. W. Larsen, Chair

Dr. N. Foster

Dr. J. E. Roberts

Dr. M. Siskin

Dr. A. H. Sperling

Dedication

To my family and to the memory of my grandmother, Hao He-Ling.

Acknowledgments

I express my appreciation to Dr. Larsen for his patience, guidance, and encouragement throughout this work, and for his critical reading of this manuscript.

I also express my appreciation to Dr. Michael Siskin of Exxon Research and Engineering Company for providing Green River and Rundle oil shales and for his help and encouragement, to Dr. Alan Burnham of Lawrence Livermore National Laboratory for providing Uinta Basin oil shales, and to Dr. Marten Ternan of Canada Center for Mineral and Energy Technology for providing Athabasca bitumen samples. A special thanks to Dr. Roberts for his help with the NMR work.

Appreciation is extended to the Petroleum Research Fund (administered by the American Chemical Society), to Lehigh University, and to the Exxon Education Foundation for the financial support.

Finally, I would like to thank my wife, her parents, and my parents. Without their support this work would not have been possible.

Table of Contents

List of Tables

List of Figures

Abstract

The solvent swelling technique was used to study the macromolecular structure of Type I kerogens. Solvent swelling of Green River kerogen followed regular solution theory well and the network did not have specific interactions with polar solvents. The measured solubility parameter of Green River kerogen was about 9.7 $(cal/cm^3)^{1/2}$ using regular solution theory. The kerogen cross-link density was calculated using swelling theories. The results demonstrate that Green River kerogen is a highly cross-linked system. Solvent swelling of Rundle kerogen followed regular solution theory except that hydrogen-bonding solvents showed slightly enhanced swelling. The solubility parameter of Rundle kerogen was estimated at ~ 10 $(cal/cm^3)^{1/2}$. Solvent swelling is a useful method for characterizing Type I kerogens.

^{252}Cf plasma desorption mass spectrometry (PDMS) was used to measure bitumen molecular weight distributions of Green River, Rundle, and Athabasca bitumens. The number average molecular weights (M_n) calculated from these PDMS spectra agreed with the values determined by vapor pressure osmometry (VPO). The PDMS molecular weight distribution of Athabasca bitumen showed a good agreement with its gel permeation chromatography (GPC)/VPO molecular weight distribution. The PDMS technique appears to be reliable for measuring molecular weight distributions of bitumens and their products.

The changes in the macromolecular structure of a Type I kerogen (Uinta Basin) maturation series were investigated. The number average molecular weight between cross-links ($\bar{M}_c$) of the kerogen, the amounts of bitumen, and bitumen molecular weight distributions were determined using the techniques developed previously. The $\bar{M}_c$ (reciprocal of the cross-link density) slowly decreases during the first 80% maturation and rapidly decreases as the kerogen matures further. These changes display a good correlation with the kinetic and thermal history models in the literature. Characterizing the changes in kerogen cross-link density which occur during maturation provides a new way of probing maturation chemistry. The amounts of bitumen extracted from the Uinta basin maturation series agreed with the literature values, but the data do not display increases with increasing kerogen maturation because (1) light hydrocarbons were lost during vacuum removal of the solvent, and (2) oil migration reduced some bitumen molecules from the 80% and 100% mature samples.

It was proposed that Type I kerogen maturation involves fragmentation accompanied by network reconstruction. The model can be used to describe the kerogen maturation process on a macromolecular level.

Chapter I

Introduction

Reported here is a study of the changes in kerogen macromolecular structure which occur during the maturation process which generates petroleum. Kerogens are the insoluble organic matter in sedimentary rocks. They occur over wide geographical areas and are present in almost all sediments. The most important occurrences of kerogens are found in oil shales, which normally contain 0.5 to 20 wt % organic carbon,[1,2] and in coals, which usually contain 80 to 95 wt % organic matter.[3] Determining kerogen macromolecular structure can reveal much about its formation and behavior. Much work has been done on coals.[3,4] Little work has been done on the macromolecular structure of Type I kerogens. The work in this thesis is the first attempt of which we are aware to measure a Type I kerogen cross-link density.

Bitumens are the soluble organic matter in sedimentary rocks. Their amount, composition, and the concentration of individual components have frequently been used as descriptors of kerogen transformations.[1,5] In this dissertation, the amount of bitumen and its molecular weight distribution were carefully examined as an important descriptor of the chemistry of kerogen maturation.

Kerogens are complex heterogeneous materials having three dimensionally cross-linked macromolecular networks.[1] They are

the most abundant form of organic carbon on earth. It has been estimated that the amount of shale kerogen is at least 1000-fold greater than the amount of coal.[6] Type I and II kerogens are the source of most petroleum and some natural gas and are thought to be formed from random condensation of monomers generated by the degradation of biopolymer precursors following sediment burial in an anoxic environment.[1,7] Because kerogens are cross-linked, they are insoluble in organic solvents. Structurally, kerogens can be classified as random geopolymers.[8,9]

Traditionally, study of kerogen is closely tied to oil shale characterization for petroleum exploration and production. The primary intent usually is to understand the origin, generation, migration, and accumulation of petroleum. The main focus of oil shale studies has continued to be the development of empirical and statistical basin models to enhance petroleum exploration and oil potential estimation. The frontier of this field has recently shifted to involve more fundamental and quantitative assessments of the geochemical origin of kerogen, the characterization of the material and its evolution, and the investigation of oil formation and migration processes. Our work characterizes the macromolecular structure of kerogen and follows the changes in its structure as the kerogen matures.

Understanding the changes in kerogen macromolecular structure during maturation is important for oil formation and

migration studies. Geochemists generally believe that the molecular evolution of kerogens involves a series of bond making and breaking reactions. Small molecular groups continuously fragment off the cross-linked macromolecular "core". The polymeric "core" network undergoes structure changes throughout maturation.[1,9,10] This thermal evolution process has been extensively characterized using many techniques, including pyrolysis, elemental analysis, spectroscopy, petrography, etc., but has not been investigated for Type I and II kerogens using polymer chemistry approaches such as measuring kerogen cross-link densities and bitumen molecular weight distributions.

Determination of the cross-link density of the kerogen network (the gel), the amount of bitumen (the sol), and its molecular weight distribution and their changes with time could lead to development of a quantitative model of kerogen maturation by applying polymer theories.[11] This approach will reveal much of the chemistry of the petroleum formation process and allow a detailed kinetic analysis of kerogen maturation. It does require samples containing all of the original bitumen; none can have diffused out.

The principal technique employed in the work described in this dissertation is solvent swelling. Application of regular solution and rubber elasticity theories allowed us to estimate the number average molecular weight between cross links ($\bar{M}_c$) in a kerogen maturation series. The relationship established

between $\bar{M}_c$ and percent kerogen maturity directly reflects bond making and breaking which occur in the kerogen network during the thermal evolution process. The solvent swelling technique applied in this work provides a very different approach from those traditionally used to study kerogen maturation and holds much promise.

The goal of this research was to study the changes in the macromolecular structure of a Type I kerogen during the oil formation stage. We achieved it in two steps. We first used readily available Green River and Rundle oil shales to develop the necessary experimental techniques which include solvent swelling methodology and determination of the bitumen molecular weight distribution. We then applied these techniques to a maturation series of kerogen from the Uinta Basin of Utah and investigated the changes in the macromolecular structure occurring during the kerogen maturation process. The work presented here provides unique new insight into the geochemistry of petroleum formation.

Chapter II

Kerogen Formation, Evolution, and Characterization

1. Production and Accumulation of Organic Carbon on Earth

Photosynthesis is the fundamental reaction that directly and indirectly produces organic matter on earth. The reaction converts light energy into chemical energy by transferring hydrogens from water to carbon dioxide to form glucose and oxygen. Organic carbon produced on earth is primarily recycled in the biochemical cycle and is accumulated in the geochemical cycle. The above concepts are well summarized by Tissot and Welte.[1]

Figure 1 shows the two major cycles of organic carbon conversion on earth. The biochemical cycle (Cycle 1) is the primary one where living organic matter is formed and mainly recycled. It comprises roughly 3.0×10^{12} tons of organic carbon which has a half-life of days up to tens of years. The geochemical cycle (Cycle 2) is the secondary one where organic matter is accumulated in sediments and is partly metamorphosed. It contains an estimated 6.4×10^{15} tons of organic carbon which has a half-life of several million years. The two cycles are joined by a tiny linkage. During the earth's history, less than 0.1% of the organic matter in Cycle 1 is diverted to Cycle 2 and preserved in sediments. Approximately 0.01% to 0.1% of the organic matter in sediments is naturally oxidized to CO_2.[1]

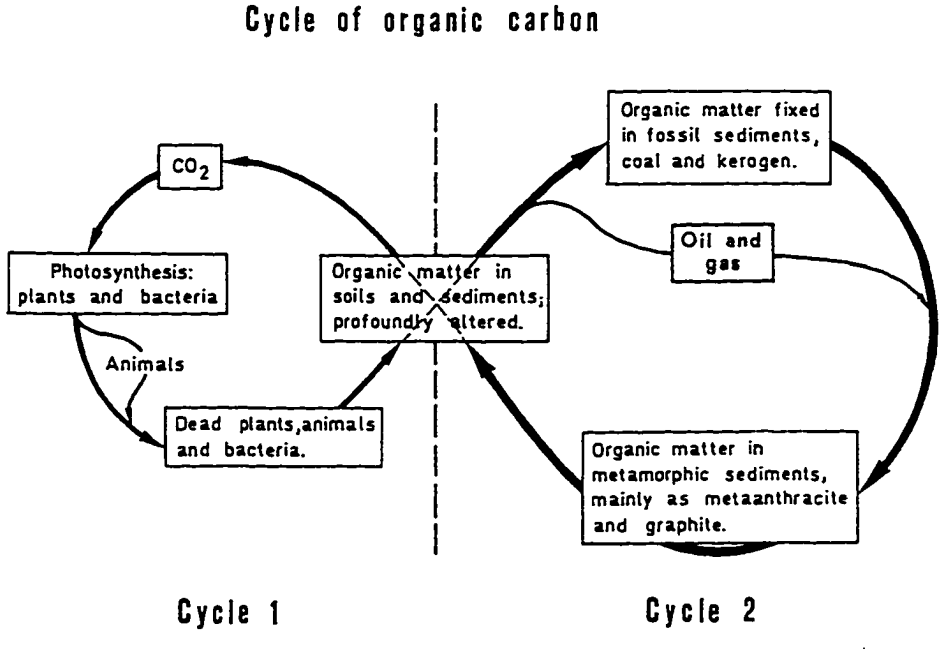

Figure 1. The two cycles of organic carbon conversion on earth.

Tissot, B. P.; Welte, D. H. *Petroleum Formation and occurrence*, Springer-Verlag: New York, 1978.

2. Geochemical Evolution of Organic Sediments

Once organic matter escapes from the biochemical cycle and enters into sediments, it is geochemically metamorphosed with increasing time and burial depth (temperature). The evolution of organic matter in sediments is a slow process and is classically divided into three stages: diagenesis, catagenesis, and metagenesis. Figure 2 shows the general scheme of kerogen evolution in a van Krevelen diagram.[1]

Diagenesis starts in the freshly deposited organic matter which is typically mixed with water, minerals, and living microorganisms at shallow depths, where biopolymers are decomposed to various degrees by microbial activity. While most of the products from decomposition are consumed by microorganisms, the rest, usually a very small fraction of the originally deposited organic matter, is transformed into kerogen by polycondensation, alkylation, dehydration, aromatization, and other insolubilization reactions.

Catagenesis results from increasing temperature with burial depth in the sedimentary basins. Temperatures generally range between 50 and 150 °C and pressures vary from 300 to 1500 bars.[1] Thermal and aqueous chemical degradations occur.[12] Because petroleum is generated during this stage, geochemists commonly call catagenesis the "oil window". The detailed chemistry of this stage is not well understood. It is not known whether the kerogen network undergoes depolymerization or small molecular groups fragment off the cross-linked "core"

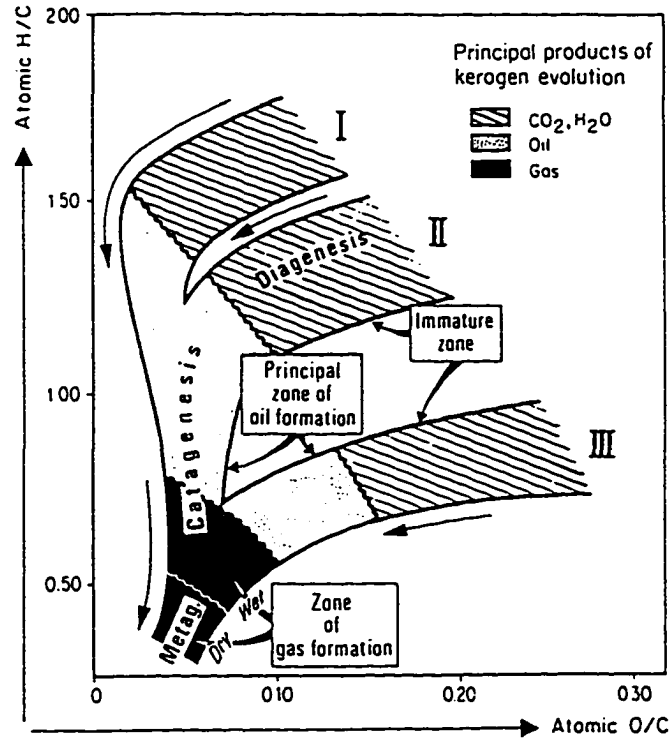

Figure 2. General Scheme of kerogen evolution in a van Krevelen Diagram.

Tissot, B. P.; Welte, D. H. *Petroleum Formation and occurrence*, Springer-Verlag: New York, 1978.

to increase the amount of soluble material (bitumen).[1] Catagenesis ends with the disappearance of the aliphatic groups in the kerogen network.

Metagenesis is the last stage, where temperature and pressure further increase and more gas is generated. The constituents of the kerogen are eventually converted into a graphitic carbonaceous material.

While the classical concept of kerogen formation through diagenesis still dominates this field, an alternate pathway emphasizing the selective preservation of biopolymers was proposed after the discovery of the insoluble non-hydrolyzable biomacromolecules.[13,14] Tegelaar et al. revised the scheme of kerogen formation after studying the biodegradability of biomacromolecules.[15] They assigned relative "preservation potentials" to known biopolymers based on the chemical stabilities of their structures and suggested that the key step in the classical mechanism of kerogen formation, random polycondensation of biomonomers formed by hydrolysis and biodegradation, is less important than previously thought. Kerogens can then be treated as physical mixtures derived from selectively preserved and partly altered resistant biomacromolecules.

3. Chemical and Petrographic Classification

Kerogen study is an interdisciplinary field. Two classification systems exist because geochemists and organic

petrographers characterize kerogens differently. Chemical classification is based on the bulk chemical composition of kerogens; petrographic classification is based on the morphological and optical properties of the elementary constituents of kerogens. The former provides direct information of bulk elemental composition and oil and gas potential; the later reveals the microscopic constituents and their thermal history. Hutton et al. reviewed important aspects of the two classification systems and compared their advantages and disadvantages.[16]

Chemically, kerogens are classified into three types dependent on their H/C ratios (see figure 2).[1] Type I kerogens have an H/C ratio of about 1.6 and contain long aliphatic chains and smaller amounts of aromatic nuclei. They are derived mainly from lacustrine deposits with organic matter enriched in lipids and have the highest potential for oil and gas generation. Type II kerogens have an H/C ratio of about 1.3 and contain more aromatic rings. They originate mainly from marine algal sediments and have lower oil and gas potential than type I kerogens. Type III kerogens (usually coals) have an H/C ratio 0.9 or less and consist of more condensed polyaromatic structures. This type of kerogen is derived mainly from terrestrial plants.

Petrographically, kerogens are divided into two main types: structured and amorphous debris.[17] Structured organic matter is further recognized as different "macerals", the

fundamental microscopic constituents in kerogens. They are vitrinite (wood remains), inertinite (carbonized remains), liptinite (spores, pollen grains, cuticles, and algae), and faunal relics (animal and plant remains which differ from the other components). Each of these structured categories has various subgroups with different optical properties. Amorphous organic matter is generated by random polycondensation of biomonomers which lose their optical identities during biodegradation.

4. Principal Techniques for Studying Kerogen Maturation

Geochemical metamorphism of kerogen changes its physical and chemical properties. Many of these changes have been utilized as kerogen maturation indicators.[18,19] A variety of techniques have been developed to characterize kerogen maturation. Elemental analysis,[1] IR,[20,21,22] NMR,[23,24,25] and biomarker analysis[26,27] are routinely applied for studying kerogen maturation; vitrinite reflectance[1,17,18,28,29] and Rock-Eval pyrolysis[1,30,31,32] are the standard methods for quantitatively determining kerogen maturation.

Elemental analysis reveals the basic chemical composition of kerogen. The H/C and O/C ratios calculated from the results of elemental analysis can be used directly to locate a kerogen on the van Krevelen diagram.[1] On the van Krevelen diagram, all kerogen types display a similar trend, a decreasing O/C ratio during diagenesis followed by a rapidly decreasing H/C ratio

during catagenesis (see Figure 2). If the type of kerogen is known, elemental analysis can be a fast technique for estimating the approximate extent of kerogen evolution.

IR is an informative tool for monitoring the functional group changes in kerogen during its maturation.[20,21] With increasing burial depth, the intensities of the aliphatic C-H (~2900-3100 cm^{-1}) and carbonyl C=O (~1700 cm^{-1}) absorptions decrease and the intensity of the aromatic peak (~1600 cm^{-1}) increases. These changes reflect chemical structure evolution and have been utilized for characterizing kerogen maturation. The IR technique was thoroughly reviewed by Rouxhet et al.[22]

NMR is another frequently used spectroscopic technique in kerogen maturation studies.[23] As kerogen matures, the amount of aliphatic carbon decreases and the amount of aromatic carbon increases. Solid state ^{13}C NMR provides a direct measurement of the ratio of aliphatic and aromatic carbons in a kerogen. This ratio has been used as an important parameter describing oil generation potential.[24,25]

The application of biological markers to kerogen study has emerged and made a great impact in the past two decades. Biomarkers are defined as the organic compounds occurring in sedimentary rocks whose carbon skeletons are preserved after losing functional groups during maturation.[26] Determining those compounds in oil shales is a valuable tool for studying kerogen maturation. Several classes of biomarkers, i.e. steranes and triterpanes, have been studied extensively for

this purpose. Maturation scales covering a wide range of maturity were established based on the relative concentrations of different isomers.[26,27]

Optical measurements, including vitrinite reflectance, liptinite florescence, and pollen-spores transmittance, are the classical quantitative techniques for studying kerogen maturation.[17] They are highly selective for particular optical particles and have be used to distinguish the different origins of kerogen and to evaluate kerogen maturity. Application of these techniques to the study of kerogen maturation was extensively reviewed by several researchers[1,17,18] Vitrinite reflectance is a standard parameter measuring the extent of coalification of coals, but it has severe limitations for determining the maturation of Type I and II kerogens.[28,29]

Pyrolysis is the most widely used technique for studying kerogen maturation.[30,31,32] Pyrolyzers are normally operated under an inert atmosphere (He or N_2) and coupled with on-line GC or MS (more frequently GC/MS) to analyze the pyrolyzed products. Rock-Eval pyrolysis, developed by Espitalie et al., is a widely used standard method for source rock evaluation.[1] T_{max} (the temperature at which the pyrolyzable hydrocarbon peak reaches its maximum evolution) and transformation ratio (the ratio of free hydrocarbons to the sum of free and pyrolyzable hydrocarbons in the oil shale) measured by this technique are the universally accepted parameters for characterizing kerogen

maturation (See Figure 3).[1] Tissot and Welte described the principles of the Rock-Eval pyrolysis device, analysis cycle, data examples, and its application to petroleum exploration.

The above techniques are practically important for petroleum exploration and have been widely used in kerogen structure characterization, kinetic studies for oil and gas formation, and reservoir modelling. But, none of them provides information reflecting the bond making and breaking reactions occurring in kerogen maturation. The solvent swelling technique employed in this work can follow macromolecular evolution during the oil formation process. A detailed discussion of its application is given in Chapter VII (Results and Discussion).

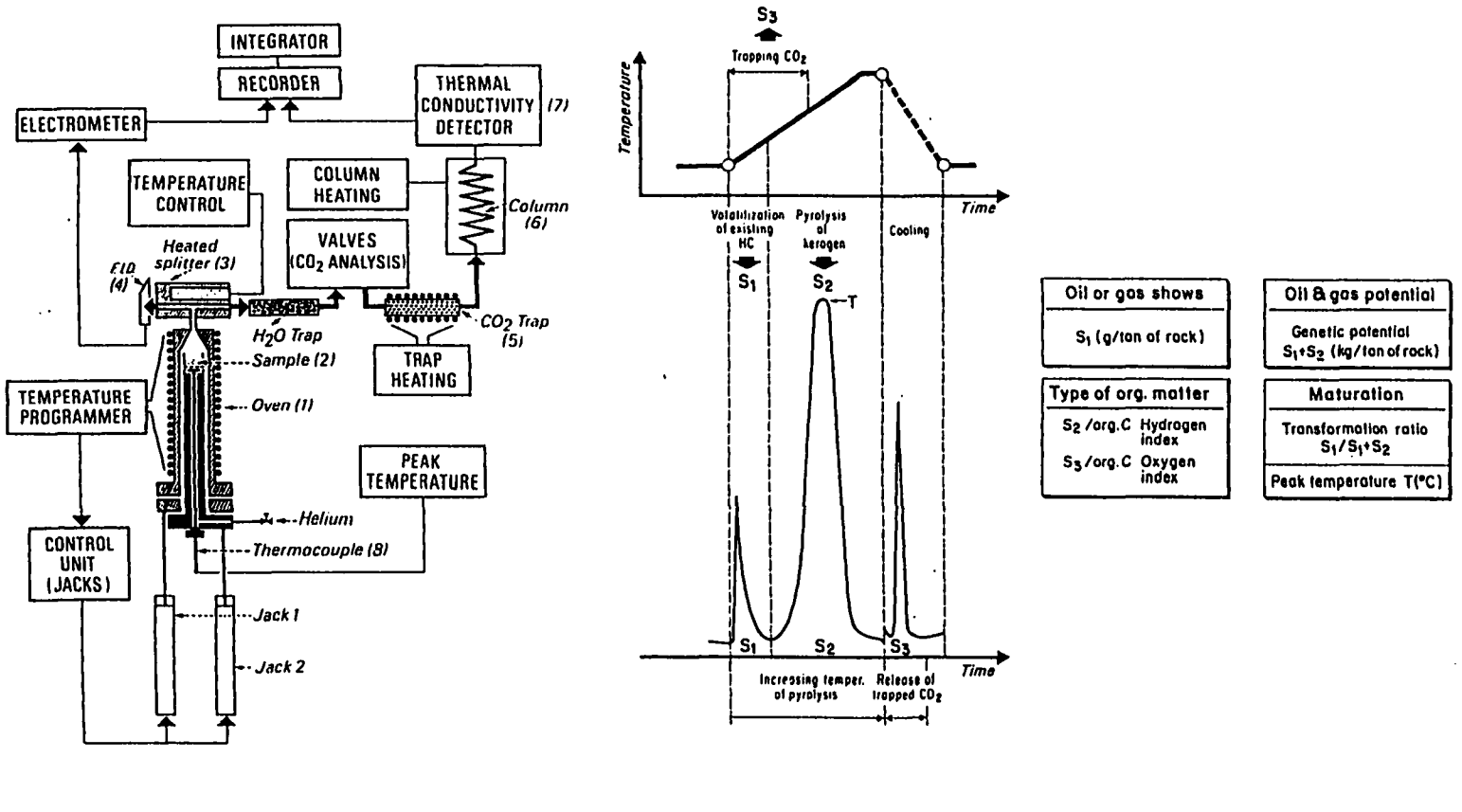

(a) (b) (c)

Figure 3. (a). Principle of the Rock-Eval pyrolysis device. (b). Typical data and significance. (c). Application to petroleum exploration.

Tissot, B. P.; Welte, D. H. *Petroleum Formation and occurrence*, Springer-Verlag: New York, 1978.

Chapter III

Structural Models of Type I Kerogen

1. Overview

The main atomic constituents of kerogens are carbon, hydrogen, oxygen, sulphur, and nitrogen.[1,33] Speight listed the elemental composition of 111 kerogen samples. For every 1000 carbon atoms, there are 500-1800 hydrogens, 25-300 oxygens, 5-30 sulphurs, and 10-35 nitrogens.[2] Kerogens are enormously complex. They are heterogenous random geopolymers, usually containing different macerals and residual minerals.[6,9] The detailed chemical structure of a kerogen depends on the original source of living organic materials, the chemical environment of sedimentation, and its geochemical evolution stage.

There is convincing evidence that the macromolecular structure of kerogen is a three dimensionally cross-linked network.[1,8,9] Kerogens are insoluble in either aqueous alkali or aqueous acids.[1,34,35] Aqueous oxidizing acids, such as chromic acid and perchloric acid, degrade kerogens to low molecular weight components without dissolving them.[36] Kerogens are also swellable in organic solvents.[4,34,37] This behavior is typical of a cross-linked polymer gel. Furthermore, kerogens exhibit rubber elasticity. It has be demonstrated that Type III kerogens can be stretched reversibly.[38,39]

A few chemical structural models of kerogens have been

described in the literature.[2,3,8,40] This section will not consider all of them, but limits the discussion to three Type I kerogen models. They are representative in different aspects. Yen's model is a multipolymer structure; Siskin's model reveals detailed chemical functionalities; and Behar and Vandenbroucke's model displays the changes in the chemical structure occurring during kerogen maturation.

2. Yen's Model[8,41]

Yen et al. used a classical chemical degradation approach to elucidate kerogen structures. Using a variety of techniques, they explored the structure of Green River kerogen isolated by HCl/HF demineralization. Green River kerogen was oxidized in a stepwise procedure into 10 successive fractions by multi-treatment with alkaline permangante. Over 90% of the original organic matter was recovered after the oxidation. Each fraction was studied by NMR, MS, and IR. The precursor material was additionally investigated by X-ray diffraction, ESR, electron spectroscopy for chemical analysis (ESCA), and IR.

Based on the experimental results, Yen et al. built a structure model of Green River Kerogen (Figure 4). This model contains almost no aromatic carbon. The bulk of the carbon skeleton is naphthenic and contains 3-4 rings. The empirical formula is $C_{235}H_{397}N_3O_5S_5$.

Yen et al. viewed this Green River kerogen model as a

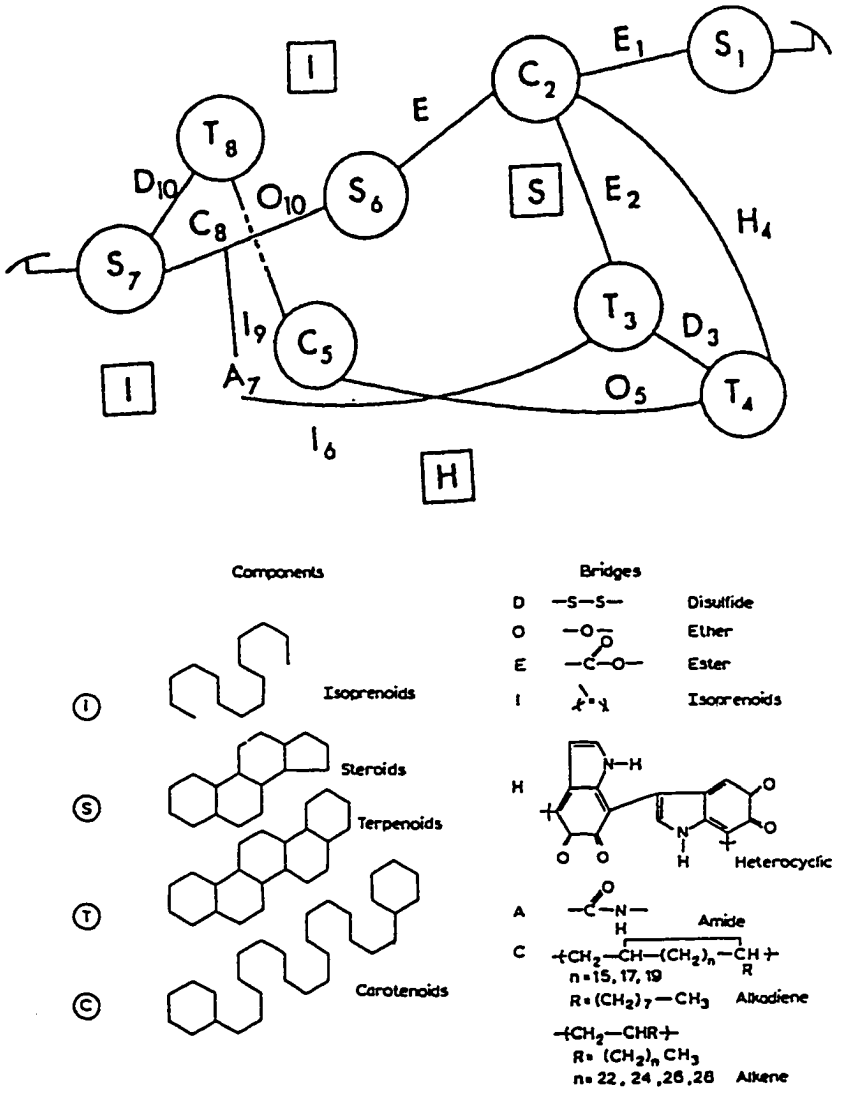

Figure 4. Yen's multipolymer model of Green River Kerogen. The squares are bitumen trapped in the kerogen network.

Yen, T. F. in *Oil Shale*, Yen, T. F.; Chilingarian, G. V. Ed., Elsevier: Amsterdam, 1976; pp 129-148.

"multipolymer". It consists of multifunctional nuclei that are cross-linked by difunctional bridges to form a three dimensional network gel. The multifunctional nuclei are the major components of the structure, and include isoprenoids, steroids, terpenoids, carotenoids, etc. The difunctional bridges are short chains, including disulfides, ethers, esters, isoprenoids, heterocyclics, alkenes, alkadienes, etc.

Yen el al. believed that Green River kerogen was highly heterogeneous exhibiting a "core-shell" structure. The shell is a more cross-linked region and contains most of the polar groups and heteroatoms; the core is a less polar region and contains more long aliphatic chains (C_{17} - C_{31}) which become more abundant toward in the center of the core.

Yen's Green River kerogen model agrees with the basic features of models previously proposed.[42,43,44] Although it lacks detailed chemical functionality, the model reveals the complexity of the Green River kerogen structure and its heterogeneous nature.

3. Siskin's Model[37]

A more sophisticated chemical model for Type I kerogen was developed by Siskin et al. They studied Green River oil shale from the Colony Mine, Parachute Creek, Colorado using mild chemical degradation, derivatization, solid state ^{13}C and ^{29}Si NMR, and other techniques. The hydrocarbon, oxygen, and nitrogen functionalities were determined after selective

derivatization of the Green River kerogen with isotopically labeled reagents.

Based on the distribution of hydrocarbon, nitrogen, and oxygen functionalities, Siskin et al. proposed a model for Green River kerogen and bitumen (see Figure 5). This model represents "one tetrafunctional cross link in an essentially infinite macromolecular network" and has the empirical formula $C_{100}H_{155}N_{3.10}S_{0.62}O_{2.17}$. It is a significantly detailed structure including multifunctional nuclei and the bridges that construct the macromolecular network. Most of this model is insoluble kerogen with a cross-linked structure. Bitumen is less than 15% of the total organic material.

Like Yen's model, the principal cross links in this model are covalent bonds. Siskin et al. pointed out that other types of cross links are also possible such as hydrogen bonding, heteroatom and mineral bonding, and physical entanglements.

Perhaps the major difference between Siskin's model and the previous ones is that the aromatic carbons make an important contribution to the structure: 22% of the total organic carbon. The relatively high aromaticity in the model differs from Yen's conclusion for Green River kerogen, but is consistent with Schmidt-Collerus and McGowan's works.[45,46] This difference may be caused by sample variability in the Green River formation.

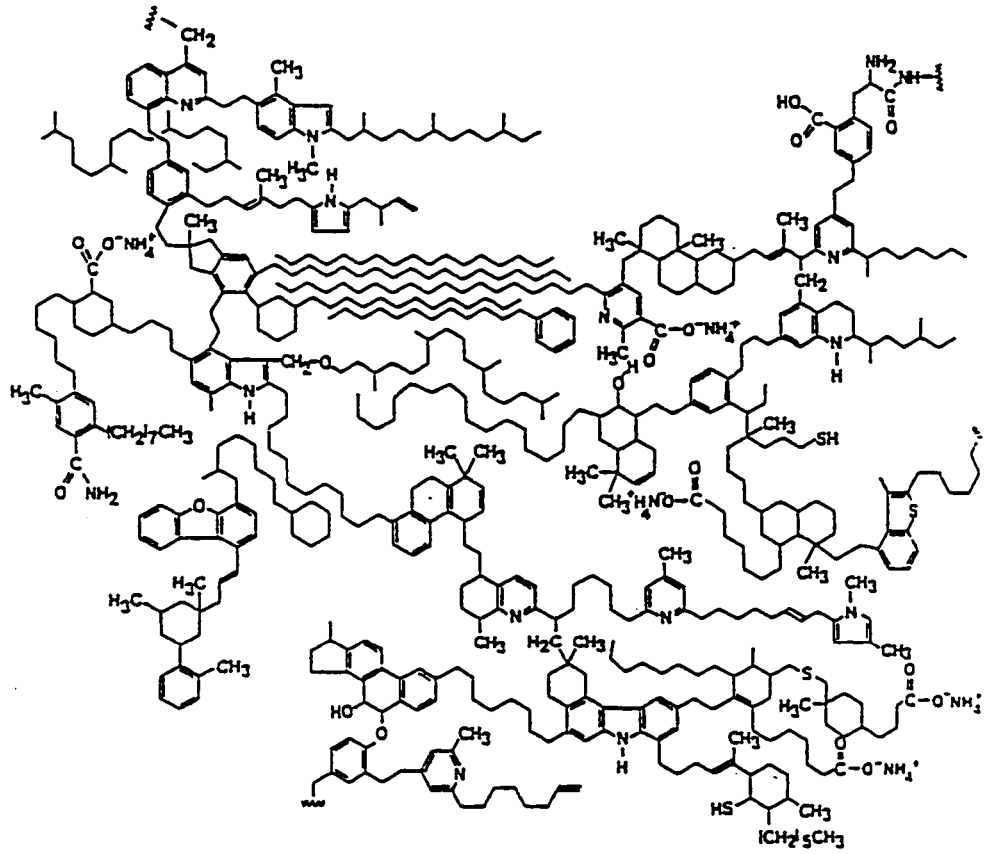

Figure 5. Siskin's detailed model of organic matter in Green River oil shale.

Siskin, M.; Scouten, C. G.; Rose, K. D.; Aczel, T.; Colgrove, S. G.; Pabst, R. E. Jr. in *Composition, Geochemistry, and Conversion of Oil Shales*, Snape, C. Ed., Kluwer Academic Publishers, 1995; pp 143-158.

4. Behar and Vandenbroucke's Model[10]

Behar and Vandenbroucke used literature data to construct generalized models for the three types of kerogens at different maturation stages.[10] Instead of modelling a particular kerogen, their goal was to demonstrate the differences between the three types of kerogens and the chemical structural changes occurring during the oil formation process.

Their models illustrate kerogen structures at the three maturation stages: (a) at the beginning of diagenesis, which excludes the very early period during which microbiologic activities are predominant; (b) at the beginning of catagenesis where kerogen loses most oxygen-containing groups and the oil window starts; and (c) at the end of catagenesis where the oil window ends and the kerogen structure has undergone reconstruction.

Because our concern in this study is solely with Type I kerogen, we have only considered Behar and Vandenbroucke's Type I kerogen model. Figure 6 shows this model at the beginning of diagenesis (Figure 6a) and at the end of catagenesis (Figure 6c). The structure at the beginning of catagenesis was not given in their paper because they stated that it almost overlaps with Figure 6a.

Table 1 compares the gross structural differences in the Type I kerogen model before and after oil formation. At the beginning of diagenesis, the kerogen has a high H/C ratio and

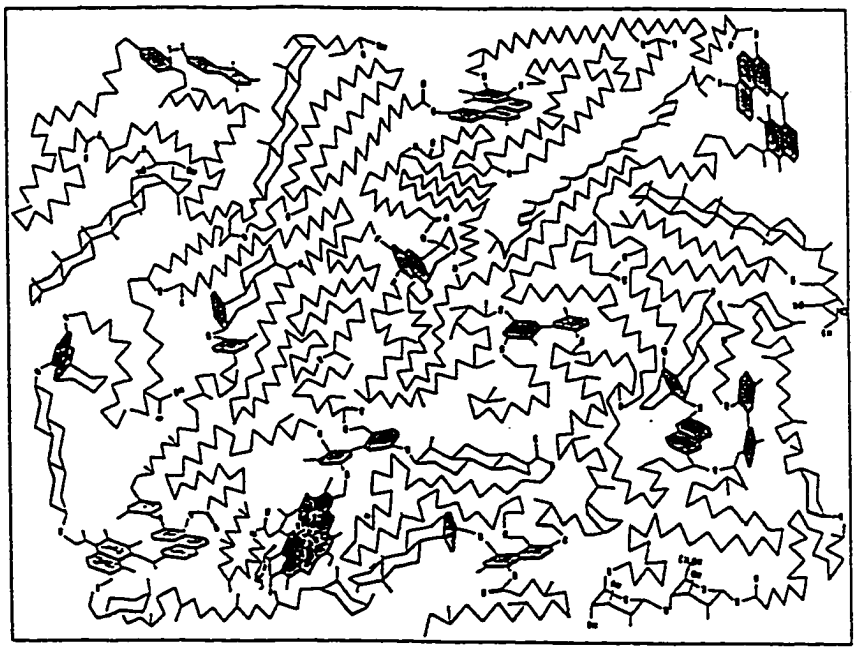

(a)

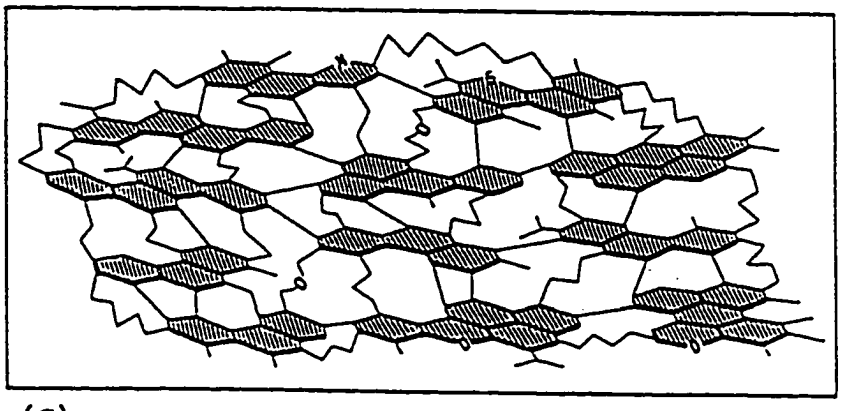

(c)

Figure 6. Behar and Vandenbroucke's statistical model of Type I kerogen. (a). At the beginning of diagenesis. (c). At the end of catagenesis.

Behar, F.; Vandenbroucke, W. *Org. Geochem.*, **1987**, 11, 15-24.

Table 1. Comparison of the H/C and O/C ratios and the carbon type distribution in a typical Type I kerogen at the beginning of diagenesis (Stage a) and at the end of catagenesis (Stage c).

Stage	H/C	O/C	ALC	CYC	ARC	PNR
a	1.64	0.060	74	12	14	1.9
c	0.83	0.013	36	0	64	3.8

ALC: % aliphatic carbons

CYC: % cycloaliphatic carbons

ARC: % aromatic carbons

PNR: average number of rings in polynuclear aromatics

Behar, F.; Vandenbroucke, W. *Org. Geochem.*, **1987**, 11, 15-24.

a high aliphatic content. The amount of oxygen is fairly low and it is present primarily in the form of ether groups. Aliphatic and cycloaliphatic carbons contribute 74% and 12%, respectively. Aromatic carbon is only 14% of the total and the average number of rings in polynuclear aromatics is 1.9. At the end of catagenesis, the H/C and O/C ratios have decreased from 1.64 and 0.060 to 0.87 and 0.013, respectively. The aliphatic carbons have decreased to 36% and cycloaliphatic carbons have disappeared. Aromatic carbons have increased to 64% of the total and the average number of rings in polynuclear aromatics is 3.8.

Behar and Vandenbroucke's model exhibits the changes in the chemical structure occurring during kerogen maturation. It is clear that catagenesis decreases the H/C ratio, O/C ratios, and aromaticity, and results in reconstruction and reorientation in the chemical structure of Type I kerogen.

Chapter IV

Macromolecular Chemistry of Kerogen Maturation

1. Isolation of Kerogen from Oil Shale

The first step in the study of kerogen is usually separation of kerogen from the mineral matrix. A variety of physical and chemical separation techniques have been reported in the literature and thoroughly reviewed.[35,47,48]

Physical methods generally do not alter the chemical structure of kerogen, but none is effective and gives a good laboratory yield. The most commonly employed physical methods are sink-float, oil agglomeration, and froth flotation.[47,48] These techniques are based on the different density of organics and minerals or on the different wettability of the two fractions in water and hydrocarbon liquids. Other reported physical techniques include ultrasonic, electrostatic, and magnetic methods.[47,48]

Chemical methods are more effective and are generally preferred on the laboratory scale. Among them, HCl/HF demineralization is classical and well studied.[35,47,48] Aqueous HCl and aqueous HF are capable of removing the carbonate and silicate minerals, respectively. Durand and Nicaise reviewed the effects of HCl and HF on kerogen and suggested that acid digestion at temperatures below 70 °C does not cause significant changes in the chemical structure.[35] IR studies of Torbanite oil shale from Australia did not show obvious

differences after HCl/HF treatment except for the disappearance of silicate absorptions near 1100 cm^{-1}.[35] CP/MAS ^{13}C NMR studies of a Kentucky and a Colorado oil shale revealed no relative changes in aliphatic and aromatic peaks after HCl/HF demineralization.[49]

McCollum and Wolff removed the silicate minerals using base instead of toxic HF.[34] They digested Green River oil shale with aqueous caustic followed by dilute mineral acid. The comparison of Base/Acid digestion and HCl/HF demineralization indicated that the effectiveness of the two techniques was comparable.

HCl may cause kerogen structural changes due to hydrolysis and chlorination.[35] Efforts have been made to avoid using strong acid in isolation procedures. Robl and Davis claimed that aqueous HF (pH = 3.45) is sufficient to remove any carbonate minerals and proposed replacing HCl/HF by a procedure using HF/BF_3.[50] In their work, HF reacts with minerals forming fluoride salts, and the salts are then selectively dissolved by reaction with BF_3 to form water soluble fluoroborates. Five carbonate and silicate oil shales were demineralized with both procedures. Elemental analysis, FTIR, and microscopic examination did not show any relative differences between HCl/HF and HF/BF_3 demineralized oil shales.

Based on the results of model compound-mineral studies, Siskin el al. identified acid-base interactions between

organics and clays as the major force binding kerogen to rock in oil shales. They developed a mild demineralization procedure utilizing aqueous ammonium sulfate (pH = 5~6) to dissolve the carbonate rock and to disrupt the organic-clay interactions.[51] The results of demineralizing Green River and Rundle oil shales demonstrated that their technique removed 85% and 50% of the clay minerals with 95% and 75% recovery of the total organic matter, respectively.[51,52]

2. Macromolecular Chemistry of Type I Kerogen Maturation

Most geochemists believe that the macromolecular structure of kerogen changes during the kerogen maturation process. Examining the thermal evolution of kerogen, it is easy to postulate that the macromolecular structure of kerogen may change in two stages. During diagenesis, polycondensation dominates and the cross-linked kerogen network is formed. Increasing cross-link density probably occurs as the polymerization proceeds. During catagenesis, oil and gas are formed and fragmentation must be occurring. This fragmentation may lead to an increase or decrease in the cross-link density of kerogen.

There have been speculations about the changes in kerogen cross-link density,[1,53,54] but the changes have never been measured. Stainforth and Reinders proposed that the petroleum formation process on a molecular scale involves a decreasing kerogen cross-link density and an increasing amount of soluble

molecules (bitumen).[53] Ungerer reviewed two possible schemes of kerogen maturation: depolymerization and defunctionalization.[54] Depolymerization decreases kerogen cross-link density and converts kerogen into small molecular groups (bitumen); defunctionalization releases appended chains from an inert carbon skeleton and leaves kerogen cross-link density unchanged. Ungerer suggested a network depolymerization being more adapted for describing Type I kerogen maturation. In this research, we set out to measure the changes in kerogen cross-link density which occur during the petroleum formation stage.

Three different models of the macromolecular chemistry of Type I kerogen maturation are possible. First, and common to all models, the kerogen network may polymerize continuously during catagenesis. The statistics of polycondensation of multifunctional monomers is well understood.[11,55] As the reaction proceeds, the infinite polymer network is first formed at the gel point. After that, the cross-link density of the polymer network increases, the amount of original monomers decreases, and the average molecular weight of oligomers decreases with increasing polymerization. The possibility of polycondensation in coalification has been rigorously examined.[56,57]

In the first macromolecular maturation model, the kerogen network undergoes depolymerization to form small molecular weight fragments. The theory of depolymerization has not been well explored, but careful studies of depolymerization of lignin and bitumious coals have been carried out.[58,59] If kerogen

network depolymerization is a random bond breaking process, large molecular groups will tend to fragment off the network later than small molecular groups because they are tied to the network by more bonds. In this case, the cross-link density of the kerogen network will decrease, and the amount of bitumen and its number average molecular weight will increase with increasing depolymerization. This seems to be the situation with coals.[57,59]

In the second model, the kerogen network is altered to a new chemical structure without changing the cross-link density. If the fragmentation reactions do not occur in cross-linking chains and only happen on appended hydrocarbon chains, the cross-link density will remain unchanged. If fragmentation from the appended chains is a random bond breaking process, the cleavage of small and large molecular groups will have a similar probability. The amount of bitumen will increase and its molecular weight distribution will remain unchanged unless the bitumen itself fragments.

In the third model, fragmentation is accompanied by a network reconstruction. Fragmentation may occur selectively on kerogen chains and the resulting intermediates react further to form cross-links. In this process, the amount of bitumen will increase and the cross-link density of the kerogen will increase with increasing maturation.

In all cases, there will exist relationships between the amount of bitumen, its molecular weight distribution, and the

cross-link density of the kerogen. Our initial goal was to determine these three quantities and follow their changes in a kerogen maturation series. The intention was to develop a model which can describe the macromolecular evolution of kerogen during maturation.

3. Solvent Swelling Theory and Technique

We selected the solvent swelling technique to measure the cross-link density of a kerogen. The theory of solvent swelling was originally developed by Flory and Rehner[11]. When a polymer network is placed in a suitable solvent, it will absorb the solvent and swell. At equilibrium, the free energy of mixing the polymer with the solvent will be exactly balanced by the elastic restoring force of the network. The total change in these two free energies must equal zero.

$$\Delta G_{mix} + \Delta G_e = 0 \qquad (1)$$

Here, ΔG_{mix} is the change in the free energy of mixing, ΔG_e is the change in free energy upon the expansion of the network.

The free energy of mixing comes from two terms: (1) the entropy change caused by mixing polymer and solvent, which favors swelling; and (2) the heat of mixing of the polymer network and solvent, which is zero in an ideal solution and has a finite positive value in a regular solution. When regular solution theory applies (the mixing is random and the total volume does not change), the change in the free energy

of mixing is expressed as equation 2.

$$\Delta G_{mix} = RT[\ln(1-v_2) + v_2 + \chi v_2^2] \qquad (2)$$

Here, v_2 is the volume fraction of the polymer network at equilibrium, χ is the Flory interaction parameter which characterizes the polymer-solvent interactions occurring during the mixing.

The elastic restoring force depends on the cross-link density of the polymer. It is entropic and opposes solvent swelling. The change in the elastic free energy of a polymer network in solution is complicated, but can be simplified when (1) the network is tetrafunctionally cross-linked; (2) the chain lengths between joining points obey the Gaussian distribution; and (3) the chains deform uniformly.

$$\Delta G_e = RT\frac{\rho V_1}{\overline{M_c}}\left(V_2^{\frac{1}{3}} - \frac{V_2}{2}\right) \qquad (3)$$

Here, V_1 is the molar volume of the solvent, ρ is the polymer density, and $\overline{M}_c$ is the number average molecular weight between cross links.

Using Equations 1, 2, and 3, the Flory-Rehner equation can be derived.[11]

$$\overline{M_c} = -\frac{V_1\rho\left(V_2^{\frac{1}{3}} - \frac{V_2}{2}\right)}{\ln(1-v_2) + v_2 + \chi v_2^2} \qquad (4)$$

The cross-link density (n) is easily calculated using equation 5.

$$n = \frac{\rho}{\overline{M_c}} \qquad (5)$$

Solvent swelling theory is widely used to determine the cross-link densities of elastomers[60] and has been extensively applied to study the macromolecular structure of coals.[4,38] It has been recognized that coal is a highly cross-linked polymer network in which the chain length between cross-links is too short and too rigid to follow the Gaussian distribution. Both Kovac and Peppas have modified the Flory-Rehner equation for highly cross-linked systems.[61,62] The principle refinement of Kovac's theory is to remove the assumption of the Gaussian chain length distribution and to introduce an additional parameter N, the number of rotatable segments between the cross-links.

$$\overline{M_c} = -\frac{V_1\rho\,(v_2^{\frac{1}{3}} + N^{-1}v_2^{-\frac{1}{3}})}{\ln(1-v_2) + v_2 + \chi v_2^2} \qquad (6)$$

Experimentally, v_2 and χ must be determined in order to calculate $\bar{M}_c$ using Equation 4 or 6. While determining v_2 is easy, χ is problematic.[63] A simple method is to use regular solution theory.[64,65] The polymer is swollen in a series of solvents. The Hildebrand solubility parameter of the network (δ_2) can be determined using the bell-shaped plot of polymer swelling ratios vs. swelling solvent solubility parameters. Using equation 7, χ can be calculated.[66,67,68]

$$\chi = \frac{V_1}{RT}(\delta_1 - \delta_2)^2 + \chi_s \qquad (7)$$

Here δ_1 and δ_2 are the solubility parameters of the solvent and the polymer, respectively. χ_S is the entropy contribution. This term depends on the size and shape of the solvent molecule and the polymer network,[66] and is generally 0.3 - 0.4 for polymers in nopolar solvents.[66,67] Sperling pointed out that $\chi_S = 0$ gives better correlations for most polymer-solvent pairs.[68] Larsen et al. and Green studied two coals swollen in various organic solvents.[4,63] Assigning $\chi_S = 0.3$ yielded scatter $\bar{M}_C$ values for the coals in different swelling solvents. Larsen et al. and Green suggested that χ_S might vary for different coal-solvent pairs.[4,63] A value of 0.3 is usually assigned in solvent swelling studies of coals.[3,4,63]

Painter has developed another theoretical treatment of coal swelling. His theory explicitly recognizes the strong specific interactions between some swelling solvents and coal.[68] As we will show, such interactions are absent in Type I kerogen. We need not consider this treatment further.

The solvent swelling technique is well developed and has been done volumetrically, gravimetrically, and on coal thin sections under a microscope.[38] A new technique based on particle size distributions before and after swelling was also developed recently.[70] The volumetric method has been carefully examined and is the easiest.[71,72] Green et al. compared the

volumetric and gravimetric experiments by swelling two coals in 10 solvents. The volumetric swelling method appeared to be more rapid and convenient and provided the same results as the gravimetric procedure.

A small amount of data on solvent swelling of Type I kerogen exists in the literature. McCollum and Wolff demineralized Green River oil shale using NaOH/HCl and swelled the kerogen concentrate in five solvents.[34] The plot of weight swelling ratio of the kerogen against solubility parameter of the solvents used yielded a bell-shaped curve with a peak at about 9.5 $(cal/cm^3)^{1/2}$. Their result agreed with the work of Shadle el al. who studied the gravimetric swelling of Green River kerogen in 8 solvents.[73] We studied Green River kerogen is 28 solvents using volumetric solvent swelling.[37] The results showed that regular solution theory is roughly followed in most of the solvents used including polar solvents and hydrogen bond acceptors. A detailed discussion of the solvent swelling experiments is given in Section VII.2.

4. Amount of Bitumen and its Molecular Weight Distribution

It has been recognized for a long time that the abundance and composition of the bitumen present in source rocks depends on the kerogen maturity. Many techniques have been developed to characterize the stage of kerogen maturation using the amount of bitumen, its composition, and the concentration of its individual components. We are interested in the amount of

bitumen and its molecular weight distribution because our goal is to characterize the changes in the macromolecular structure of kerogen by following the relationship between the amount of bitumen, its molecular weight distribution, and kerogen cross-link density.

The amount of bitumen is normally determined using an organic solvent to extract the demineralized oil shale. The result is commonly expressed as the transformation ratio, the ratio of bitumen to the total organic matter, and is used to characterize the stage of petroleum formation. For oil shales, bitumen is 2 to 20 wt % of the total organic matter.[1] Tissot and Welte demonstrated that the amount of bitumen changed progressively with increasing burial depth in four basins. A bell-shaped plot of the bitumen to the total organic carbon ratio vs burial depth was observed during catagenesis in the Douala Basin.[1]

The bitumen molecular weight distribution can be determined by several methods. The most frequently used technique is gel permeation chromatography (GPC), which separates bitumen based on molecular size.[74] It is generally accepted that there are no adequate calibration standards for analyzing kerogen products because adsorption, association, and partition effects influence the size-based separation.[75,76] A more reliable approach is to collect individual fractions separated by GPC and to measure the number average molecular weight of each fraction. Vapor pressure osmometry (VPO) is

commonly used to measure the number average molecular weight of the separated GPC fractions. Freezing point depression (FPD) and gas chromatography/mass spectrometry (GC/MS) have also been employed for this purpose.[77] Champagne el al. fractionated Athabasca bitumen using GPC and measured the number average molecular weight of the separated fractions by VPO, FPD, and GC/MS.[77] The results showed good agreement among these techniques.

Field-ionization mass spectrometry (FIMS) has been used to determine the bitumen molecular weight distributions.[78,79,80] FIMS generates molecular ions with little fragmentation and responds with approximately equal sensitivity to almost all classes of compounds. Payzant et al. determined molecular weight distributions of the hydrocarbon-substituted aromatic, sulphur-containing aromatic, thiourea adduct, and thiourea non-adduct fractions isolated from a series of Alberta bitumens and studied the effect of biodegradation on molecular weight distributions of these components.[78] McKay et al. characterized molecular weight distributions of Green River bitumen isolated by pyridine extraction, and CH_3OH/H_2O and CO_2/H_2O supercritical extraction.[79,80]

We used ^{252}Cf plasma desorption mass spectrometry (PDMS) to measure molecular weight distributions of Green River, Rundle, and Athabasca bitumens and compared our results with those obtained by VPO and GPC/VPO.[81] The number average molecular weights measured by VPO and PDMS agreed well, and

the GPC/VPO molecular weight distribution of Athabasca bitumen agreed with the one determined by PDMS. This application of ^{252}Cf plasma desorption mass spectrometry is discussed in Section VII.2b.

Chapter V

Maturation Studies of Uinta Basin Oil Shale

1. Geographical Features

The Uinta basin is a topographic depression which covers over 24,000 km^2 in northeast Utah.[82,83,84] It is an asymmetric syncline with an east-west-trending axis near the northern side. The basin is surrounded by the Uinta Mountains to the north, the Wasatch Mountains to the west, the San Rafael Swell to the southwest, and the Uncompahgre Uplift to the southeast (see Figure 7). The geological structure of the Uinta basin is complex and variable. The detailed geological and geochemical factors which lead to the formation of this basin are not well understood.[84]

The Uinta Basin provides an ideal geological setting to study the evolution of kerogen to petroleum. During the early Tertiary (57.8 - 30 million years ago), approximately 6000 meters of sediments were accumulated in a lacustrine and alluvial environment.[84,85,86] Today, a variety of hydrocarbon deposits, including oil, gas, coal, tar sand, solid bitumen, and oil shale, have been discovered in this region. The basin currently contains more than 100 oil and natural gas fields.[85]

Currently, the primary source of oil and gas formed in the Uinta basin is the Green River formation, which is carbonate mudstone with 610-2500$^+$ meters thick and is located in the north central region of the basin. The Green River

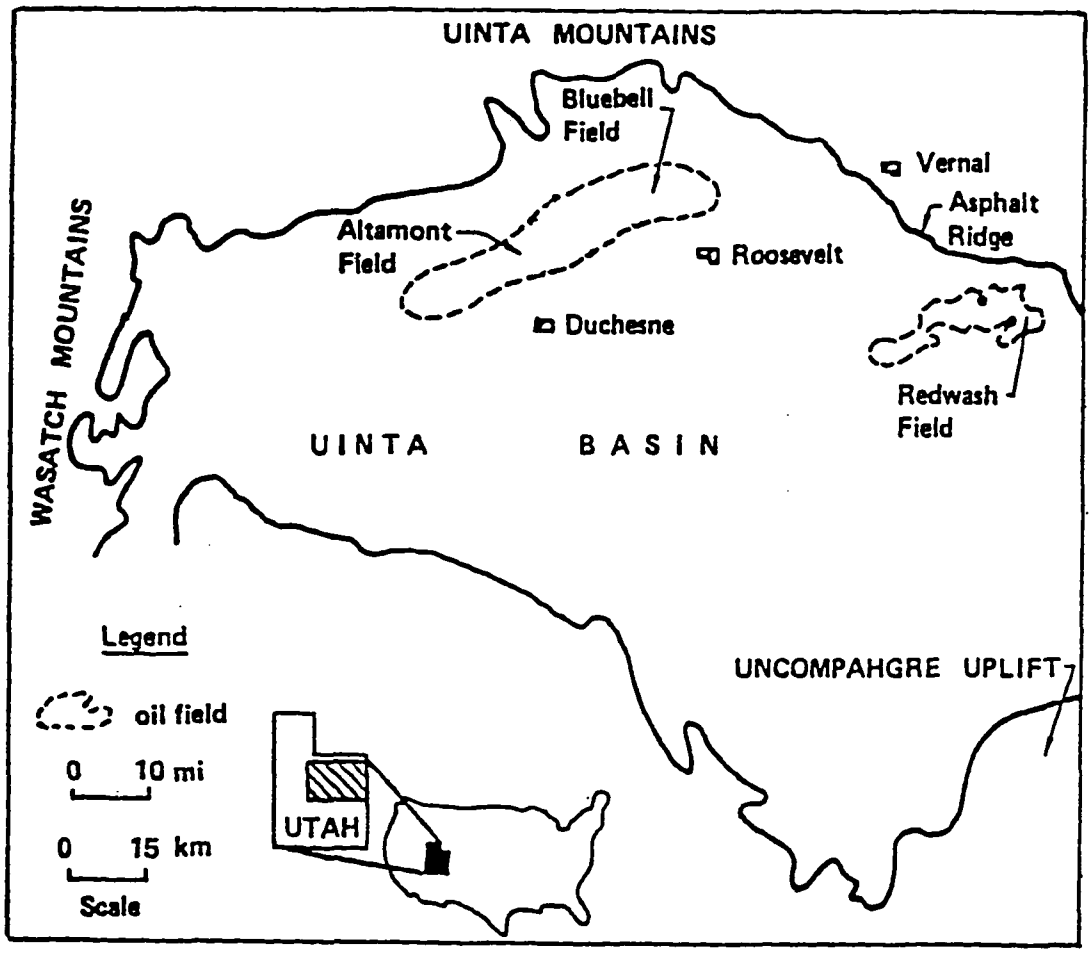

Figure 7. Structural setting of the Uinta Basin showing locations of the Altamont-Bluebell and Redwash oil fields.

Sweeney, J. J.; Burnham, A. K.; Braun, R. L. *Am. Assoc. Petro. Geol. Bull.*, **1987**, 71, 967-985.

formation is overlain by the Uinta formation and the Duchesne River formation (see Figure 8).[82,85,86] The lower part of the Green River formation is in the mature stage and petroleum and natural gas are recovered from the deeply buried rocks. Five samples representing different maturation stages of the Green River formation were used in this study. Four of these shales were collected from the Altamont field and one was collected from the Redwash field (see Figure 7). The detailed burial histories and geological structures of these two fields were described previously.[87,88]

2. Maturation Geochemistry

Uinta basin kerogen is a typical Type I kerogen in the classification scheme of Tissot and Welte.[1] It is derived from lipid-rich lake algae and terrestrial spores and pollen and consists of primarily amorphous materials.[89] The Uinta basin oil shale usually contains 1 to 20 wt.% organic matter. More than 80 wt.% of that organic matter is kerogen.[84,89,90,91] The mineral content of the oil shale is variable depending on the specific geographical location, but most samples contain dolomite, calcite, quartz, illite, feldspars, pyrite, and analcime.[91]

Extensive maturation studies of the Uinta basin oil shale have been performed.[1,83,84,90,92] A general conclusion is that the lower part the Green River formation has reached the principal stage of oil generation. The mature zone appears to occur in

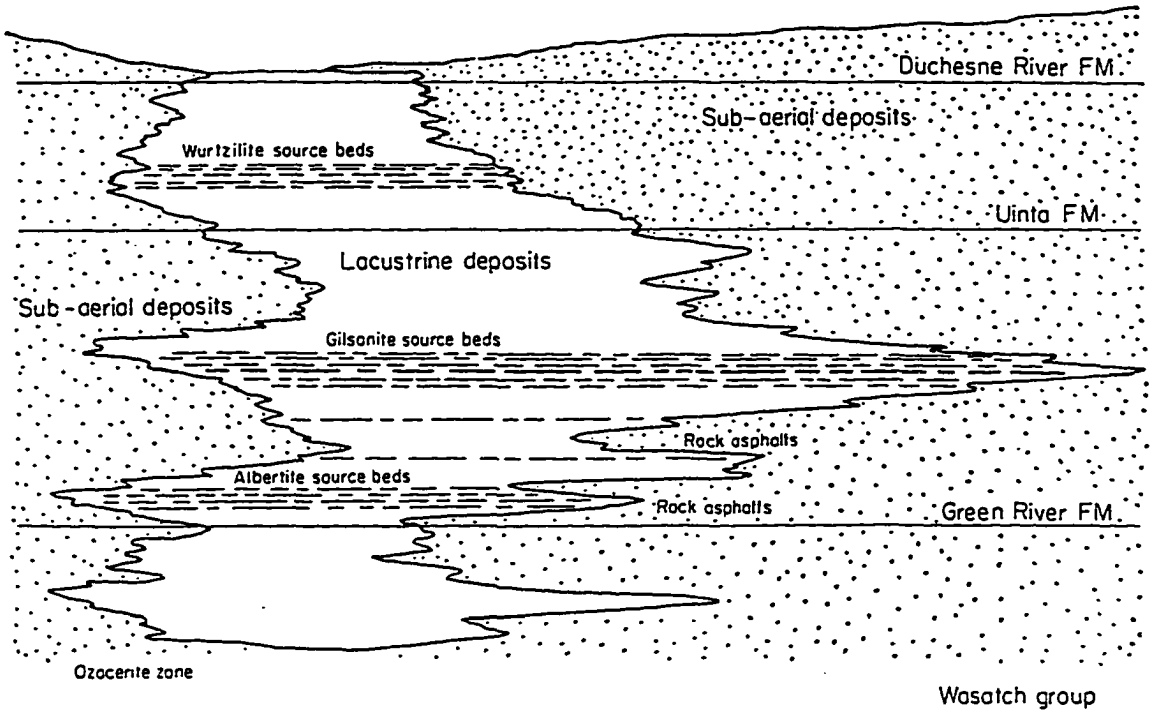

Figure 8. A generalized section of the Uinta Basin assuming no deformation and erosion.

Bell, K. G.; Hunt, J. M. in *Organic Geochemistry*, Breger, I. A. Ed., Pergamon Press: New York, 1963; pp. 333-366.

the burial depth of 3930-5590 meters.

Elemental analysis of the kerogen from the Green River formation of the Uinta Basin shows that the average H/C and O/C ratios are about 1.5 and 0.05 at the beginning of diagenesis (see Figure 9).[84] With increasing thermal evolution, the O/C ratio decreases to 0.03 during the early diagenesis due to loss of CO_2 and H_2O. The H/C ratio is rapidly reduced to 0.8 during catagenesis.

Figure 10 displays IR spectra of the Uinta basin kerogen obtained from 9 different maturation stages.[84] With increasing burial depth, aliphatic CH_2 and CH_3 bands (2950 and 1450 cm^{-1}) continuously decrease and aromatic C=C bonds (1600 cm^{-1}) continuously increase. Long aliphatic chains (750 cm^{-1}) become undetectable in the deeply buried samples. C=O functional groups (1700 cm^{-1}) decrease initially and then appear to increase slightly with the extent of maturation. The conclusions derived from the IR spectra agree with that based on the van Krevelen diagram (Figure 11). The initial decrease of C=O functional groups corresponds to the formation of CO_2 and H_2O during diagenesis. With more burial, the large decrease in the aliphatic groups corresponds to hydrocarbon formation from the kerogen.

The amount of bitumen and its individual components have often been used to characterize kerogen maturation processes in the Uinta basin.[1,83,84,90,92] Tissot and Welte displayed the concentration changes in C_{14}-C_{30} n-alkanes, cycloalkanes,

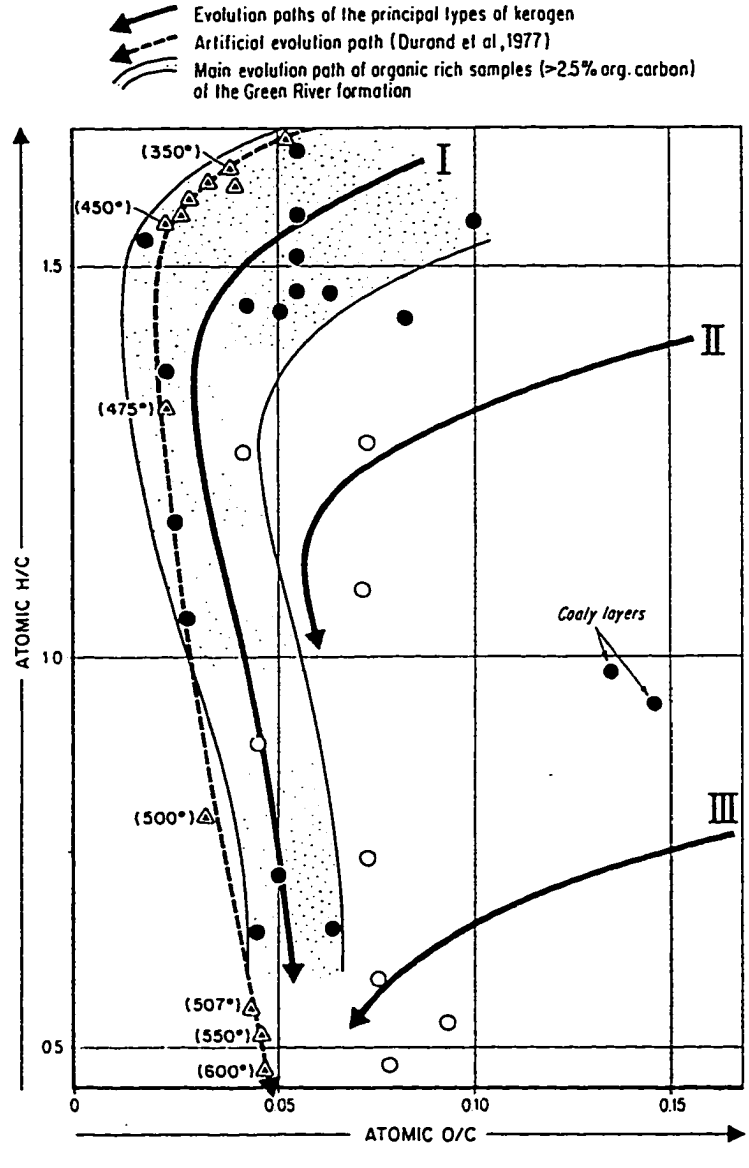

Figure 9. Elemental analysis of kerogen from the Uinta basin Green River formation.

Tissot, B.; Deroo, G.; Hood, A. *Geochim. Gosmochim. Acta*, **1978**, 42, 1469-1486.

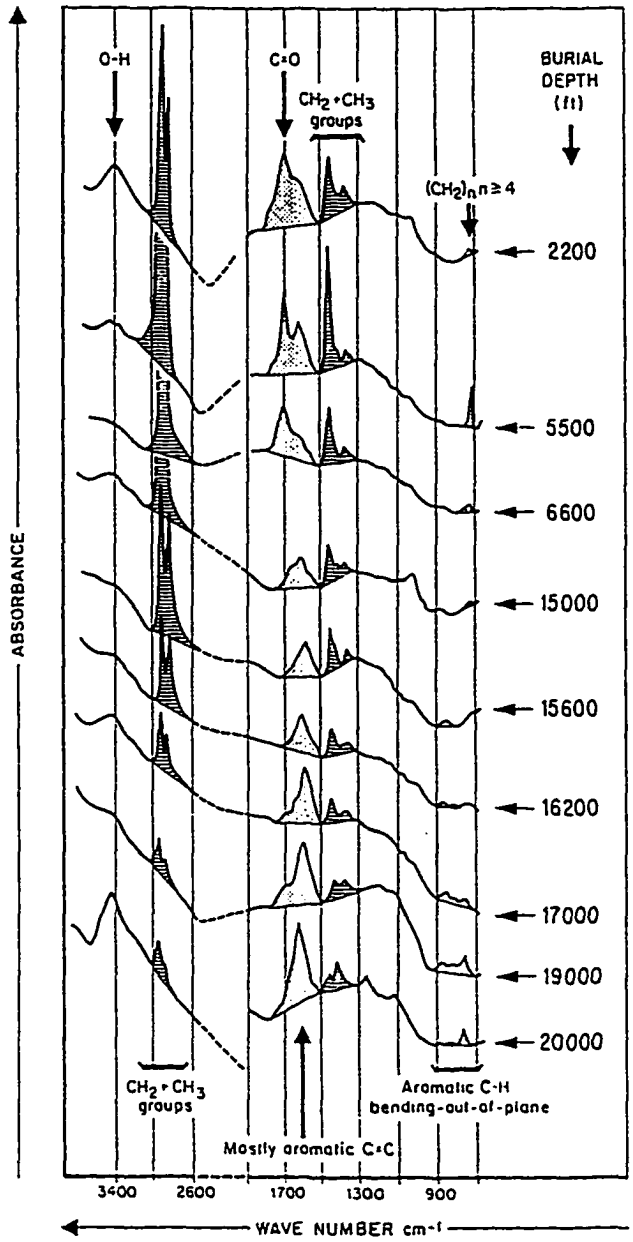

Figure 10. Evolution of IR spectra of Uinta basin kerogen from Green River formation as a function of increasing burial depth.

Tissot, B.; Deroo, G.; Hood, A. *Geochim. Gosmochim. Acta*, 1978, 42, 1469-1486.

isoalkanes, and aromatics generated from the kerogen during the oil formation process.[1] The amounts of these hydrocarbons change progressively and plots of bitumen components to the total organic carbon vs burial depth display the bell-shaped curves (Figure 11).[1] Tissot et al. analyzed 38 Uinta basin bitumens and plotted the ratio of bitumen to the total organic carbon as a function of burial depth.[84] The amount of bitumen generated from the Uinta basin kerogen does not reveal an obvious pattern throughout the whole burial range (Figure 12a). When the ratio of bitumen to the total "useful organic carbon", sum of pyrolyzable and extractable organic carbon, is used, the plot displays a familiar bell-shaped curve like the major hydrocarbon components generated from the kerogen (Figure 12b).

Tissot et al. investigated 28 samples with various maturities in the Altamont field using the vitrinite reflectance technique.[84] Vitrinite reflectance gradually increases from 0.5 to 1.7 as burial depth changes from 3350 m (11000 ft) to 7010 m (23000 ft) (see Figure 13).

Much work has been done using Rock-Eval pyrolysis to evaluate the Uinta basin kerogen maturation process and to model the kinetics of oil formation.[1,83,84,90,92] Anders and Gerrild characterized Uinta basin rock samples collected from six wells at various depths.[90] Their results revealed that as Uinta basin kerogen matures, the hydrogen index (the ratio of pyrolyzable hydrocarbons to the total organic carbon)

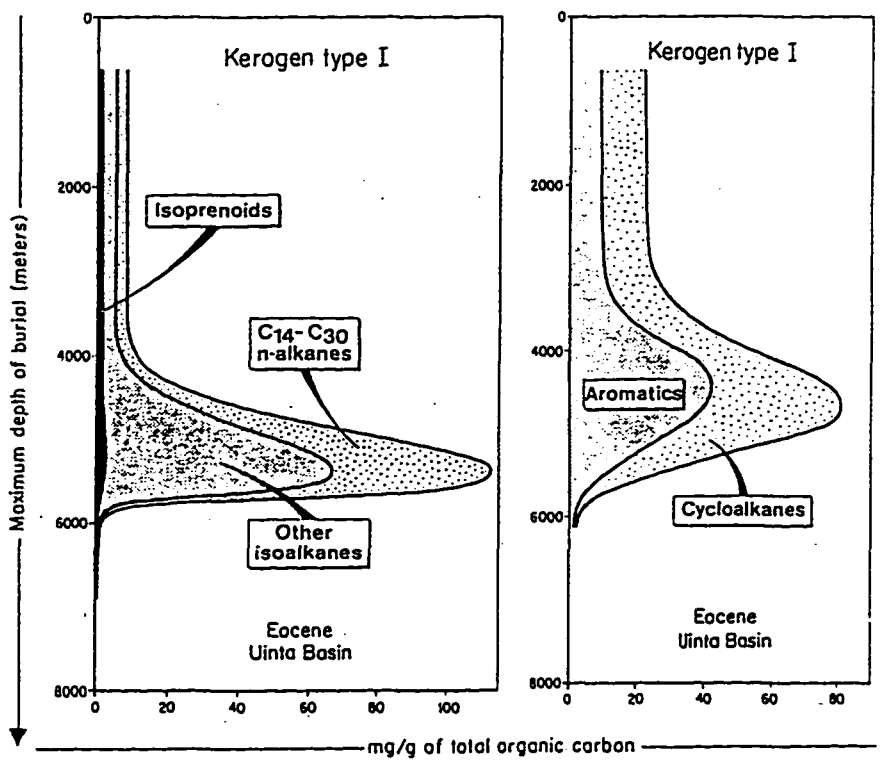

Figure 11. Formation of hydrocarbons as a function of burial depth in the Uinta basin.

Tissot, B. P.; Welte, D. H. *Petroleum Formation and occurrence*, Springer-Verlag: New York, 1978.

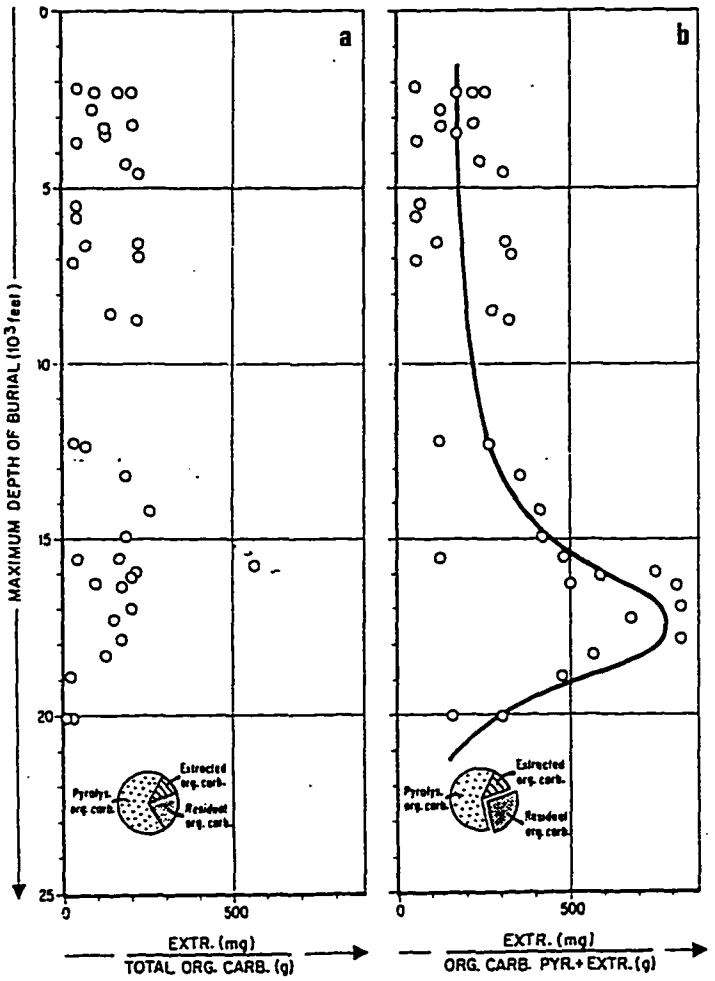

Figure 12. The amount Uinta basin bitumen as a function of burial depth. a. The amount of bitumen is expressed as mg/g of total organic carbon. b. The amount of bitumen is expressed as mg/g of pyrolyzable and extractable organic carbon.

Tissot, B.; Deroo, G.; Hood, A. *Geochim. Gosmochim. Acta*, **1978**, 42, 1469-1486.

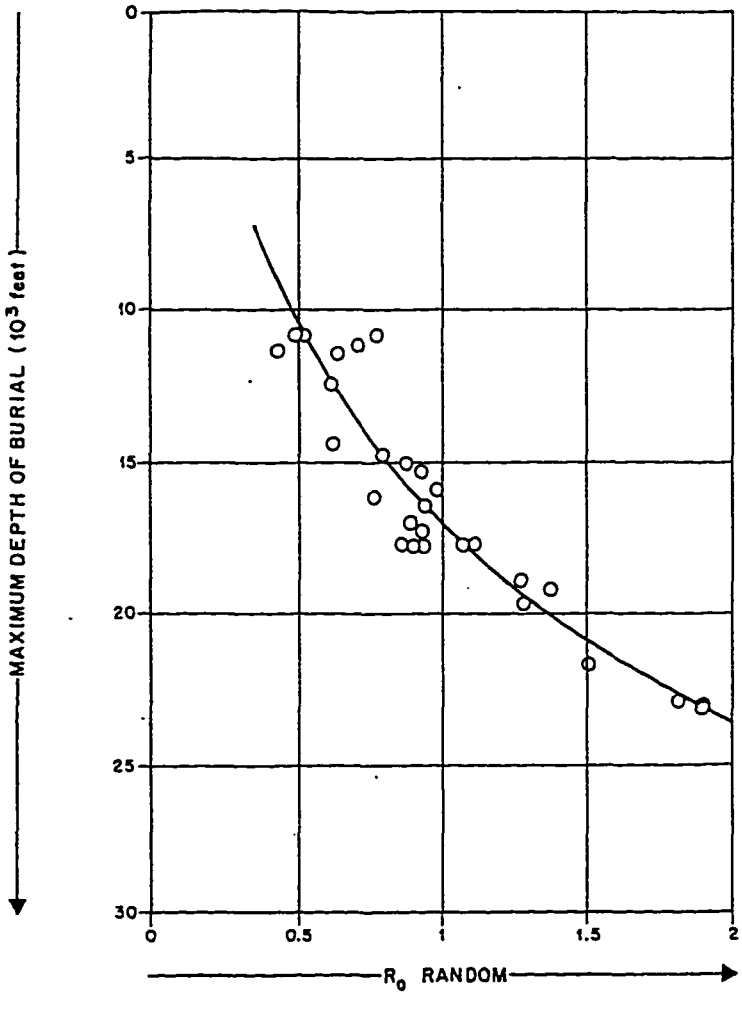

Figure 13. Vitrinite reflectance as a function of burial depth in the Altamont field.

Tissot, B.; Deroo, G.; Hood, A. *Geochim. Gosmochim. Acta*, **1978**, 42, 1469-1486.

decreases, the production index (the ratio of free hydrocarbons to the sum of free and pyrolyzable hydrocarbons) increases, and T_{max} (the temperature of the maximum oil generation) has no obvious trend (Figure 14).

Sweeney et al. reviewed the previous studies of the burial history of the Uinta basin and concluded that erosion has taken place everywhere in the depression.[83,92] The present burial depth of the oil shale does not represent the maximum burial depth. Therefore, without an accurate estimation of the amount of erosion in each field, the maximum burial depth and T_{max} can not be determined. They estimated 1800 m for the amount of erosion in the Altamont and Redwash fields and reconstructed the relationship between the maximum burial depth and temperature for the selected wells in the fields. Based on these relationships, Sweeney et al. developed a kinetic model which is capable of predicting the timing and the rate of oil and gas generation. Their published results showed that the predicted kerogen maturation levels at different depths agreed well with the experimental results from the literature. Figure 15 is a comparison of the predicted transformation ratio (% oil generated) with the actual generated saturated hydrocarbons in the Altamont field.[83] The model curve assumes no cracking or migration occurred and 1800 m of erosion in the field.

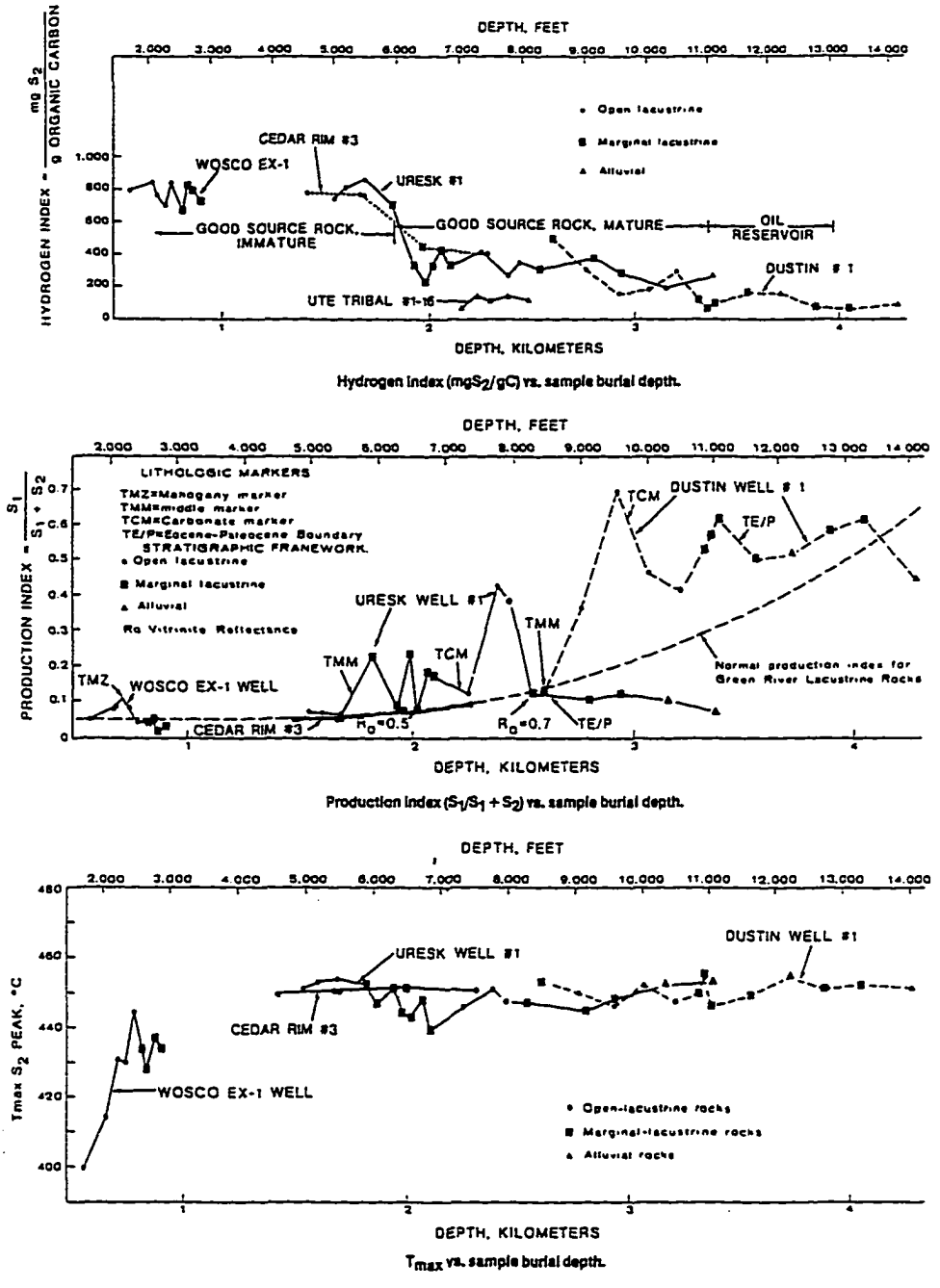

Figure 14. The Hydrogen index, transformation ratio, T_{max} as a function of increasing burial depth in the Uinta basin.

Anders, D. E.; Gerrild, P. M. in *Hydrocarbon Source Rocks of the Greater Rocky Mountain Region*, Woodward, J.; Meissner, F. F.; Clayton, J. L. Ed., Rocky Mountain Assoc. Geol., 1984; pp. 513-529.

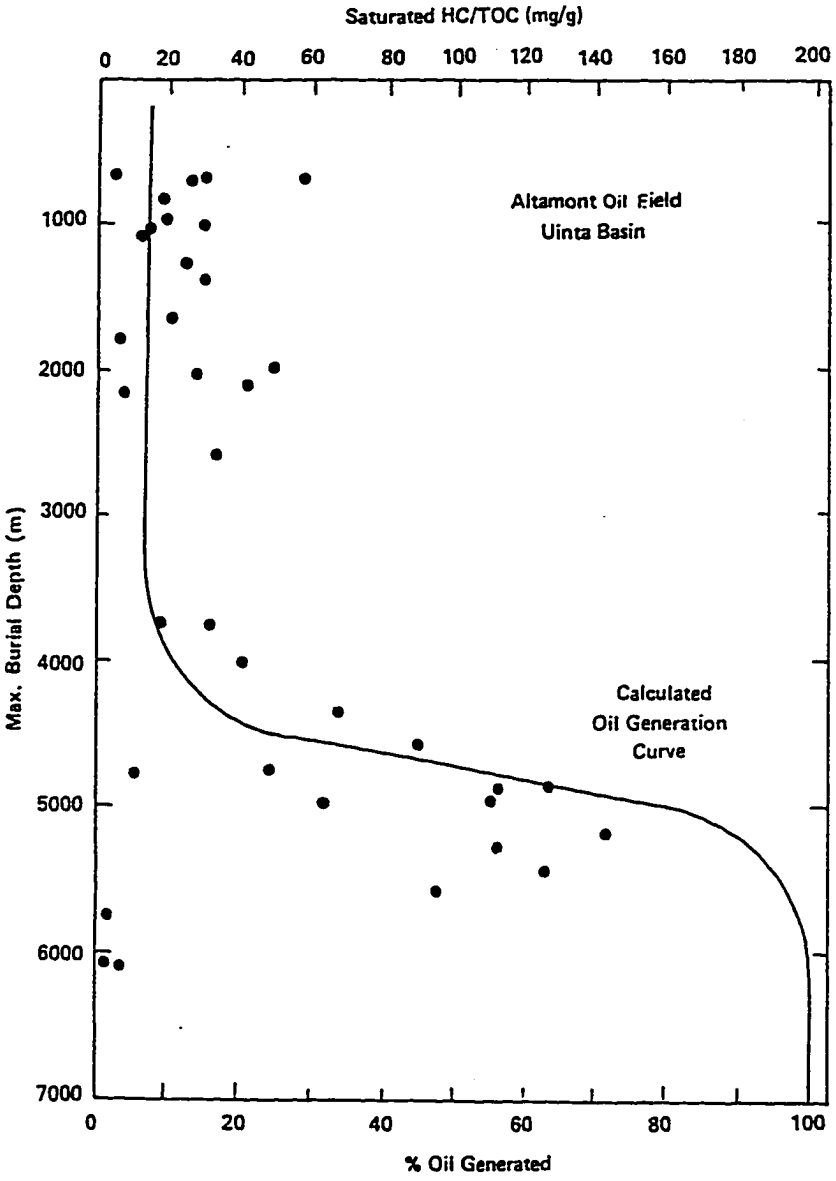

Figure 15. A comparison of the predicted transformation ratio (% oil generated) with the actual generation of saturated hydrocarbons in the Altamont field.

Sweeney, J. J.; Burnham, A. K.; Braun, R. L. *Am. Assoc. Petro. Geol. Bull.*, **1987**, 71, 967-985.

Chapter VI

Experimental Procedures

IV.1. Sample Origins

Green River and Rundle oil shales were kindly supplied by Dr. Michael Siskin of Exxon Research and Engineering Company. Their compositions have been published.[40,51] The maturation series of oil shale samples from the Uinta Basin of Utah were kindly supplied by Dr. Alan Burnham of Lawrence Livermore National Laboratory. Table 2 displays the elemental analyses of the Uinta Basin oil shales.

Green River oil shale was received as 20-100 mesh ground particles. Rundle and Uinta Basin oil shales were received as <20 mesh ground particles. All oil shales were stored under a dry N_2 atmosphere.

Athabasca bitumen, the +525 °C boiling point fraction of Athabasca bitumen, and the +525 °C boiling point fraction from the hydrocracked bitumen prepared using a unimodal catalyst were kindly supplied by Dr. Marten Ternan of the Canada Center for Mineral and Energy Technology. Table 3 shows the % mass and number average molecular weight in each fraction of these samples obtained by preparative scale gel permeation chromatography.[77,93] All solvents used in this research were high-purity grades purchased from Aldrich or Fisher and were used without further purification.

Table 2. Elemental analyses of Uinta Basin maturation series of oil shales

Sample	Depth(m)	%Maturation	%C	%H	%N	%S	$\%CO_2$	%Org C
Government 33-4[a,b]	1630	<5	9.2	1.3	0.5	0.7	9.9	6.5
Brotherson 1-23B4-A[a,b]	2560	20	9.1	0.7	0.2	0.2	20.4	3.5
Brotherson 1-23B4-B[a,b]	2780	35	8.0	0.4	0.2	0.1	24.0	1.5
Brotherson 1-3B4[b]	3260	80	5.5	0.6	0.4	1.5	10.6	2.6
Christensen 1-33A5[b]	3610	100	5.3	0.5	0.1	1.0	13.0	1.8

[a]Burnham, A. K. *Energy Fuels*, **1991**, 5, 205-214.

[a]Reynolds, J. G.; Grawford, R. W.; Burnham, A. K. *Energy Fuels*, **1991**, 5, 507-523.

[b]Burnham, A. K. *Personal Communication*.

Table 3. % Mass and M_n of each fraction of Athabasca bitumen[a], its +525 °C b.p. fraction[b,c], and the +525 °C b.p. fraction from the hydrocracked bitumen[b,c]

	Athabasca Bitumen		+525 °C b.p. Fraction		Hydrocracked +525 °C b.p.	
Fraction No.	% Mass	M_n	% Mass	M_n	% Mass	M_n
1	4.51	6690	22.6	1642	21.4	4986
2	5.46	5470	15.7	1473	18.7	1931
3	6.86	1680	16.5	1185	18.7	1378
4	12.20	1420	19.4	912	29.0	872
5	19.40	713	25.8	688	12.2	623
6	23.14	504				
7	16.80	371				
8	7.82	368				
9	2.99	284				
10	0.48	271				
11-16	0.34	250				

[a]Champagne, P. J.; Emmanuel, M.; Ternan, M. *Fuel*, 1985, *64*, 423-425. [b]Ternan, M.; Rahimi, P. M.; Clugston, D. M. *Energy Fuels*, 1994, *8*, *518-530*. [c]Ternan, M. *personal communication*.

IV.2. HCl/HF Demineralization[35,47]

Approximately 10 g of oil shale was placed in a Nalgene Erlenmeyer flask. 5 N HCl (150 mL) was added to the flask. The oil shale/HCl mixture was heated to 55-65 °C and magnetically stirred under an N_2 atmosphere for 24 hours. The mixture was filtered through a porcelain funnel using a Teflon filter membrane and was washed with 2 liters of warm distilled water. After the oil shale was transferred back to the Nalgene flask, 150 mL of 1:1 HF reagent (49% aqueous solution) was added to the flask. The oil shale/HF mixture was heated to 55-65 °C and magnetically stirred under an N_2 atmosphere for another 24 hours. After the heat was removed, the mixture was diluted to 600 mL with warm distilled water and filtered through a porcelain funnel using a Teflon filter membrane. A large quantity of distilled water was used to wash the sample until the wash water was neutral to blue litmus paper. The product was transferred to a tared beaker and dried to constant weight in a vacuum oven at 105 °C and < 1 mm of Hg pressure.

Uinta Basin oil shales have low organic carbon contents. The above procedure was scaled up and the HCl/HF treatment time was extended as necessary (see VII.1., Results and Discussion chapter).

IV.3. Soxhlet Extraction

Approximately 5 g of the HCl/HF demineralized oil shale

was transferred to a dried and weighed Whatman cellulose extraction thimble. The thimble with sample was placed in a Soxhlet extraction apparatus. The sample was extracted with ~200 mL of toluene under a dry N_2 atmosphere until the toluene in the Soxhlet remained clear for at least 24 hours. Toluene was removed using rotary evaporation followed by vacuum drying to constant weight at 105 °C and < 1 mm of Hg pressure.

IV.4. Aqueous Ammonium Sulfate Demineralization[51]

Approximately 10 g of Green River oil shale was used for aqueous $(NH_4)_2SO_4$ demineralization. The literature procedure was used without modification.[51]

IV.5. Volumetric Solvent Swelling[71,94,95]

Approximately 50-100 mg of demineralized kerogen was used for each volumetric solvent swelling experiment. The procedure described by Larsen and Shawver was used as modified by Suuberg.[94,95]

IV.6. ^{252}Cf Plasma Desorption Mass Spectrometry[96]

^{252}Cf plasma desorption time-of-flight mass spectrometry was used to determine molecular weight distributions. The instrument is a Bio Ion 20 instrument equipped with a 13 μCi ^{252}Cf source and 15-cm fight tube. Aluminized Mylar disks purchased from Applied Biosystems Inc. were used as the sample supports. Bitumen solutions were prepared in concentrations of

ca. 10 mg/mL. Sample disks were coated by dropping 20-40 μL of bitumen solutions onto aluminized Mylar disks followed by drying in a gentle stream of dry N_2. Positive 10 kV acceleration voltage and 1 ns/channel time resolution were used. 10^6 primary ion events were collected for each sample spectrum and 10^7 primary ion events were collected for the background spectrum. H^+ and Na^+ were used as the calibration standards.

IV.7. Vapor Pressure Osmometry[97]

A Knauer Dampfdruck - Osmometer was used to determine the number average molecular weight of Green River bitumen and the toluene-soluble fraction of Rundle bitumen. The principles and procedure of VPO are given in reference 97.

IV.8. Fourier Transform Infrared Spectrometer[98]

A Mattson Sirius 100 Fourier transform infrared spectrometer was used to record the IR absorbance spectra. Each sample was prepared by mixing the dried oil shale, or kerogen, and KBr to approximately 10 mg of sample/1 g of KBr in an N_2 filled dry box. The mixture was then ground in a Wig-L-Bug for 3 minutes. A portion of the ground mixture (100 mg) was transferred to a bolt KBr pellet press. The pellet was prepared by hand tightening the nuts. Each spectrum was recorded for 128 scans at 4 cm^{-1} resolution against a pure KBr pellet background.

IV.9. Nuclear Magnetic Resonance Spectroscopy[99]

A General Electric model GN-300 FT-NMR spectrometer equipped with a Doty Scientific 5 mm Magic Angle Sample Spinning probe was used for solid state ^{13}C NMR measurements. The reduced pulse angle protocol for Bloch decay experiments was used as previously described.[99] Natural abundance ^{13}C NMR spectra were recorded at 75.47 MHz, with magic angle sample spinning at 9 KHz and proton decoupling at 300 MHz. The instrument was operated using the following conditions: the spectrometer sweep width of 25,000 Hz, a 10° pulse angle of 400 μs, an acquisition time of 20 ms, and 1 s time delay between acquisitions. The spectra of the raw and demineralized Brotherson 1-23B4-A oil shale accumulated 416,000 and 80,000 scans, respectively. The spectra were processed using zero-fill, baseline correction, a line broadening factor equivalent to 100 Hz, Fourier transformation, and manual phasing.

Chapter VII

Results and Discussion

The aim of this research was to investigate the changes in the macromolecular structure of a Type I kerogen which occur during the maturation process. The key experiments were performed on a kerogen maturation series from the Uinta Basin. The changes in the macromolecular structure of the kerogen were characterized by following changes in three quantities: (1) the number average molecular weight between cross-links of the kerogen; (2) the amount of bitumen; and (3) the bitumen molecular weight distribution. These experimental results were used to model the maturation of Type I kerogen.

This research began with technique development and methods testing. Kerogens and bitumens isolated from the readily available and widely studied Green River and Rundle oil shales were used for method development. The oil shales were demineralized using the classical HCl/HF method, and the isolated kerogen concentrates were Soxhlet-extracted to remove the bitumens (see VII.1). Volumetric solvent swelling methodology and ^{252}Cf plasma desorption mass spectrometry (PDMS) were adapted to kerogens and bitumens and were used to measure the number average molecular weight between cross-links of the kerogen and the bitumen molecular weight distributions, respectively. (see VII.2).

In the second phase of this research, the developed

techniques were applied to a maturation series of Uinta basin oil shales. The number average molecular weight between cross-links of the kerogens, the amounts of bitumen, and bitumen molecular weight distributions were measured (see VII.3a). The results were used to characterize the kerogen macromolecular evolution occurring during the petroleum formation process (see VII.3b).

1. Kerogen and bitumen isolation

a. Oil shale demineralization and bitumen isolation

Green River oil shale was demineralized using both $(NH_4)_2SO_4$ and HCl/HF procedures.[35,47,51] The HCl/HF demineralization was carried out for three time periods: 2, 8, and 48 hours. Following the 8-hour and 48-hour demineralizations, the kerogen concentrates isolated were Soxhlet-extracted with toluene to remove the bitumen.

Rundle oil shale was demineralized using HCl/HF.[35,47] The kerogen concentrate was Soxhlet-extracted with toluene to remove the bitumen. At room temperature, the toluene extract from the kerogen concentrate separated into two fractions: toluene-solubles and a toluene-insoluble solid. The solid was isolated by filtration using Whatman #50 filter paper followed by vacuum oven drying at 105 °C. The toluene-soluble fraction was isolated by removing toluene using a rotary evaporator followed by vacuum oven drying at 105 °C.

Uinta Basin oil shale samples were demineralized using

HCl/HF.[35,47] An elemental analyses was performed after each demineralization. The demineralization was repeated and the acid treatment time was lengthened as necessary in order to isolate the kerogen concentrates with low mineral matter contents. Table 4 shows the % ash remaining in Uinta Basin kerogen concentrates after different time periods of acid treatments. Following HCl/HF demineralization, each kerogen concentrate isolated was Soxhlet-extracted with toluene to remove the bitumen.

Table 5 displays the demineralization procedures used for the studied samples, elemental analyses of kerogen concentrates, amounts of kerogen concentrate isolated, and amounts of bitumen extracted.

b. *Failed control experiments*

Uinta Basin oil shale samples have low organic carbon contents (1.5 to 6.5 wt %). The HCl/HF demineralization times used for these samples were long. Data in the literature support the conclusion that HCl/HF digestion does not alter kerogen structure.[35,49] To examine this for our samples, two control experiments were performed in an attempt to reveal the impact of the demineralization on the kerogen functional group distribution. Unfortunately, both experiments gave inconclusive results.

FTIR spectra of Brotherson 1-3B4 oil shale (80% maturation) were obtained before and after HCl/HF

Table 4. % Ash remaining in Uinta Basin kerogen concentrates after HCl/HF demineralizations[@]

HCl/HF Demineralization	%Ash Government 33-4	%Ash Brotherson 1-23B4A	% Ash Brotherson 1-23B4B	% Ash Brotherson 1-3B4	% Ash Christansen 1-33A5
2 days	40.2				
6 days	24.7				
12 days	13.3	33.1			
24 days		5.3			
28 days			57.8	41.3	-[#]
56 days			3.3	29.9	31.3

[@]Galbraith Laboratories.

[#]Not available.

Table 5. Elemental analyses of kerogen concentrates[@], the amounts of kerogen concentrate isolated, and the amounts of bitumen extracted

Sample	Method	%C	%H	%Ash	%Bitumen[#]	%Kerogen concentrate[•]
Green River[$]	$(NH_4)_2SO_4$	40.3	5.2	41.9		27.9
Green River[$]	HCl/HF 2 hr	40.7	5.8	38.2		28.2
Green River[$]	HCl/HF 8 hr	59.1	7.7	17.0	7.8	26.1
Green River[$]	HCl/HF 48 hr	73.3	9.4	5.2	7.5	26.5
Rundle	HCl/HF 48 hr	55.1	8.0	20.1	5.8	22.7
Government 33-4	HCl/HF 12 d	61.4	7.4	13.3	13.4	9.8
Brotherson 1-23B4-A	HCl/HF 24 d	77.2	9.6	5.3	13.2	5.2
Brotherson 1-23B4-B	HCl/HF 56 d	75.1	6.7	3.3	13.5	1.7
Brotherson 1-3B4	HCl/HF 56 d	44.2	4.1	29.9	7.8	7.7
Christansen 1-33A5	HCl/HF 56 d	41.5	3.6	31.3	10.6	3.4

[@]Galbraith Laboratories. [#]On a dry mineral matter free basis. [•]By weight of starting shale.

[$]Larsen, J. W.; Li, S. *Energy Fuels*, **1994**, 8, 932-936.

demineralization (see Figure 16).[98] Disappearance of carbonate (~1450 cm^{-1}) and silicate (~1100 cm^{-1}) peaks in the demineralized sample spectrum demonstrates that these minerals were effectively removed, but the intense carbonate and silicate peaks existing in the raw shale spectrum block the region from 1000 to 1600 cm^{-1}, which, coupled with the weak organic spectrum in the original shale, makes it impossible to determine whether the HCl/HF demineralization changed the kerogen functional group distribution.

The solid state ^{13}C NMR technique of Bloch decay with magic angle sample spinning and proton decoupling was used to measure the carbon distributions in the raw and demineralized Brotherson 1-23B4-A oil shale (20% maturation).[99] Figures 17 and 18 display the NMR spectra before and after the acid demineralization. The peak at ~180 ppm in the raw shale spectrum is due to carbonate minerals.

Aromatic and aliphatic carbon fractions determined by integrating the apparent aromatic and aliphatic peaks in these spectra lead to a contradiction. The demineralized sample has 35% aromatic carbon and 65% aliphatic carbon; the raw shale has 66% aromatic carbon and 34% aliphatic carbon. The aromaticity of the raw shale is abnormally and unbelievably high. Because this sample contains only 3.5 wt % organic matter, the large amount of mineral matter present may affect the carbon distribution measurement.[100] A ^{13}C CP/MAS spectrum of a low rank inertinite-rich coal showing anomalously high

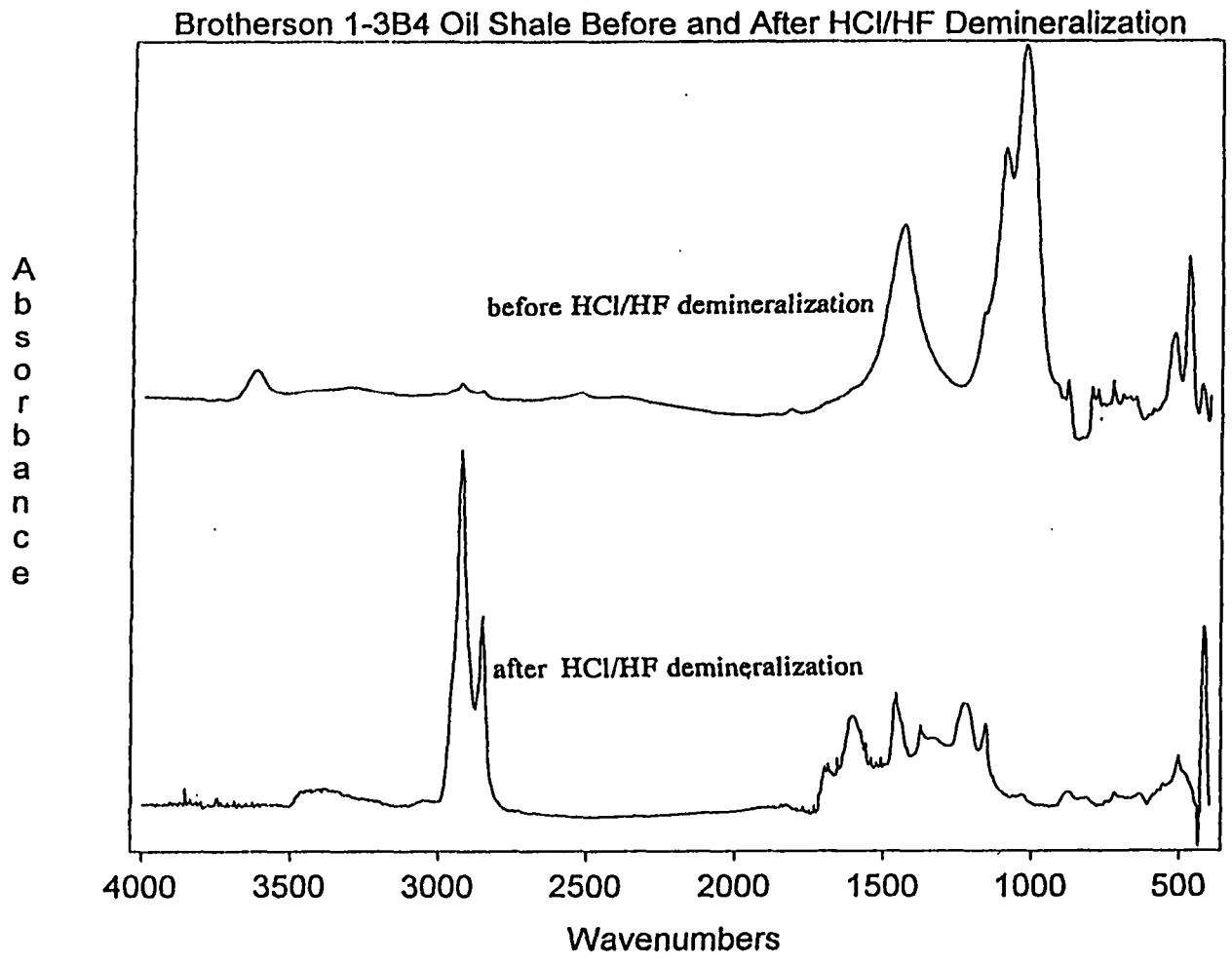

Figure 16. FTIR spectra of Brotherson 1-3B4 oil shale before and after HCl/HF demineralization.

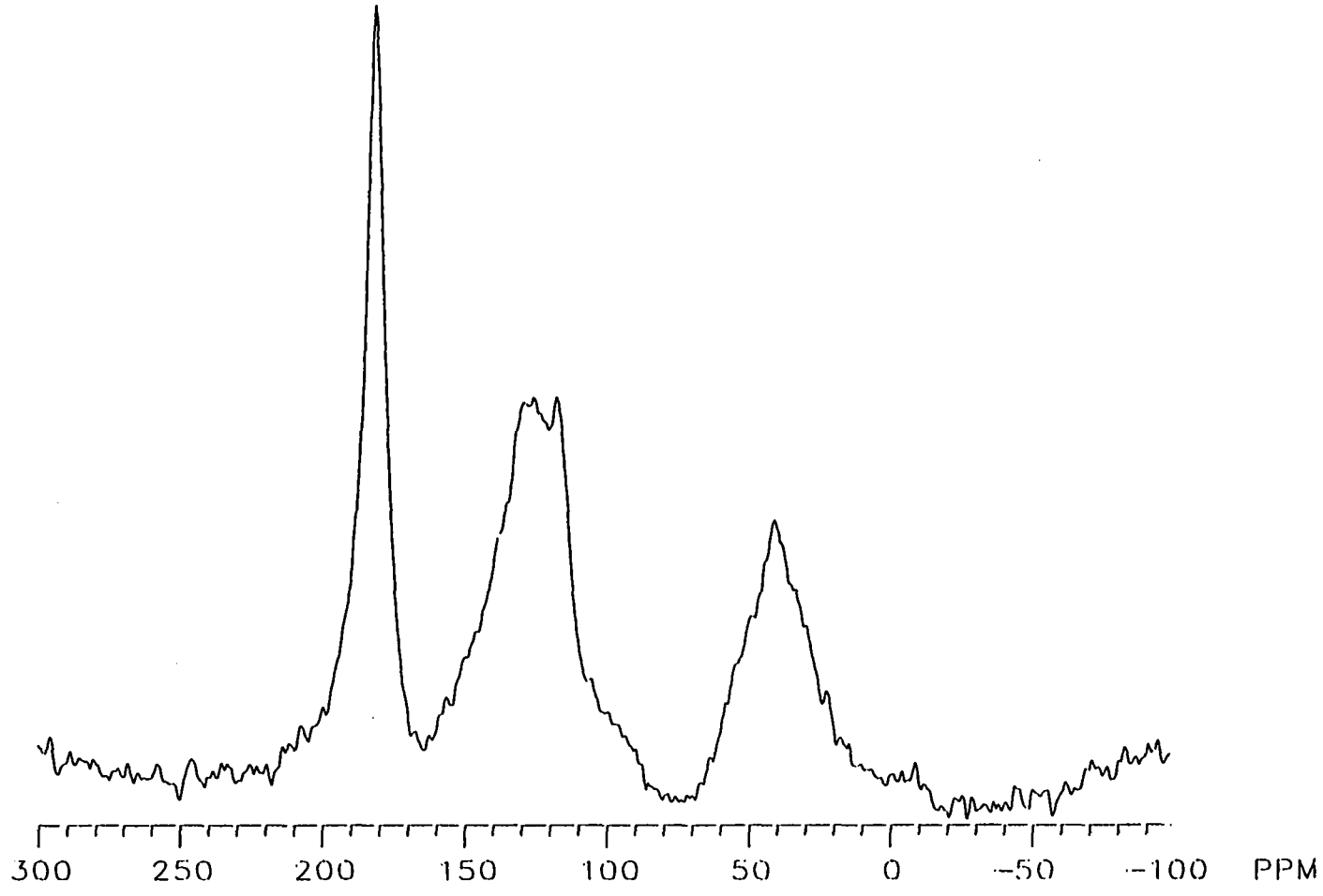

Figure 17. Solid state ^{13}C NMR spectrum of Brotherson 1-23B4-A oil shale.

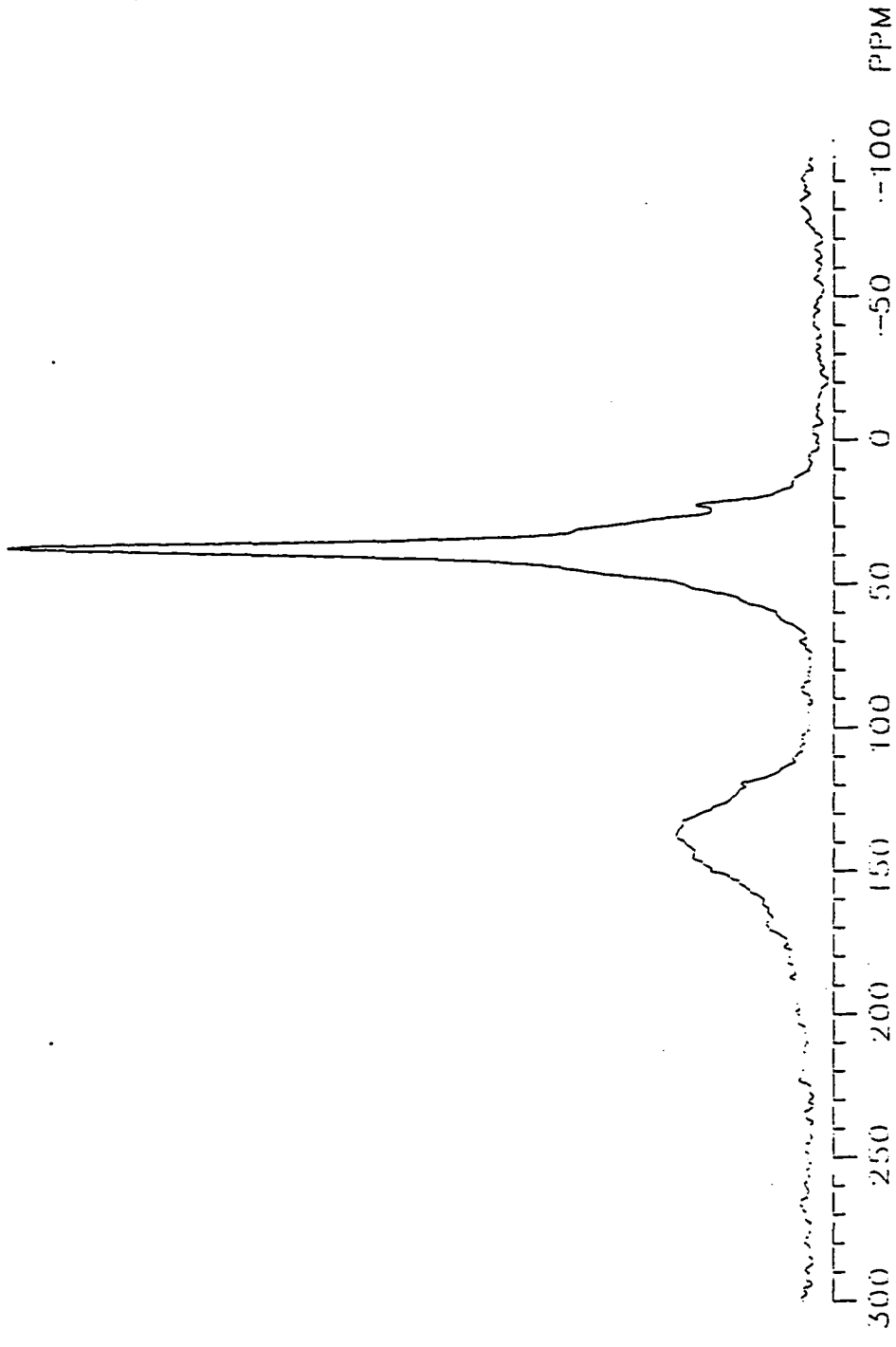

Figure 18. Solid state ^{13}C NMR spectrum of HCl/HF demineralized Brotherson 1-23B4-A oil shale.

aromaticity has been reported and the high aromaticity was assigned to the influence of iron-bearing minerals.[101] There is abundant evidence in the literature that HCl/HF demineralization under 70 °C does not significantly alter the kerogen chemical structure.[35,49] We have no reason to believe that our samples are unique. We proceeded assuming that the isolation procedures do not change kerogen or bitumen chemical structure.

2. Technique Development

a. Solvent Swelling

A method which could measure the kerogen cross-link density was needed. The solvent swelling technique was chosen over others because it is experimentally easy and has been successfully applied to the study of the macromolecular structure of coals.[4,94] Solvent swelling theories existing in the literature could be used to treat experimental data and to calculate the kerogen cross-link density.[11,61,62]

We started with solvent swelling studies of Green River kerogen.[37] This Type I kerogen was selected for five reasons: (1) it had been well characterized and a detailed chemical structure was available;[40] (2) Green River oil shale is a carbonate rock from which kerogen can be isolated using mild conditions;[51] (3) it is a Type I kerogen which is similar to the maturation series to be studied; (4) its high organic content easily provides ample amount of sample; and (5) it is

readily available.

Volumetric solvent swelling measurements were performed on Green River kerogen samples isolated using both $(NH_4)_2SO_4$ and HCl/HF procedures.[71,94] The kerogen was placed in a 6-mm o.d. glass tube which was sealed on one end. The tube was centrifuged for 5 minutes and then was repeatedly tapped on a hard surface until the height of the kerogen reached a minimum, H_1. The packed kerogen was then disturbed and immersed in a large excess of the swelling solvent. The tube was centrifuged again and the height was measured after 24 hours. This process was repeated for several days until the height of the kerogen reached a constant value, H_2. The volumetric swelling ratio (Q_v) was calculated using

$$Q_v = \frac{H_2}{H_1} \qquad (8)$$

a.1 Measurement reproducibility[37]

The reproducibility of volumetric solvent swelling measurements using $(NH_4)_2SO_4$ demineralized Green River kerogen and chlorobenzene was studied. Table 6 contains the volumetric swelling ratios measured at three different times. Each listed Q_v is calculated using four measurements and the standard deviation of Q_v is usually about 2-3% of the reported value. The data shown here are typical and demonstrate the

Table 6. Reproducibility of the volumetric swelling ratio (Q_v) using ammonium sulfate demineralized Green River kerogen and chlorobenzene

	11/20/92	1/31/93	3/26/93
Run 1 Q_v	1.57	1.62	1.61
Run 2 Q_v	1.56	1.62	1.64
Run 3 Q_v	1.60	1.61	1.57
Run 4 Q_v	1.53	1.67	1.62
Average Q_v	1.57 $\pm$0.03	1.63 $\pm$0.03	1.61 $\pm$0.03

Larsen, J. W.; Li, S. *Energy Fuels*, **1994**, 8, 932-936.

reproducibility of the technique.

a.2 Effect of mineral matter content on swelling measurements[37]

We next studied the effect of mineral matter content on solvent swelling measurements. Green River kerogen samples containing four different quantities of mineral matter were isolated using two different methods. $(NH_4)_2SO_4$ demineralization gave a sample with 42 wt % mineral matter. HCl/HF demineralization of a fresh sample for 2, 8, and 48 hours gave samples with 38 wt %, 17 wt %, and 5.2 wt % mineral matter, respectively. Kerogen samples isolated by all four methods were swollen in 28 organic solvents (see Table 7). The data in Table 7 demonstrate that samples containing 38 wt % and 42 wt % of mineral matter have swelling ratios similar to the one containing 5.2 wt % mineral matter. The swelling ratios of the demineralized kerogen samples do not depend on the amount of mineral matter remaining. It seems that demineralization procedures are effective for disrupting kerogen-mineral interactions and mineral matter remaining in the kerogen is not cross-linking the organic matter.

a.3 Solubility parameter (δ) of Green River kerogen[37]

Figures 19-22 show the volumetric swelling ratios of four demineralized Green River kerogen samples as a function of swelling solvent solubility parameter. These plots show that polar solvents and hydrogen bonding solvents (e.g. THF and

Table 7. Volumetric swelling ratios of differently demineralized Green River kerogens in organic solvents

No.	Solvent	δ (cal/cm^3)$^{1/2}$@	Q_v $(NH_4)_2SO_4$ 42% Ash	Q_v HCl/HF 2h 38% Ash	Q_v HCl/HF 8h 17% Ash	Q_v HCl/HF 48h 5.2% Ash
1	n-pentane	7.0	1.23	1.08	1.18	1.14
2	n-heptane	7.4	1.25	1.11	1.14	1.18
3	methylcyclohexane	7.8	1.34	1.22	1.32	1.31
4	cyclohexane	8.2	1.36	1.28	1.33	1.31
5	o-xylene	8.8	1.52	1.43	1.35	1.40
6	toluene	8.9	1.47	1.41	1.34	1.38
7	benzene	9.2	1.49	1.43	1.37	1.40
8	tetralin	9.5	1.51	1.51	1.46	1.51
9	chlorobenzene	9.5	1.57	1.51	1.49	1.45
10	1-methylnaphthalene	9.9	1.49	1.55	1.45	1.58
11	carbon disulfide	10.0	1.62	1.43	1.42	1.49
12	o-dichlorobenzene	10.0	1.67	1.52	1.63	1.59
13	nitrobenzene	10.0	1.54	1.41	1.52	1.50
14	biphenyl	10.6	1.66	1.54	1.53	1.46
15	propionitrile	10.8	1.19	1.05	1.24	1.16
16	nitroethane	11.1	1.32	1.10	1.23	1.14
17	acetonitrile	11.9	1.18	1.02	1.18	1.07
18	chloroacetonitrile	12.6	1.31	1.12	1.24	1.31
19	nitromethane	12.7	1.24	1.07	1.13	1.12
20	pyridine	10.7	1.64	1.70	1.54	1.54
21	tetrahydrofuran	9.1	1.64	1.61	1.61	1.61
22	carbon tetrachloride	8.6	1.72	1.64	1.33	1.63
23	1,1,2-trichloroethane	9.6	1.67	1.76	1.43	1.46
24	1,2-dibromoethane	10.4	1.70	1.54	1.37	1.44
25	2-propanol	11.5	1.22	1.28	1.22	1.27
26	ethanol	12.7	1.15	1.22	1.18	1.21
27	acetone	9.9	1.17	1.23	1.21	1.25
28	dimethyl sulfoxide	12.0	1.21	1.33	1.27	1.35

@Brandrup, J. and Immergut, E. H., *Polymer Handbook, 3rd ed.*, John Wiley & Sons, 1989.

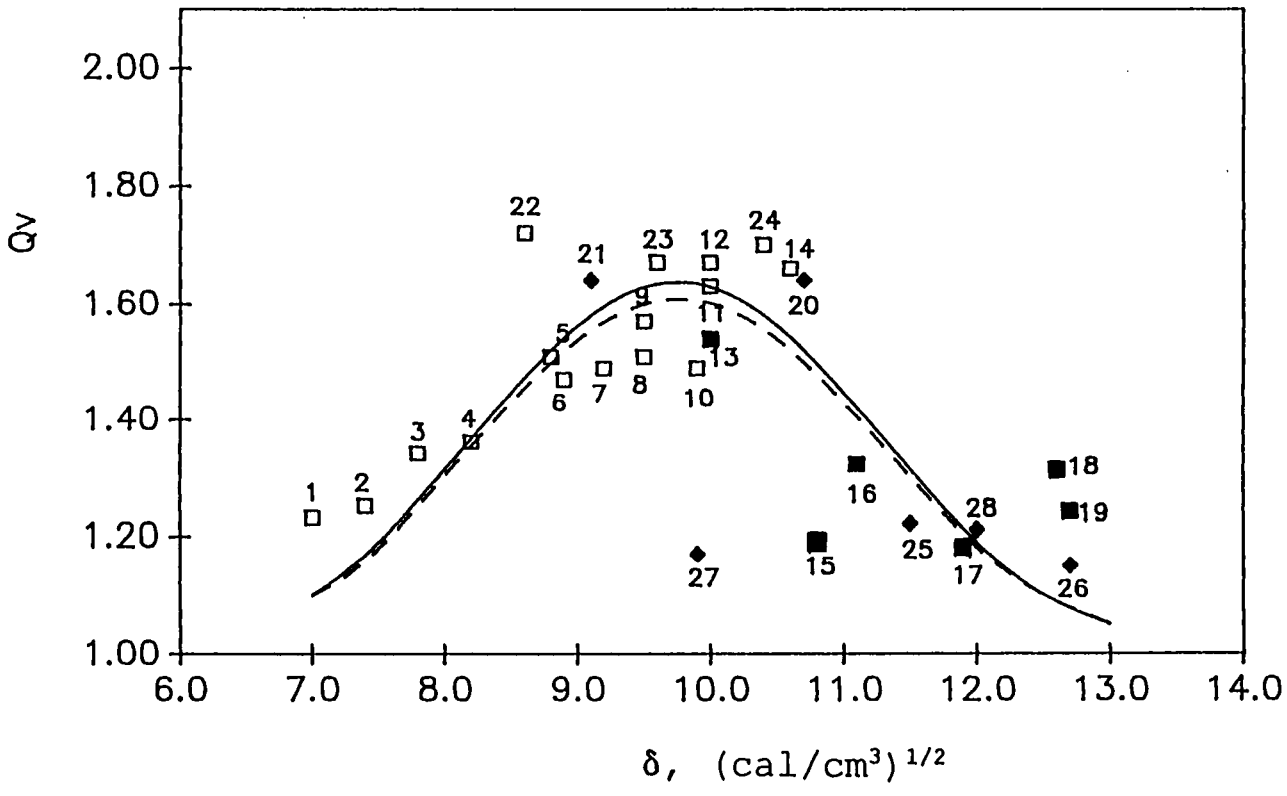

Figure 19. Swelling ratio of $(NH_4)_2SO_4$ demineralized Green River kerogen as a function of swelling solvent solubility parameter. (□) nonpolar solvents, (■) polar solvents, (♦) H-bonding solvents. The solid line is the theoretical prediction by Kovac's model assuming N = 1 and $\bar{M}_c$ = 1200. The dashed line is the theoretical prediction by Flory's model assuming $\bar{M}_c$ = 280. See Table 7 for solvent identification.

Larsen, J. W.; Li, S. *Energy Fuels*, **1994**, 8, 932-936.

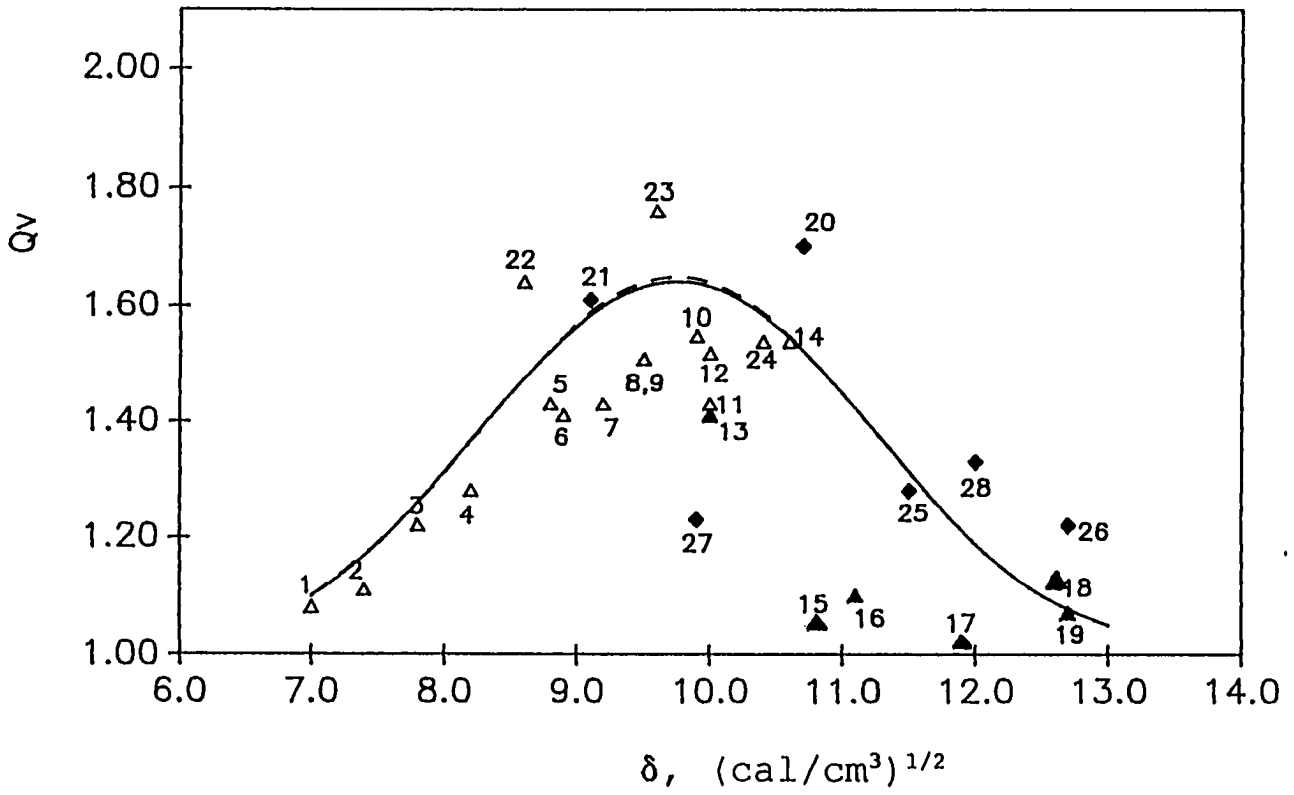

Figure 20. Swelling ratio of HCl/HF demineralized (2 hr) Green River kerogen as a function of swelling solvent solubility parameter. (△) nonpolar solvents, (▲) polar solvents, (◆) H-bonding solvents. The solid line is the theoretical prediction by Kovac's model assuming N = 1 and $\bar{M}_c$ = 1100. The dashed line is the theoretical prediction by Flory's model assuming $\bar{M}_c$ = 270. See Table 7 for solvent identification.

Larsen, J. W.; Li, S. *Energy Fuels*, **1994**, 8, 932-936.

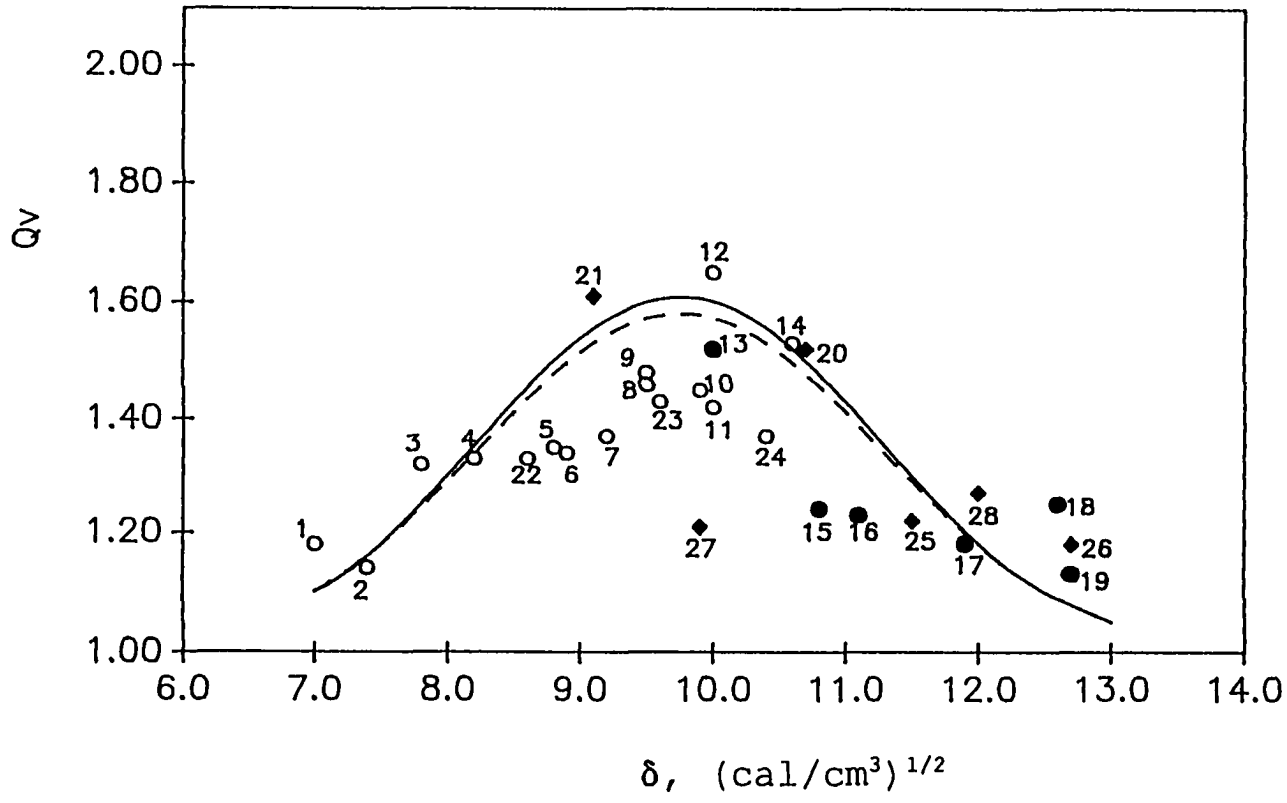

Figure 21. Swelling ratio of HCl/HF demineralized (8 hr) Green River kerogen as a function of swelling solvent solubility parameter. (O) nonpolar solvents, (●) polar solvents, (♦) H-bonding solvents. The solid line is the theoretical prediction by Kovac's model assuming $N = 1$ and $\bar{M}_c = 730$. The dashed line is the theoretical prediction by Flory's model assuming $\bar{M}_c = 190$. See Table 7 for solvent identification.

Larsen, J. W.; Li, S. *Energy Fuels*, **1994**, 8, 932-936.

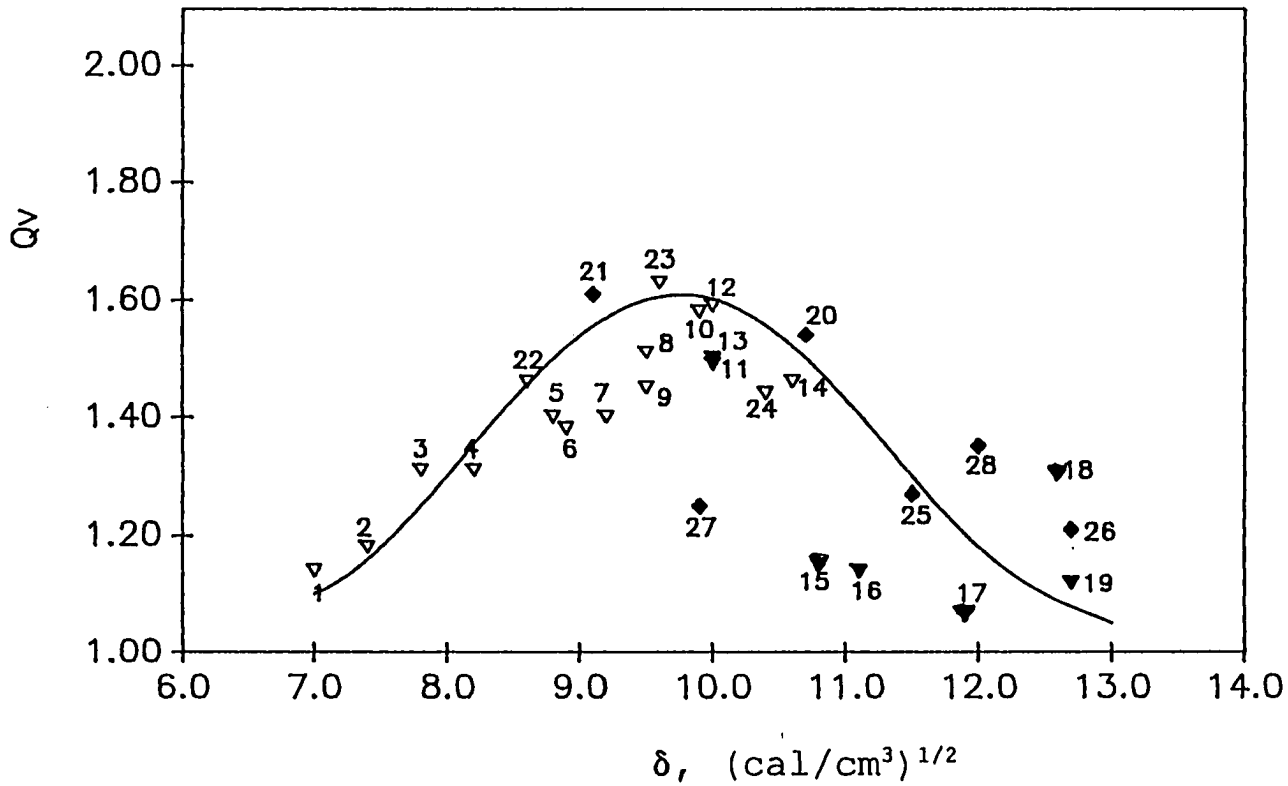

Figure 22. Swelling ratio of HCl/HF demineralized (48 hr) Green River kerogen as a function of swelling solvent solubility parameter. (▽) nonpolar solvents, (▼) polar solvents, (◆) H-bonding solvents. The solid line is the theoretical prediction by Kovac's model assuming N = 1 and $\bar{M}_c$ = 810. The dashed line is the theoretical prediction by Flory's model assuming $\bar{M}_c$ = 220. The curves are identical. See Table 7 for solvent identification.

Larsen, J. W.; Li, S. *Energy Fuels*, **1994**, 8, 932-936.

pyridine) behave similarly to nopolar solvents with similar solubility parameters. These results demonstrate that regular solution theory roughly applies to these systems. Regular solution theory assumes that the mixing between the polymer network and a solvent is random, without any specific interactions such as hydrogen bonding, and predicts the maximum swelling ratio will occur when the network and a swelling solvent have the same solubility parameter.[102,103] Figures 19-22 also display bell-shaped curves predicted by regular solution theory and allow the kerogen to be assigned a solubility parameter of 9.7 $(cal/cm^3)^{1/2}$. The solubility parameter of Green River kerogen was calculated to be 9.4 $(cal/cm^3)^{1/2}$ using Siskin's structure and van Krevelen's atom and group contributions.[3,40] The lines in the figures were calculated using the Flory-Rehner and Kovac treatments and will be discussed in section a.5.

a.4 Swelling Reversibility[37]

Mined coals are in a strained state and their glassy nature prevents the structures from attaining equilibrium.[104] This phenomenon leads to an initial irreversible swelling after which repetitive swellings are reversible.[104,105,106] Because of this behavior of coals, the swelling reversibility of Green River kerogen was examined.

The data in Table 8 demonstrate irreversible swelling of $(NH_4)_2SO_4$ demineralized kerogen and reversible swelling of

Table 8. Repetitive swelling of HCl/HF (8 hours) and $(NH_4)_2SO_4$ demineralized Green River kerogen in chlorobenzene at room temperature@.

	Q_v	
	$(NH_4)_2SO_4$	HCl/HF 8 hr
1st swelling	1.57	1.49
2nd swelling	1.50	1.50
3rd swelling	1.44	
4th swelling	1.27	
5th swelling	1.27	

@Kerogen was swollen in chlorobenzene at room temperature and chlorobenzene was removed using rotary evaporation followed by vacuum drying after each swelling.

HCl/HF (8 hr) demineralized kerogen in chlorobenzene. $(NH_4)_2SO_4$ demineralized kerogen was swollen in chlorobenzene and the solvent was removed after the swelling measurement. Kerogen swelling and solvent removal were repeated 5 times and reversible swelling was observed only after 3 repetitions. In contrast, chlorobenzene swells HCl/HF (8 hr) demineralized kerogen reversibly.

To confirm these repetitive swelling results, we swelled both kerogen samples in chlorobenzene at 60-70 °C under a dry N_2 atmosphere overnight and removed the chlorobenzene after swelling. Elemental analysis revealed that the chlorine content was 0.14 wt % before the chlorobenzene treatment and 0.17 wt % after for $(NH_4)_2SO_4$ demineralized kerogen. This analysis proved that within experimental error, no chlorobenzene remained in the kerogen. The data in Table 9 show that exposure to chlorobenzene reduced the swelling ratios of $(NH_4)_2SO_4$ demineralized kerogen in 3 organic solvents. The data in Table 10 show that HCl/HF demineralized kerogen was swollen reversibly and the bitumen remaining in the kerogen does not influence the swelling measurements.

The above results demonstrate that demineralization methods affect the chemical/physical structure of isolated Green River kerogen. We have made no investigations into the structures of these samples, so it is premature to speculate the origin of the irreversibility. Since HCl/HF and $(NH_4)_2SO_4$ demineralized Green River kerogen samples have the same

Table 9. Swelling of $(NH_4)_2SO_4$ demineralized Green River kerogen in three solvents before and after chlorobenzene treatment@

Solvent	Q_v Before chlorobenzene treatment#	After chlorobenzene treatment*
benzene	1.50	1.31
chlorobenzene	1.63	1.43
carbon disulfide	1.60	1.42

@Kerogen was swollen in chlorobenzene at 60-70 °C under a dry N_2 atmosphere overnight, and the chlorobenzene was removed under vacuum.

#The Cl content of this sample was 0.14%. Elemental analysis was performed by Galbraith Laboratories.

*The Cl content of this sample was 0.17%. Elemental analysis was performed by Galbraith Laboratories.

Larsen, J. W.; Li, S. *Energy Fuels*, **1994**, 8, 932-936.

Table 10. Reversible swelling of HCl/HF (8 hours) demineralized Green River kerogen in chlorobenzene before and after chlorobenzene treatment[@]

sample	Q_v Before chlorobenzene treatment	After chlorobenzene treatment
HCl/HF 8 hr w/o toluene extraction	1.45	1.53
HCl/HF 8 hr w/ toluene extraction	1.49	1.54

[@]Kerogen was swollen in chlorobenzene at 60-70 °C under a dry N_2 atmosphere overnight, and the chlorobenzene was removed under vacuum.

Larsen, J. W.; Li, S. *Energy Fuels*, **1994**, 8, 932-936.

solubility parameter (see Figures 19-22), the two isolation procedures cannot have caused kerogen a significant difference in the functional group distributions.

For our purpose, the crucial result is that solvent swelling of HCl/HF demineralized Green River kerogen is reversible. Solvent swelling theories are derived under the assumption of thermodynamic equilibrium. Swelling reversibility of the kerogen allows us to estimate $\bar{M}_c$ using thermodynamic treatments (see a.5).

a.5 Estimation of the number average molecular weight between cross-links ($\bar{M}_c$) of Green River kerogen[37]

The Flory-Rehner and Kovac equations were used to calculate the ideal solvent swelling curves. The lines shown in Figures 19-22 are the theoretical predictions of the Flory-Rehner and Kovac models assuming (1) solubility parameter of Green River kerogen is 9.75 $(cal/cm^3)^{1/2}$, (2) the molar volume of swelling solvent is 95 cm^3/mol, and (3) the number average molecular weight between cross-links of the kerogen is the value given in each figure legend. These calculations fit experimental results reasonably well. This agreement induces us to calculate the number average molecular weight between cross-links of Green River kerogen.

Since regular solution theory is followed, the Flory χ parameters for Green River kerogen-solvents pairs can be calculated using Equation 7. As stated earlier (see section

IV.3), calculation of the Flory χ parameters for kerogen-solvents pairs requires the knowledge of kerogen solubility parameter and the entropy contribution, χ_s. The former is directly available from swelling measurements. The later depends on both the size and shape of the swelling solvent for a given polymer-solvent pair.[66,67] Different χ_s values for polymer-solvents pairs have been assigned in the literature.[66,67,68] We have no basis for estimating χ_s values for Green River kerogen-solvent pairs. Determining these values is beyond the scope of this thesis. We arbitrarily assigned χ_s = 0.3, a value which is usually accepted in solvent swelling of coals,[4,63] in χ calculations.

Because mineral matter remaining in the kerogen occupies a volume and does not swell, it is necessary to convert the volumetric swelling ratios (Q_v) measured by experiment to the values on a dry mineral matter free basis ($Q_{v,dmmf}$) before calculating $\bar{M}_c$.

$$Q_{v,\,dmmf} = \frac{Q_v - f_m/\rho_m}{1 - f_m/\rho_m} \qquad (9)$$

Here, ρ_m is the density of the mineral matter. A commonly accepted value of 2.7 g/cm^3 is used in this work.[3,63] f_m is the weight fraction of mineral matter remaining in the kerogen. This value can be calculated using Equation 10.

Table 11. χ parameters for Green River kerogen-solvent pairs

Solvent	V_S cm^3/mol[@]	δ $(cal/cm^3)^{1/2}$[@]	χ[#]
n-pentane	116.2	7.0	1.78
n-heptane	147.4	7.4	1.67
methylcyclohexane	128.3	7.8	1.12
cyclohexane	108.7	8.2	0.74
o-xylene	121.2	8.8	0.48
toluene	106.8	8.9	0.43
benzene	89.4	9.2	0.35
tetralin	136.0	9.5	0.31
chlorobenzene	102.1	9.5	0.31
1-methylnaphthalene	138.8	9.9	0.31
carbon disulfide	60.0	10.0	0.31
o-dichlorobenzene	112.8	10.0	0.31
nitrobenzene	102.7	10.0	0.31
biphenyl	154.1	10.6	0.46[$]
propionitrile	70.9	10.8	0.43
nitroethane	71.5	11.1	0.52
acetonitrile	52.6	11.9	0.71
chloroacetonitrile	63.3	12.6	1.17
nitromethane	54.3	12.7	1.10
pyridine	80.9	10.7	0.42
tetrahydrofuran	81.7	9.1	0.36
carbon tetrachloride	97.1	8.6	0.36
1,1,2-trichloroethane	92.7	9.6	0.30
1,2-dibromoethane	86.2	10.4	0.36
2-propanol	76.8	11.5	0.70
ethanol	58.5	12.7	1.16
acetone	74.0	9.9	0.30
dimethyl sulfoxide	71.3	12.0	0.91

[@]Brandrup, J. and Immergut, E. H., *Polymer Handbook, 3rd ed.*, John Wiley & Sons, 1989.

[#]Calculated using Equation 2 assuming solubility parameter of the kerogen is 9.75$(cal/cm^3)^{1/2}$ and χ_S is 0.30.

[$]Calculated at 75 °C.

$$f_m = \frac{\%\ Ash}{\%\ Ash + (1-\%\ Ash) \times (1-\%\ Bitumen)} \qquad (10)$$

Here, % Ash is determined by elemental analysis of the kerogen concentrate. % Bitumen is determined by Soxhlet extraction of the kerogen concentrate on a dry mineral matter free basis.

Having demonstrated solvent swelling of Green River kerogen follows regular solution theory and HCl/HF demineralized Green River kerogen swells reversibly, the number average molecular weight between cross links ($\bar{M}_c$) for Green River kerogen was calculated using both the Flory-Rehner and Kovac equations. Table 12 lists the Flory-Rehner and Kovac $\bar{M}_c$ values for Green River kerogen in 18 swelling solvents. The $\bar{M}_c$ values in the other swelling solvents are unreasonable and discarded. The Flory-Rehner equation yields $\bar{M}_c$ of 190 ±60 and 220 ±70 amu for HCl/HF (8 hr) and HCl/HF (48 hr) demineralized samples, respectively. These small values of $\bar{M}_c$ indicate that Green River kerogen is a highly cross-linked network. The results also lead us to question the validity of applying the Flory-Rehner equation. One of the key assumptions of the Flory-Rehner equation is that chain lengths between cross links obey a Gaussian distribution. The small $\bar{M}_c$ values calculated using this equation clearly violate this assumption. The Kovac equation describes the system better and will give greater values for $\bar{M}_c$. It does require a correct

Table 12. Number average molecular weight between cross-links of the HCl/HF demineralized Green River kerogen

Solvent	HCl/HF (8h) demineralization $\bar{M}_c$ (Flory)	$\bar{M}_c$ (Kovac)			HCl/HF (48h) demineralization $\bar{M}_c$ (Flory)	$\bar{M}_c$ (Kovac)		
		N=1	N=2	N=3		N=1	N=2	N=3
cyclohexane	290	1100	800	700	240	920	670	580
o-xylene	210	770	560	490	230	860	620	540
toluene	160	600	440	380	170	650	470	410
benzene	130	490	360	310	140	510	370	320
tetralin	250	920	660	580	260	990	710	610
chlorobenzene	200	730	520	450	170	630	460	400
1-methylnaphthalene	240	910	650	570	310	1200	830	720
carbon disulfide	97	360	260	230	110	410	290	260
o-dichlorobenzene	320	1200	840	730	260	980	700	600
nitrobenzene	220	810	580	500	190	720	520	450
pyridine	210	780	550	480	210	760	550	470
tetrahydrofuran	230	860	610	530	220	810	570	490
carbon tetrachloride	160	610	440	390	210	890	640	550
1,1,2-trichloroethane	150	570	410	360	230	870	610	530
1,2-dibromoethane	130	490	350	310	150	560	400	350
2-propanol	100	390	290	250	130	480	350	310
ethanol	180	690	510	450	250	940	690	610
dimethyl sulfoxide	220	830	610	530	370	1400	1000	870
average	190	730	520	460	220	810	580	500

Larsen, J. W.; Li, S. *Energy Fuels*, **1994**, 8, 932-936.

estimate of the number of freely rotatable group (N) between cross links. Since our goal is to study the changes in $\bar{M}_c$ occurring during kerogen maturation, we can avoid quantitatively assigning N. We have no basis for estimating it. It is clear that Green River kerogen is a highly cross-linked macromolecular network.

a.6 Solvent swelling studies of Rundle kerogen

Rundle kerogen is a Type I kerogen from Queensland, Australia. Its organic functionalities have been carefully studied and a detailed chemical structure has been proposed.[40] Table 13 compares organic functionality distributions in Green River and Rundle oil shales.[40]

We briefly conducted solvent swelling studies of Rundle kerogen in order to compare the behaviors of Type I kerogens from different geological environments. Table 14 lists the volumetric swelling ratios of Rundle kerogen in 23 organic solvents and Figure 23 displays a plot of the swelling ratio of this kerogen as a function of swelling solvent solubility parameter. The results again show that polar and nonpolar solvents with similar solubility parameters swell the kerogen similarly. Good hydrogen-bond-acceptors (pyridine and THF) and hydrogen-bond-donors (2-propanol and ethanol) swell the kerogen more than nopolar solvents with similar solubility parameters. Specific interactions clearly exist between hydrogen bonding solvents and the kerogen network.

Table 13. Comparison of organic functionality distributions in Green River and Rundle oil shales.[40]

	Green River oil shale	Rundle oil shale
Org. H/C	1.55	1.60
carbon		
aliphatic	74%	77%
C=O	1%	4%
C=C	3%	3%
aromatic	22%	16%
oxygen	2.95 O's /100 C's	9.2 O's /100 C's
-O-	0.4	2.3
-OH	0.55	0.6
-COO-	2.0	4.5
-CHO		1.4
$-CO-NH_2$		0.45
nitrogen	3.1 N's /100 C's	2.3 N's/100 C's
sulphur	0.62 S's/100 C's	0.68 S's/100 C's

Table 14. Volumetric swelling ratios of Rundle kerogen in organic solvents[@]

No.	Solvent	δ $(cal/cm^3)^{1/2}$	Q_v
1	n-pentane	7.0	1.23
2	n-heptane	7.4	1.24
3	methylcyclohexane	7.8	1.27
4	cyclohexane	8.2	1.18
5	o-xylene	8.8	1.52
6	toluene	8.9	1.52
7	benzene	9.2	1.45
8	tetralin	9.5	1.58
9	chlorobenzene	9.5	1.61
10	1-methylnaphthalene	9.9	1.62
11	carbon disulfide	10.0	1.46
12	nitrobenzene	10.0	1.55
13	biphenyl	10.6	1.55
14	propionitrile	10.8	1.21
15	nitroethane	11.1	1.33
16	acetonitrile	11.9	1.20
17	nitromethane	12.7	1.24
18	pyridine	10.7	1.76
19	tetrahydrofuran	9.1	1.70
20	2-propanol	11.5	1.44
21	ethanol	12.7	1.38
22	acetone	9.9	1.33
23	dimethyl sulfoxide	12.0	1.53

[@]Brandrup, J. and Immergut, E. H., *Polymer Handbook, 3rd ed.*, John Wiley & Sons, Inc., 1989.

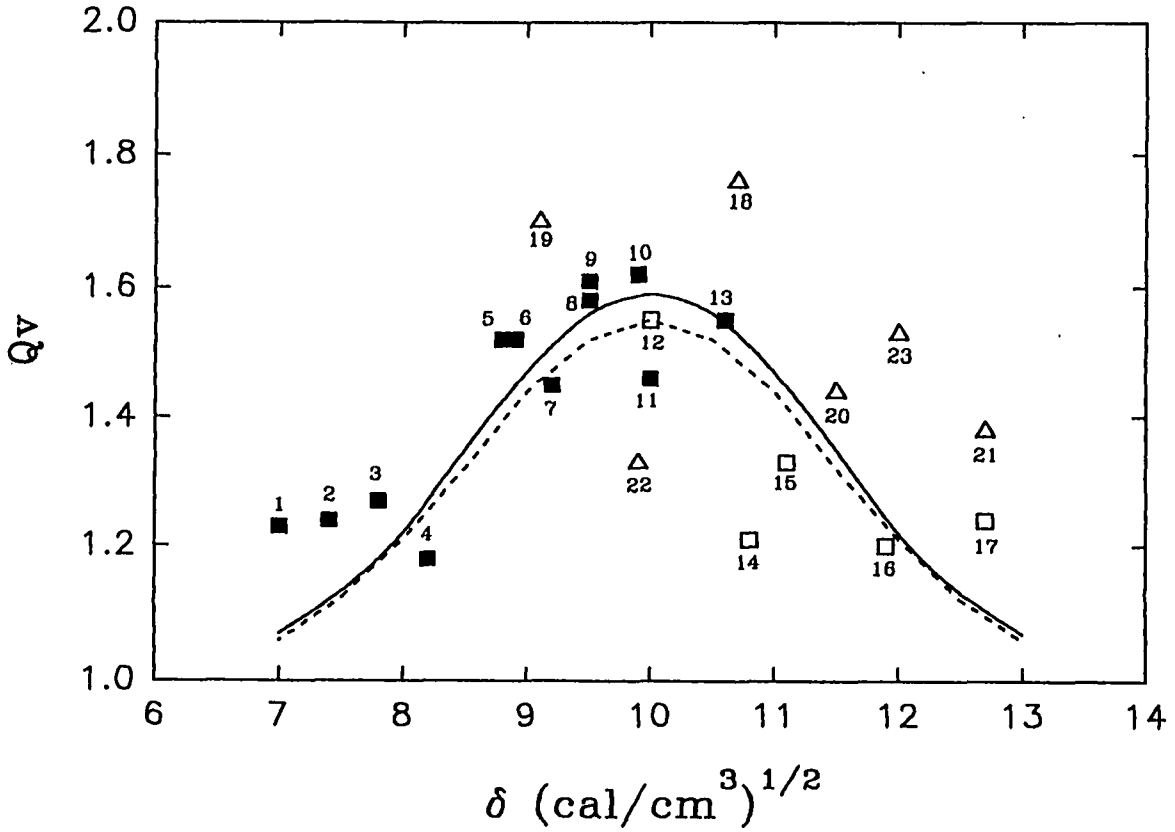

Figure 23. Swelling ratio of Rundle kerogen as a function of swelling solvent solubility parameter. (■) nonpolar solvents, (□) polar solvents, (▵) H-bonding solvents. The dash line is the theoretical prediction by Kovac's model assuming N = 1 and $\bar{M}_c$ = 760. The solid line is the theoretical prediction by Flory's model assuming $\bar{M}_c$ = 220. See Table 14 for solvent identification.

Nevertheless, the bell-shaped curve predicted by regular solution theory is visible in Figure 23, although with more scatter compared with Green River kerogen. A solubility parameter of about 10 $(cal/cm^3)^{1/2}$ can be assigned to this kerogen and could be useful for the estimation of solvent-kerogen interactions. The solubility parameter of Rundle kerogen was calculated to be 9.8 $(cal/cm^3)^{1/2}$ using Siskin's structure and van Krevelen's atom and group contributions.[3,40]

The enhanced swelling ratios of Rundle kerogen in hydrogen bonding solvents may be caused by the chemical nature of this kerogen. Siskin et al. previously showed that Green River and Rundle kerogens contain 2.2 O's/100C's and 9.2 O's/100C's, respectively.[40] Because Rundle kerogen has a much greater oxygen content than Green River kerogen, the interactions between hydrogen bonding solvents and the Rundle kerogen network will be stronger, that will enhance the swelling ratios of Rundle kerogen in these solvents. Also, Rundle kerogen has a greater chance to form hydrogen bonding cross-links.[40] If these cross-links exist in Rundle kerogen, some of them can be disrupted when the kerogen is swollen in good hydrogen bonding solvents and that will decrease the cross-link density of the network and enhance the swelling ratio of the kerogen in these solvents.

It is clear from the data presented above that different Type I kerogens behave differently in solvent swelling studies. Solvent swelling of Green River kerogen follows

regular solution theory. Its solubility parameter can be directly determined using swelling measurements. Solvent swelling of Rundle kerogen roughly follow regular solution theory. Hydrogen bonding solvents enhance swelling ratios, but polar and nopolar solvents behave similarly. The solubility parameter of Rundle kerogen can be measured using a series of nopolar and polar solvents.

The work described so far demonstrates that there is a realistic basis for the expectation that solvent swelling measurements of a Type I kerogen maturation series will succeed and give meaningful data. We have demonstrated that kerogens isolated by demineralization of oil shales can be used for solvent swelling studies. The mineral matter remaining in kerogens does not hinder the swelling measurements. Solvent swelling of Green River kerogen follows regular solution theory. The $\bar{M}_c$ of Type I kerogen can be calculated using both the Flory-Rehner and Kovac equations, but the results on the Green River kerogen studied are not to be quantitatively trusted because the kerogen is so highly cross-linked. We believe that the method used can be applied to study the changes of $\bar{M}_c$ values during the kerogen maturation process.

b. Bitumen Molecular Weight Distribution

The second part of technique development was to develop a method which could dependably measure bitumen molecular weight distributions. As mentioned in chapter IV, the amount of bitumen and its molecular weight distribution are directly related to kerogen cross-link density. These data can provide additional information about the kerogen maturation process.

Few techniques have been used for determining bitumen molecular weight distributions (see chapter IV.4) and none meets our needs. GPC is a frequently used method for bitumen studies. A careful study of this technique showed that it lacked good calibration standards for kerogen products.[75,76] GPC/VPO is an accepted technique for determining bitumen molecular weight distributions, but it is very laborious and requires more sample than was available to us.

Seeking a reliable way to measure bitumen molecular weight distributions, we studied three bitumens and two bitumen derivatives using ^{252}Cf plasma desorption mass spectrometry (PDMS).[81] The PDMS technique utilizes highly energetic ^{252}Cf fission fragments to volatilize and to ionize solid materials deposited on an aluminized Mylar disk.[107,108] It is capable of producing primarily molecular ions with much less fragmentation than conventional electron ionization. The technique is fast, requires limited sample quantities (<10 mg), and has approximately equal sensitivity to aliphatic and aromatic compounds.[96] It has been successfully applied to the

measurements of molecular weight distributions of coal hydrogenation products.[96] We explored its application to bitumens.[81]

b.1 Molecular weight distributions of Green River, Rundle, and Athabasca bitumens and two Athabasca bitumen products[81]

Green River, Rundle, and Athabasca bitumens and two Athabasca bitumen products were used for PDMS molecular weight distribution studies. Green River and Rundle bitumens were isolated by Soxhlet extraction (toluene) of the HCl/HF demineralized kerogen concentrates. Athabasca bitumen and its two derivatives were kindly supplied by Dr. Marten Ternan of CANMET. The molecular weight distributions of Athabasca bitumen and its two derivatives had been measured by GPC/VPO and the results had been published.[77,93]

The ^{252}Cf plasma desorption mass spectrometer (Bio Ion 20) used in this research calibrates PDMS spectra using H^+ and Na^+ ion masses. We checked the instrument calibration with Porcine insulin (purchased from Sigma) of molecular weight 5778 amu. The measured molecular weight was 5790 amu, within the instrument specifications.

Figure 24 shows the PDMS spectrum of an aluminized Mylar disk. The intense peaks at low mass are due to aluminum oxide cluster ions and pump oil fragment ions.[109] This background spectrum must be subtracted from the sample spectra in order to compare molecular weight distributions and to calculate

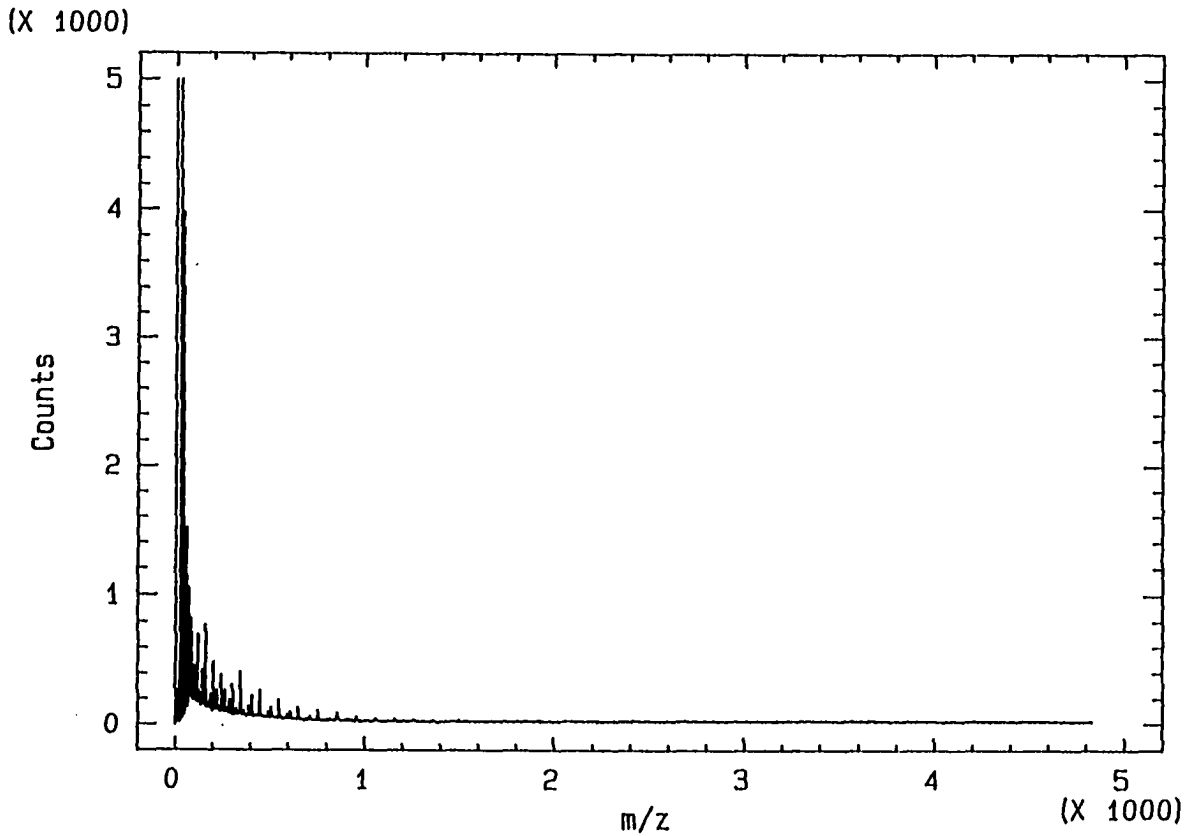

Figure 24. PDMS spectrum of an aluminized Mylar disk.

Larsen, J. W.; Li, S. *Energy Fuels*, **1995**, 9, 760-764.

number average molecular weights (M_n).

Figures 25-30 present the molecular weight distributions of Green River, Rundle, and Athabasca bitumens and two Athabasca bitumen products. In each plot, the upper line is the raw data and the lower line is the smoothed spectrum with the Mylar disk background subtracted. The simple moving average of 5 points on Y axis was used to smooth these molecular weight distribution curves.

Green River and Athabasca bitumens and two Athabasca bitumen products display continuous molecular weight distributions up to about 3000 amu (see Figures 25, 28-30). Rundle bitumen behaves differently. Figures 26 and 27 show molecular weight distributions of the toluene-soluble and toluene-insoluble portions of Rundle bitumen. The toluene-soluble fraction displays a narrower molecular weight distribution compared to Green River and Athabasca bitumens. We could not find a good room-temperature solvent to dissolve the toluene-insoluble fraction. The sample was dissolved in toluene at 80 °C, deposited on a Mylar disk, and run under normal conditions. Figures 26 and especially 27 reveal a trimodal molecular weight distribution of Rundle bitumen with peaks at about 400, 900, and 1300 amu. This trimodal distribution differs from a previously reported bimodal distribution measured by GPC.[110] PDMS provides more detailed information on the Rundle bitumen than GPC.

In the PDMS molecular weight distributions shown above,

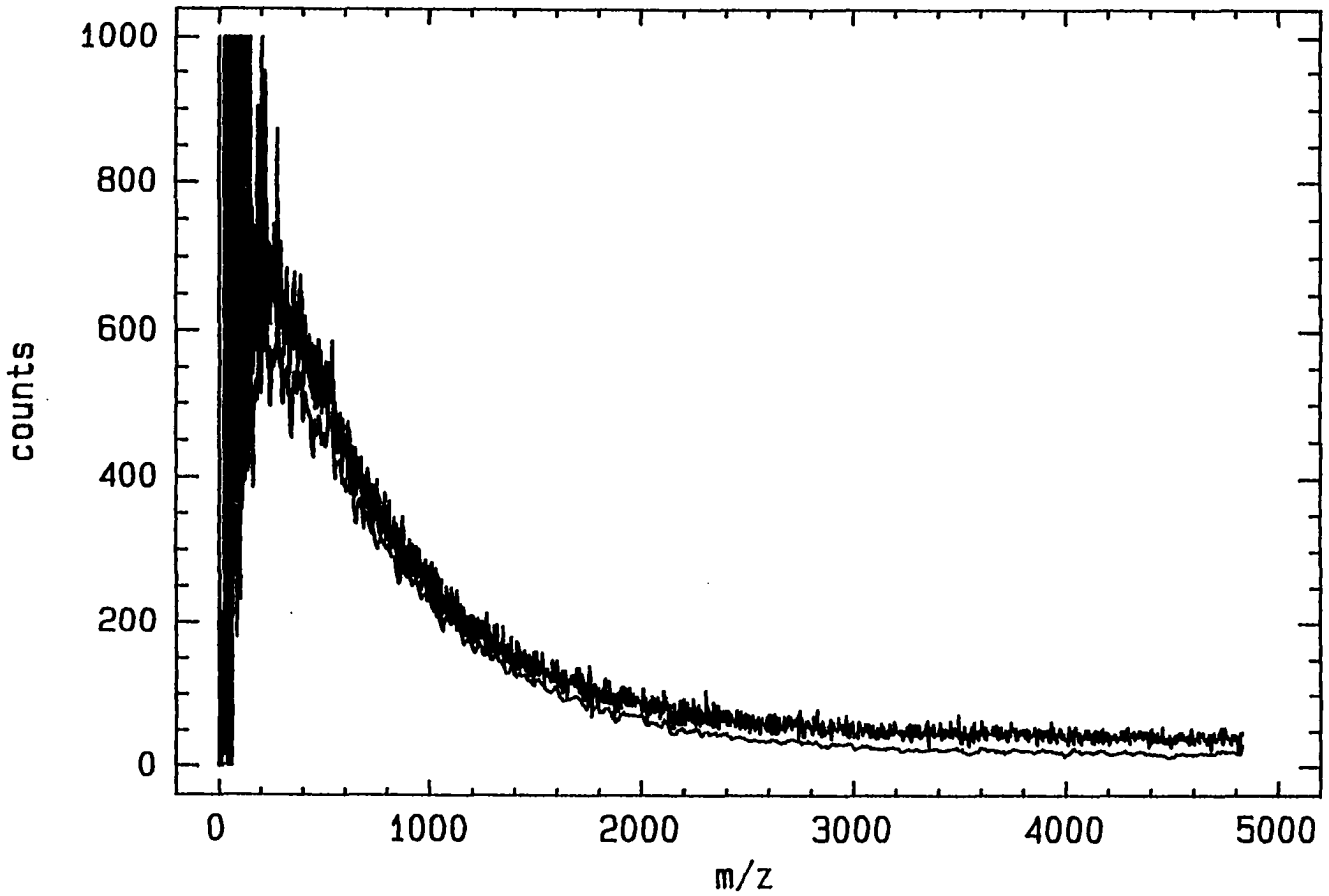

Figure 25. PDMS spectrum of Green River bitumen. Raw data (upper line) and the smoothed spectrum with the Mylar disk background subtracted (lower line).

Larsen, J. W.; Li, S. *Energy Fuels*, **1995**, 9, 760-764.

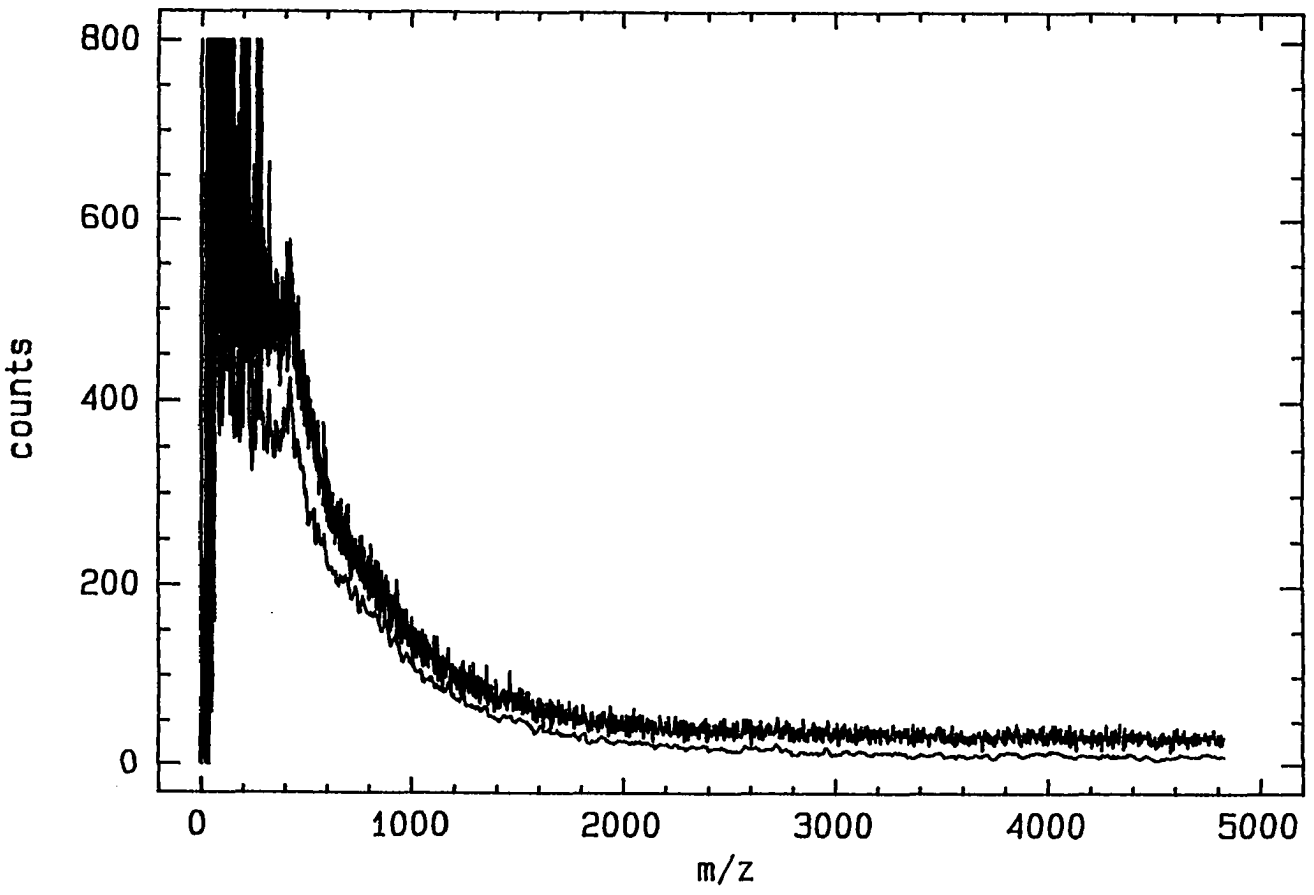

Figure 26. PDMS spectrum of toluene-soluble fraction of Rundle bitumen. Raw data (upper line) and the smoothed spectrum with the Mylar disk background subtracted (lower line).

Larsen, J. W.; Li, S. *Energy Fuels*, **1995**, 9, 760-764.

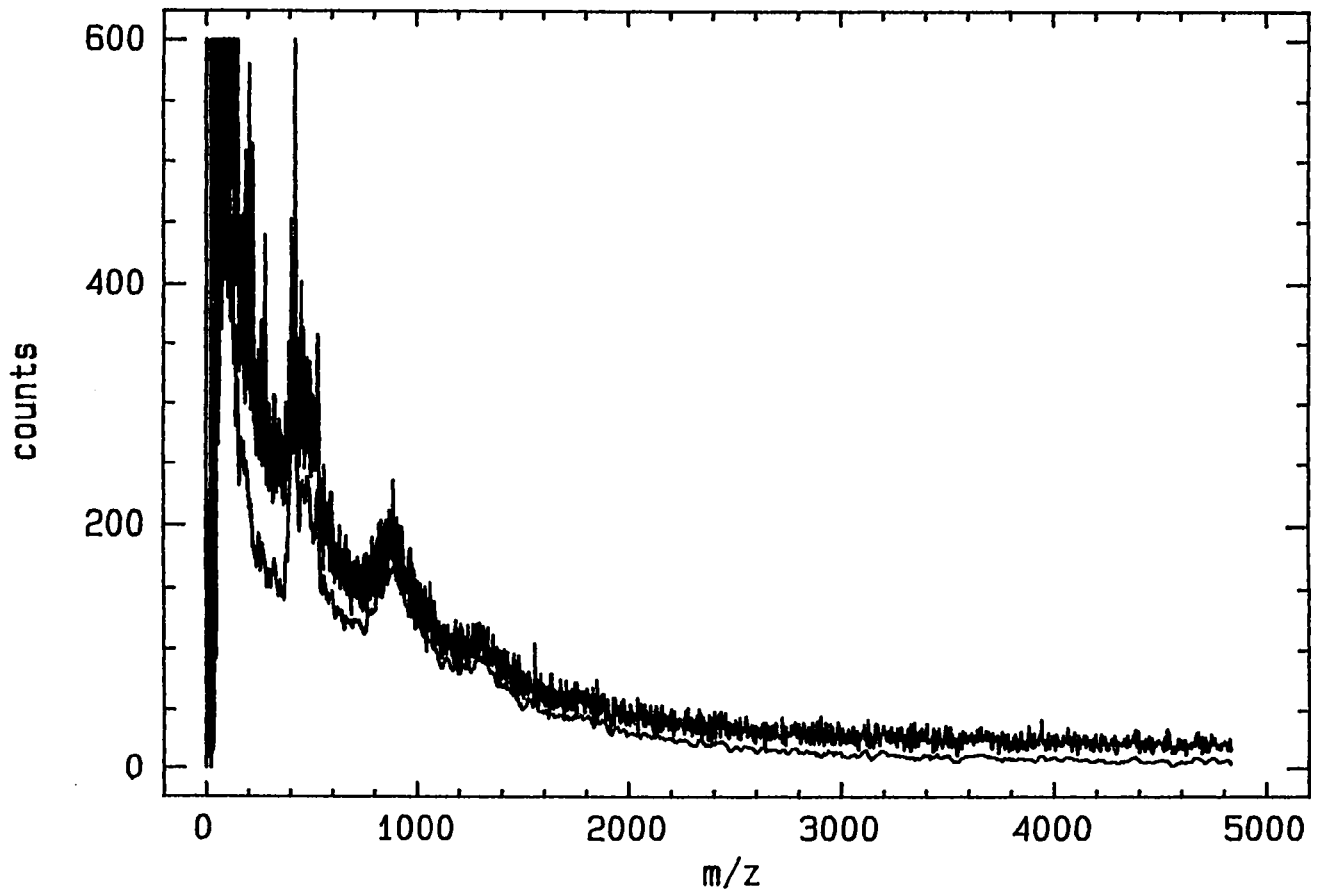

Figure 27. PDMS spectrum of toluene-insoluble fraction of Rundle bitumen. Raw data and the smoothed spectrum with the Mylar disk background subtracted (lower line).

Larsen, J. W.; Li, S. *Energy Fuels*, **1995**, 9, 760-764.

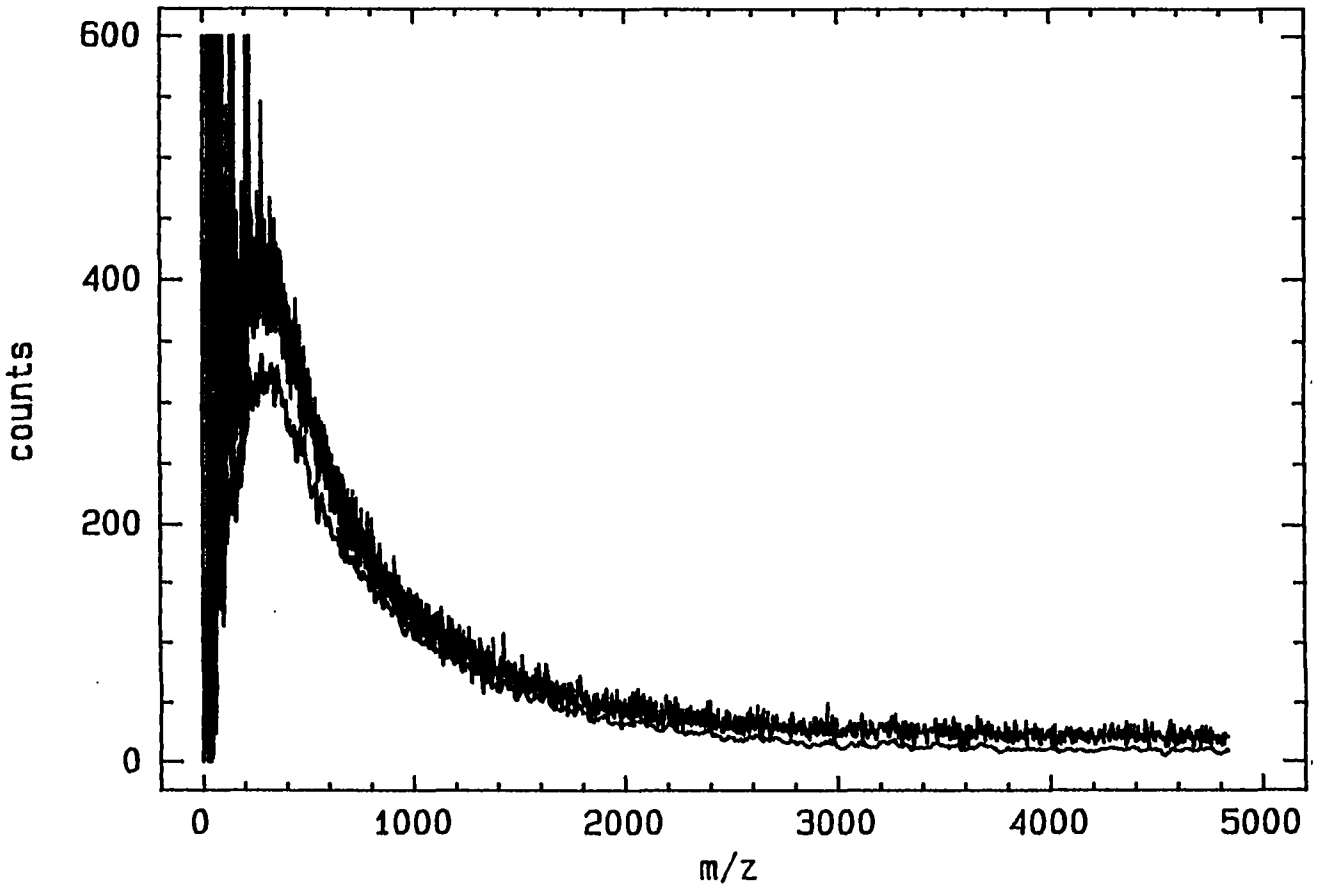

Figure 28. PDMS spectrum of Athabasca bitumen. Raw data and the smoothed spectrum with the Mylar disk background subtracted (lower line).

Larsen, J. W.; Li, S. *Energy Fuels*, **1995**, 9, 760-764.

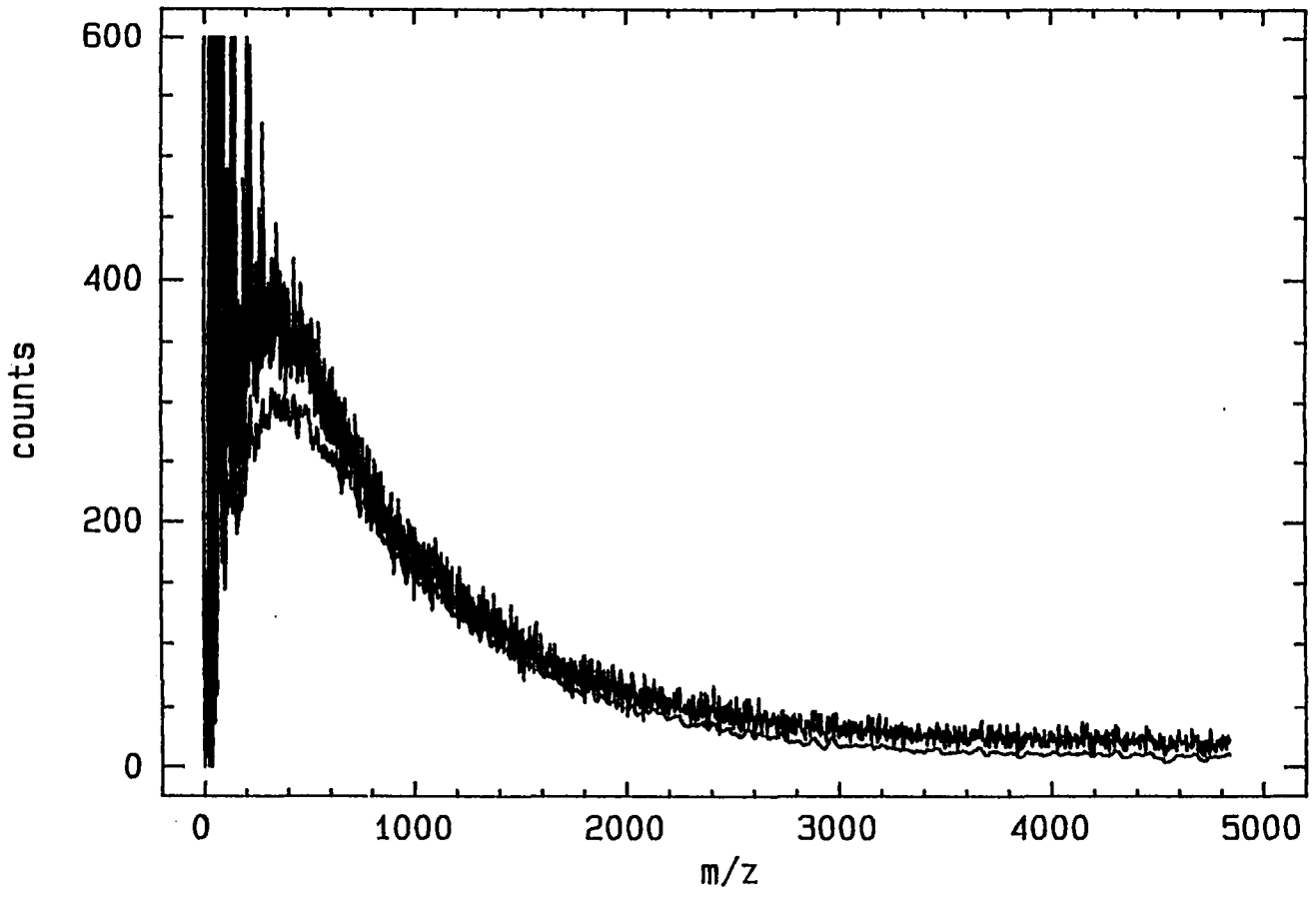

Figure 29. PDMS spectrum of +525 °C residue from Athabasca bitumen. Raw data and the smoothed spectrum with the Mylar disk background subtracted (lower line).

Larsen, J. W.; Li, S. *Energy Fuels*, **1995**, 9, 760-764.

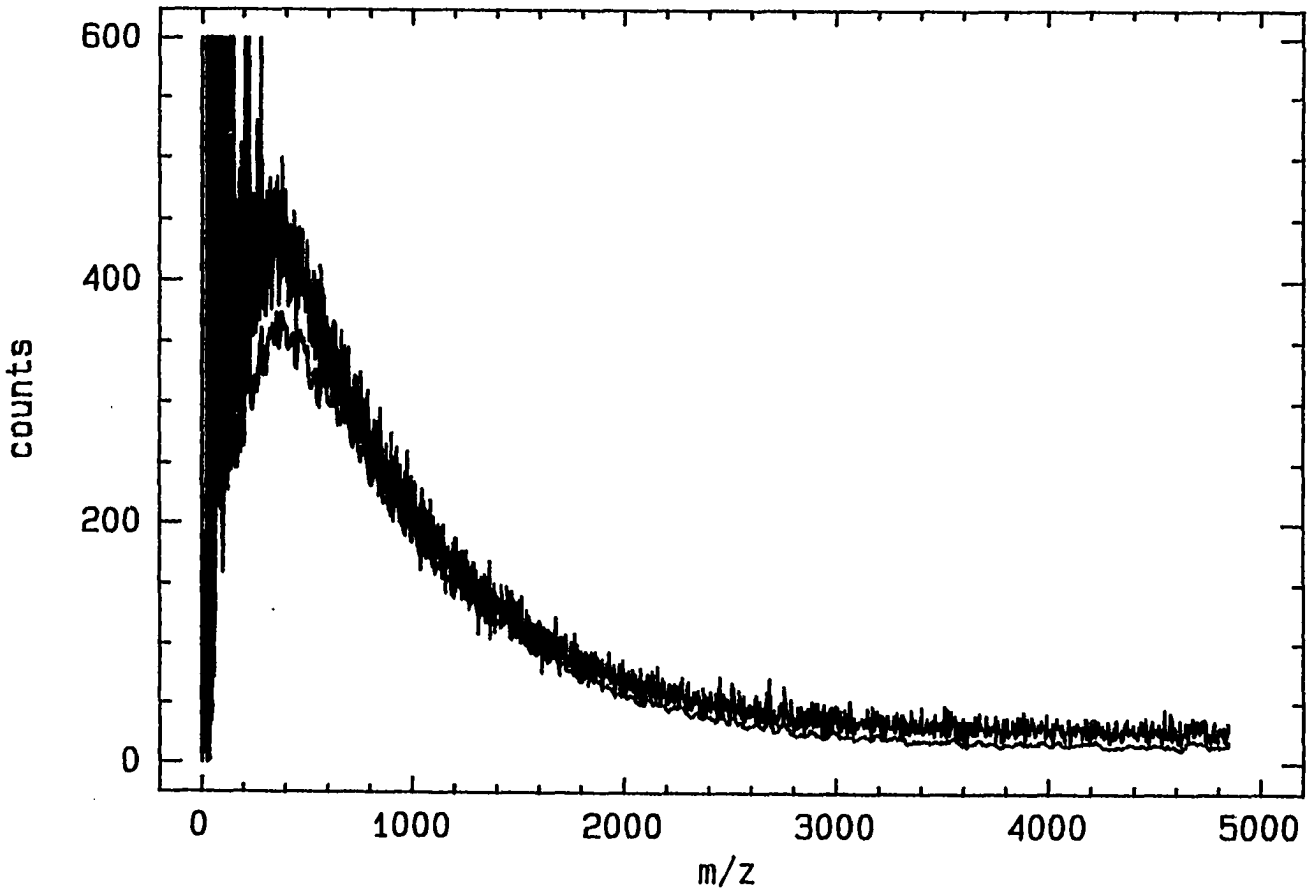

Figure 30. PDMS spectrum of +525 °C residue from unimodal catalyst. Raw data and the smoothed spectrum with the Mylar disk background subtracted (lower line).

Larsen, J. W.; Li, S. *Energy Fuels*, **1995**, 9, 760-764.

all spectra display high-mass tails over 4000 amu. There are two possible explanations for these long high-mass tails. First, high molecular weight species may exist in these samples. The published VPO/GPC molecular weight distributions of Athabasca bitumen and its +525 °C unimodal catalyst residue revealed that 10 wt % of Athabasca bitumen separated by preparative GPC has M_n over 5470 amu and 21 wt % of the +525 °C unimodal catalyst residue separated by preparative GPC has M_n of 4990.[77,93]

Second, the high-mass tails in the spectra may originate from the ^{252}Cf plasma desorption time-of-flight spectrometer. Metastable decompositions, uncorrelated events, and dimerizations all can result in broad high-mass tails.[111,112] The metastable decomposition of ions in the PDMS flight tube has been carefully studied.[111] The decayed fragments in the flight tube usually have longer flight times than their unfragmented parent ions and are detected at the higher mass region. Uncorrelated events may be the major source of the high mass background.[112] After detecting a ^{252}Cf fission fragment, the time interval digitizer (TID) of PDMS opens a time window during which any number of stop pulses are accepted and no new fission is counted. If the second ^{252}Cf fission occurs during this time window, the ions generated artificially appear in the high mass region. It has been estimated that the probability for a second fission occurring in a TID time window is on the order of a few percent.[96,112] Also, the

ionization of PDMS is a complex process during which both molecular and fragment ions produced can be dimerized to form high mass species.[113]

Because of the above three factors, PDMS spectra never reach zero at high mass. It is important to determine the point at which to cut off the high-mass tails for the M_n calculation. In practice, the intensities of the last 100 data points of each spectrum were averaged and the value was assumed to be the noise. In each spectrum, the high mass signals were compared with the assumed noise values and the high-mass tail was cut off when the signal to noise ratio was smaller than 2. As we shall see, M_n of three bitumens calculated from the truncated PDMS spectra agree well with that determined by VPO (see b.3). The results demonstrated that this truncation method is reasonable.

b.2 Vapor pressure osmometry measurements

We determined M_n of Green River bitumen and the toluene-soluble fraction of Rundle bitumen using vapor pressure osmometry. This technique detects the temperature difference between two thermistors, one immersed in a drop of pure solvent and the other in a drop of solution.[97] At low solute concentration, the temperature difference (R) can be expressed as a function of concentration (C) using Equation 11.

$$\frac{R}{C} = \frac{K}{M_n}(1 + A_2C) \qquad (11)$$

Here, A_2 is the second virial coefficient. K is a calibration constant, which can be determined using a compound of known molecular weight. Experimentally, R values are determined for solutions having different concentrations. A plot of R/C against C is usually made and the intercept of the plot is used to calculate M_n.[97]

Table 15 lists the experimental results of VPO for Green River bitumen and the toluene-soluble fraction of Rundle bitumen. Figures 31 and 32 are the plots of R/C vs. C for these samples. These plots are very close to straight lines. The intercept of each plot was computed using linear regression and the number average molecular weights of these bitumens were calculated using benzil as the calibration standard. The molecular weight of 2500 amu polystyrene purchased from Polysciences, Inc. was measured as a reliability check. It was 2270 ± 180.

b.3 Comparison of M_n and molecular weight distributions measured by PDMS, VPO, and GPC/VPO[81]

To test the PDMS technique for measuring bitumen molecular weight distributions, The number average molecular weights (M_n) of Green River, Rundle, and Athabasca bitumens and two Athabasca bitumen products were calculated from their PDMS spectra and the results were compared with those measured

Table 15. VPO measurements for Green River bitumen and the toluene-soluble fraction of Rundle bitumen.

Green River bitumen in toluene at 48 °C		Toluene-soluble fraction of Rundle bitumen in THF at 45 °C	
C (g/kg)	R	C (g/kg)	R
9.62	31.5	10.5	95.0
7.13	26.5	7.60	71.5
4.86	17.5	5.63	50.5
4.21	13.5	4.06	36.5
2.98	9.0	3.34	31.5
1.86	6.5	1.88	16.0
1.26	3.8		

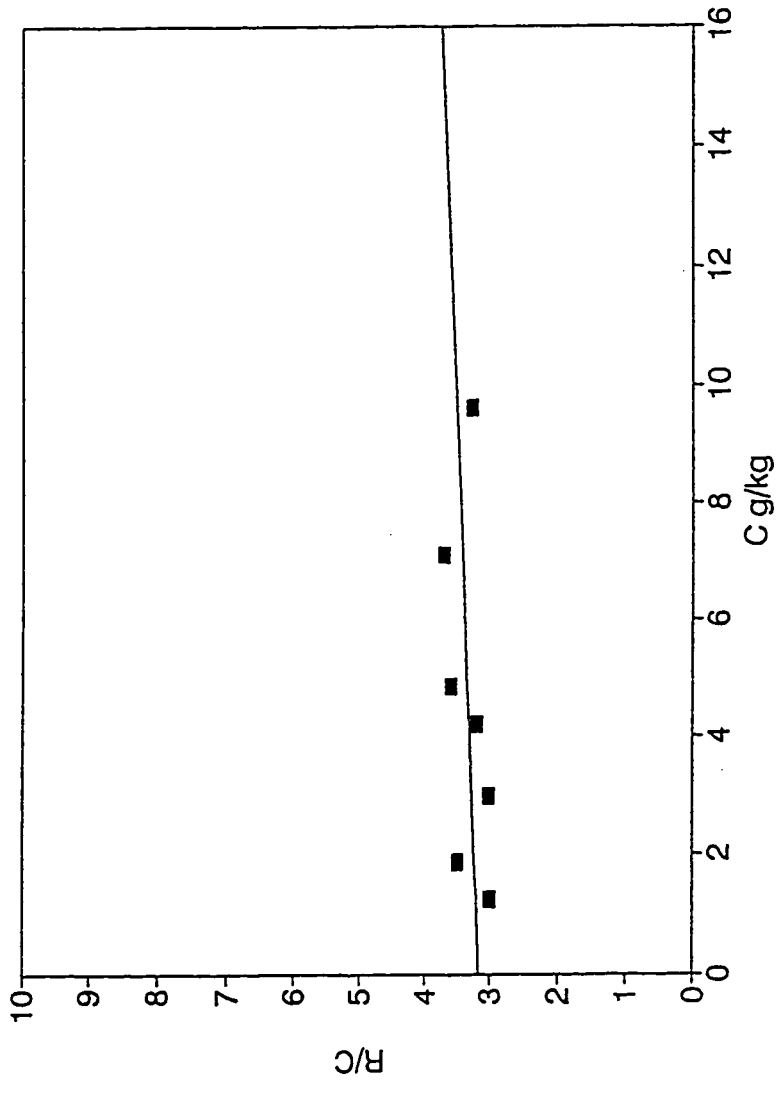

Figure 31. A plot of R/C vs. C for VPO measurements of Green River bitumen.

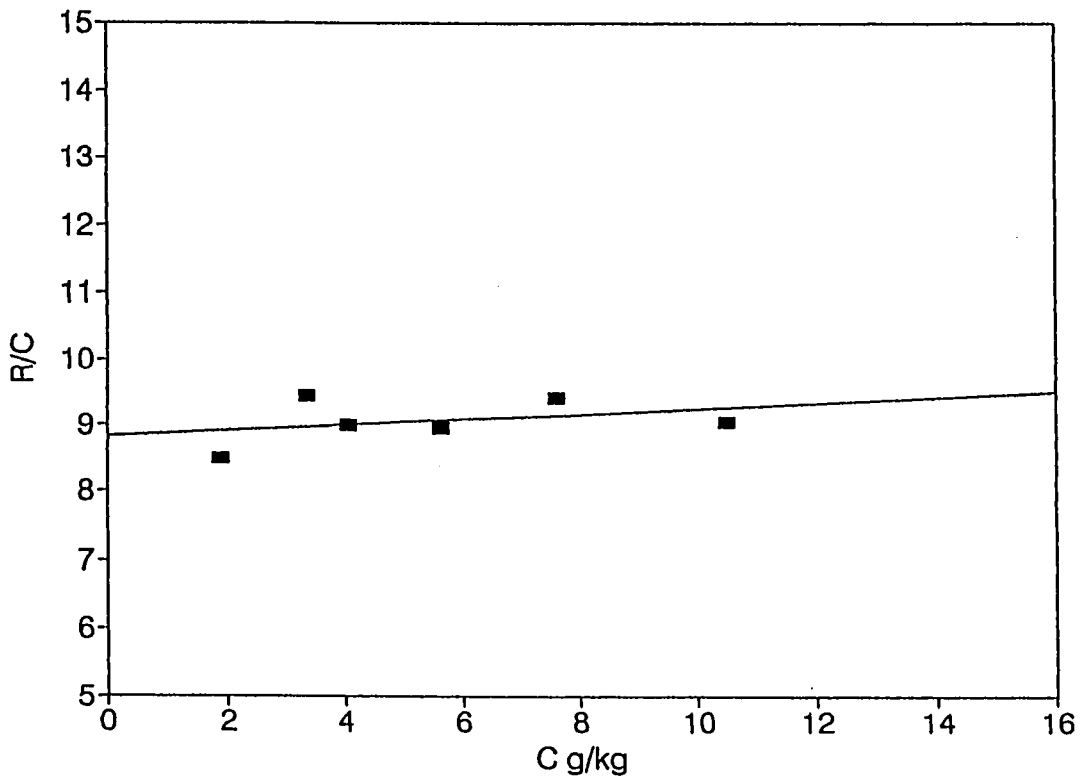

Figure 32. A plot of R/C vs. C for VPO measurements of the toluene-soluble fraction of Rundle bitumen.

by VPO (see Table 16). The VPO M_n of Athabasca bitumen and its two derivatives were calculated from their GPC/VPO molecular weight distributions reported in the literature.[77,93] In general, the number average molecular weights measured by VPO and PDMS agree well for three bitumens and do not agree for the two Athabasca bitumen products.

The agreement of bitumen M_n measured by PDMS and VPO encouraged us to further compare the shape of the PDMS molecular weight distribution of Athabasca bitumen with the GPC/VPO results published by Ternan et al.[77] Figure 33 compares the molecular weight distribution of Athabasca bitumen measured by GPC/VPO with that determined by PDMS. Two distributions display a similar shape above 300 amu and differed significantly below 300 amu.

The difference between the PDMS and VPO/GPC molecular weight distributions at low mass may have three explanations. First, molecular association may occur in the solvent during the VPO measurement. This will reduce the concentration at low mass in the GPC/VPO measurements. Second, large molecules can fragment into small species during the PDMS measurement. This will result in higher low-mass fractions in the PDMS molecular weight distribution. Significant fragmentation of different classes of hydrocarbon compounds has been reported in the literature,[113,114] but fragmentation did not appear to be a problem for M_n measurements of coal hydrogenation products.[96] Finally, PDMS using the aluminized Mylar target has strong

Table 16. Number and Weight Average Molecular Weights (Daltons) Determined Using VPO and PDMS.

	VPO		PDMS	
Sample	M_n	M_w	M_n	M_w
Green River	720±70[@]		580	980
Rundle, Toluene Soluble	400±20[@]		460	830
Rundle, Toluene Insoluble			540	1040
Athabasca	600[#]	1250[#]	600	1010
Athabasca, +525 °C fraction	1030[$]	1150[$]	710	1150
Athabasca, +525 °C unimodal catalyst	1240[$]	2010[$]	680	1100

[@]Standard deviation calculated from the result of linear regression.

[#]Data from Champagne, P. J.; Emmanuel, M.; Ternan, M. *Fuel,* **1985**, *64,* 423-425.

[$]Data from Ternan, M.; Rahimi, P. M.; Clugston, D. M. *Energy Fuels,* **1994**, *8, 518-530.*

Larsen, J. W.; Li, S. *Energy Fuels*, **1995**, 9, 760-764.

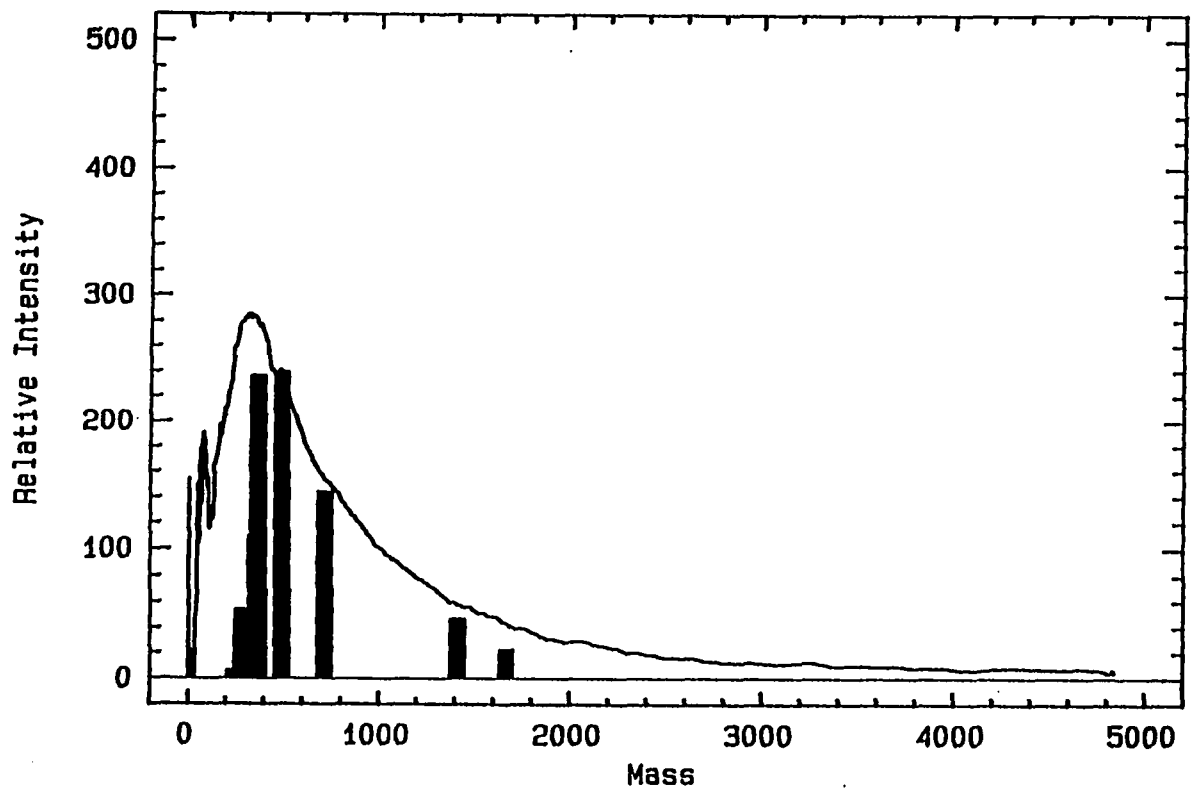

Figure 33. Comparison of the smoothed PDMS spectrum (Mylar disk background subtracted) with GPC/VPO molecular weight distribution of Athabasca bitumen.

Larsen, J. W.; Li, S. *Energy Fuels*, **1995**, 9, 760-764.

background peaks at low mass, which may influence the molecular weight distributions measured. Aluminum oxide cluster ions, pump oil molecular ions, and pump oil fragments are abundant below 1000 m/z in the PDMS spectra.[109] Our method of background subtraction takes an identical ratio of the sample spectrum and the Mylar disk background at high mass. This may result in errors at the low mass.

In spite of the molecular fagmentations and the aluminized Mylar background at low mass, the PDMS M_n of three tested bitumens agreed well with that measured by VPO (see Table 16). The bias of PDMS spectra at low mass seems not to be a problem for M_n measurements of bitumens. It is certain that more study is necessary to resolve the discrepancy between PDMS and GPC/VPO at low mass. The technique is adequate for comparing the changes in the bitumen molecular weight distribution during kerogen maturation.

In this section, we have demonstrated that PDMS is a useful technique for measuring bitumen molecular weight distributions. It is easier, faster, and more sensitive than other currently available techniques, such as GPC or GPC/VPO. M_n of bitumens calculated from PDMS spectra were in overall agreement with that measured by VPO. PDMS can reveal changes in bitumen molecular weight distributions during Type I kerogen maturation.

3. Type I Kerogen Maturation Studies

The study of kerogen maturation is important for petroleum exploration and production. Kerogen maturation is responsible for petroleum formation.[1] This process has been extensively studied and the changes in physical and chemical properties of kerogen during maturation have been thoroughly investigated.[1] Many kinetic models have been developed in the past 20 years.[83,92,115,116,117] Most of these models are empirically calibrated using pyrolysis experiments and predict the timing and quantity of petroleum generation, but the detailed mechanisms of bond making and breaking occurring during kerogen maturation are not understood. The changes in the macromolecular structure of kerogen have never been experimentally established. There are some speculations on this point in the literature.[53,54]

The ultimate goal of the research of which this project is the beginning is to develop a Type I kerogen maturation model which includes the bond making and breaking occurring during maturation. The experimental approach involves measuring the kerogen cross-link density, measuring the amount of bitumen and its molecular weight distribution, and following the changes in these quantities with increasing maturation in a Type I kerogen maturation series. During kerogen maturation, kerogen fragments to produce bitumen and wet gas.[1] For Type I kerogen, formation of gas directly from the kerogen network is insignificant within the oil window.[118]

Thus characterizing the kerogen and bitumen will be sufficient to describe the macromolecular structural changes occurring during maturation.

a. Type I kerogen maturation Experiments

Kerogen maturation experiments were performed on a maturation series of Uinta Basin oil shale samples (see Figure 2) kindly supplied by Dr. Alan Burnham (Lawrence Livermore National Laboratory). These samples, collected from different depths in the Uinta Basin of Utah, represent Uinta Basin kerogen at different maturation stages. Government 33-4 is from the Redwash field and the other four samples (Brotherson 1-23B4-A, Brotherson 1-23B4-B, Brotherson 1-3B4, and Christansen 1-33A5) are from the Altamont field. The locations of the two oil fields are indicated in Figure 7 (section V.1). The maturities of these samples had been estimated using a kinetic and thermal history model (a computer model) developed by Sweeney et al.[83,92] The percent of kerogen maturation (or % of kerogen converted) of each sample is equivalent to the transformation ratio (the ratio of free hydrocarbons to the sum of free and pyrolyzable hydrocarbons in the kerogen) determined by Rock-Eval pyrolysis.[83]

Uinta Basin kerogen samples were isolated using HCl/HF demineralization and the bitumen samples were extracted with toluene from the isolated kerogen concentrates. Table 5 (section VII.1) displays amounts of kerogen isolated,

elemental analyses of the kerogen concentrates, and amounts of bitumen extracted. Because the source rock samples have low organic carbon contents (1.5 to 6.5 wt %), demineralization times were long. Table 4 (section VII.1) details the times required to demineralize these samples.

Government 33-4 (<5% maturation) and Brotherson 1-23B4A (20% maturation) oil shale samples were demineralized for 12 and 24 days using HCl/HF and the kerogen concentrates isolated contain 13 and 5 wt % minerals, respectively. The other samples were demineralized for 56 days using HCl/HF. Brotherson 1-23B4B (35% maturation) kerogen concentrate contains 3 wt % minerals. Brotherson 1-3B4 (80% maturation) and Christansen 1-33A5 (100% maturation) kerogen concentrates contain 30 and 31 wt % minerals, respectively the results of 56 days of acid digestions. Further reduction of the mineral matter would require unrealistically longer times. Our earlier study of Green River kerogen demonstrated that mineral matter remaining in the kerogen, even at the 40% level, does not alter the solvent swelling measurements (see section VII.2a).[37]

The techniques developed in the earlier studies for Green River and Rundle oil shales were used to determine the number average molecular weight between cross-links (reciprocal of the cross-link density) of the kerogen, the amount of bitumen, and the bitumen molecular weight distribution in the maturation series. The experimental results were used to characterize the changes in the macromolecular structure of

Type I kerogen with increasing maturation.

a.1 Solvent swelling experiments

Five Uinta Basin kerogen samples were swollen in a set of 10 organic solvents which have solubility parameters between 7.4 $(cal/cm^3)^{1/2}$ and 11.9 $(cal/cm^3)^{1/2}$. Limited sample quantities prevented the use of more solvents. These solvents were chosen because (1) they cover a large solubility parameter range, and (2) they were well behaved in the earlier solvent swelling experiments (see section VII.2a).

Volumetric swelling ratios of the Uinta Basin kerogen samples in the organic solvents are given in Table 17. The swelling ratios of these samples are plotted as a function of swelling solvent solubility parameter in Figures 34-38. The swelling of Government 33-4 kerogen (<5% maturation) displays a bell-shaped curve and the maximum of the swelling ratio occurs at 9.5 $(cal/cm^3)^{1/2}$. Regular solution theory is nicely followed except biphenyl swells the kerogen slightly more than expected.

The behavior of Brotherson 1-23B4-A kerogen (20% maturation) is very similar to Government 33-4 kerogen. The maximum of the swelling ratio remains at 9.5 $(cal/cm^3)^{1/2}$. The magnitudes of swelling the kerogen in good solvents, such as toluene, benzene, tetralin and methylnaphthalene, are lower than that of the <5% mature sample.

The swelling of Brotherson 1-23B4-B kerogen (35%

Table 17. Volumetric swelling ratios (Q_v) of Uinta Basin maturation series kerogen samples in organic solvents[@]

			G33-4 <5% Matu.	B1-23B4A 20% Matu.	B1-23B4B 35% Matu.	B1-3B4 80% Matu.	C1-33A5 100% Matu.
No.	Solvent	δ $(cal/cm^3)^{1/2}$	Q_v	Q_v	Q_v	Q_v	Q_v
1	n-heptane	7.4	1.74	1.81	1.69	1.61	1.28
2	methylcyclohexane	7.8	2.09	2.00	1.96	2.04	1.36
3	cyclohexane	8.2	2.16	2.02	1.96	2.00	1.32
4	toluene	8.9	2.87	2.42	2.44	2.36	1.55
5	benzene	9.2	2.87	2.46	2.49	2.30	1.55
6	tetralin	9.5	3.18	2.74	2.83	2.44	1.59
7	1-methylnaphthalene	9.9	2.86	2.68	3.08	2.47	1.56
8	biphenyl	10.6	2.92	2.39	2.37	2.44	1.44
9	nitroethane	11.1	1.64	1.63	1.65	1.43	1.33
10	acetonitrile	11.9	1.20	1.30	1.36	1.24	1.26

[@]Brandrup, J. and Immergut, E. H., *Polymer Handbook, 3rd ed.*, John Wiley & Sons, Inc., 1989.

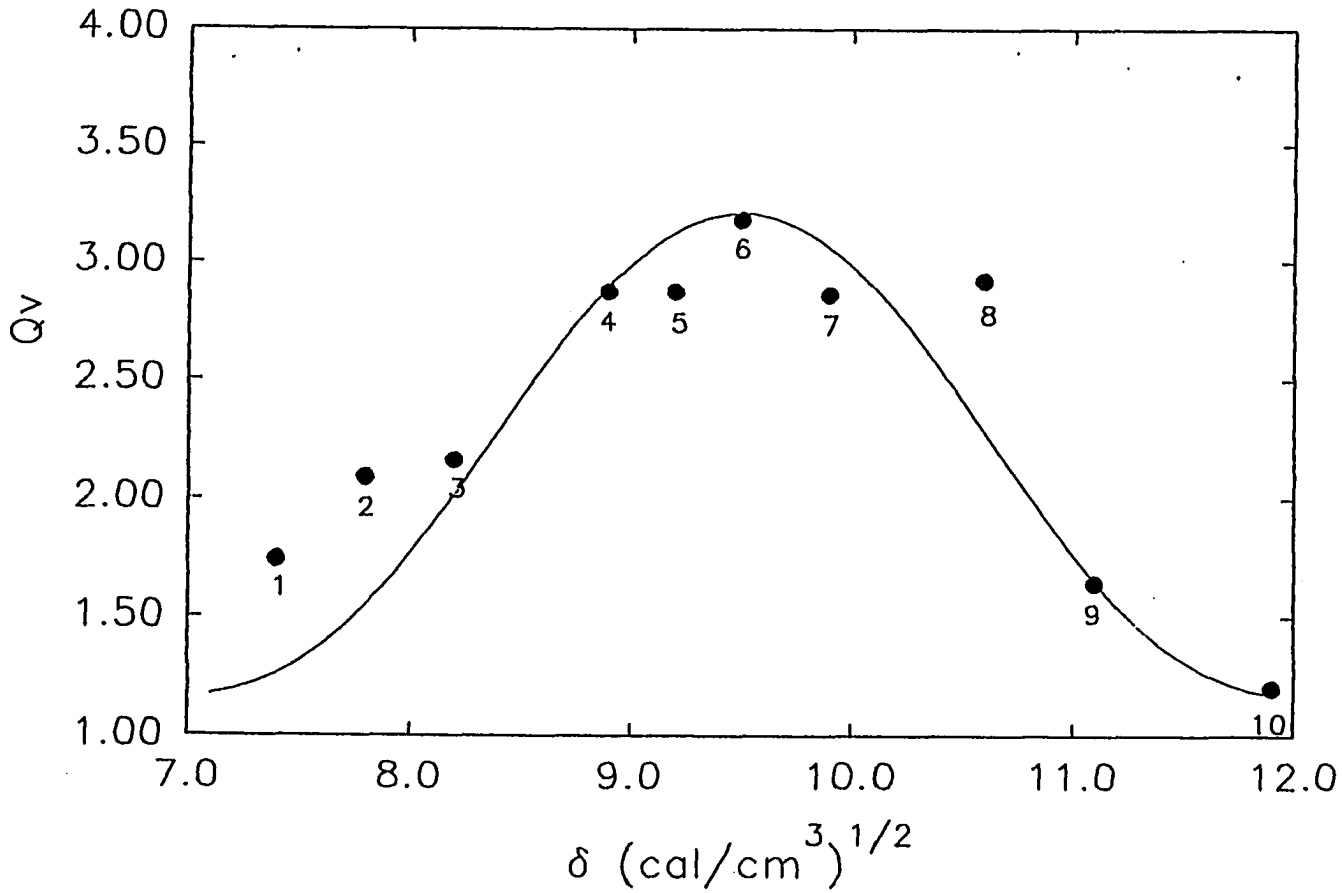

Figure 34. Swelling ratio of Government 33-4 kerogen (<5% maturation) as a function of swelling solvent solubility parameter. The line is the theoretical prediction by Flory's model assuming $\bar{M}_c$ = 1970. See Table 17 for solvent identification.

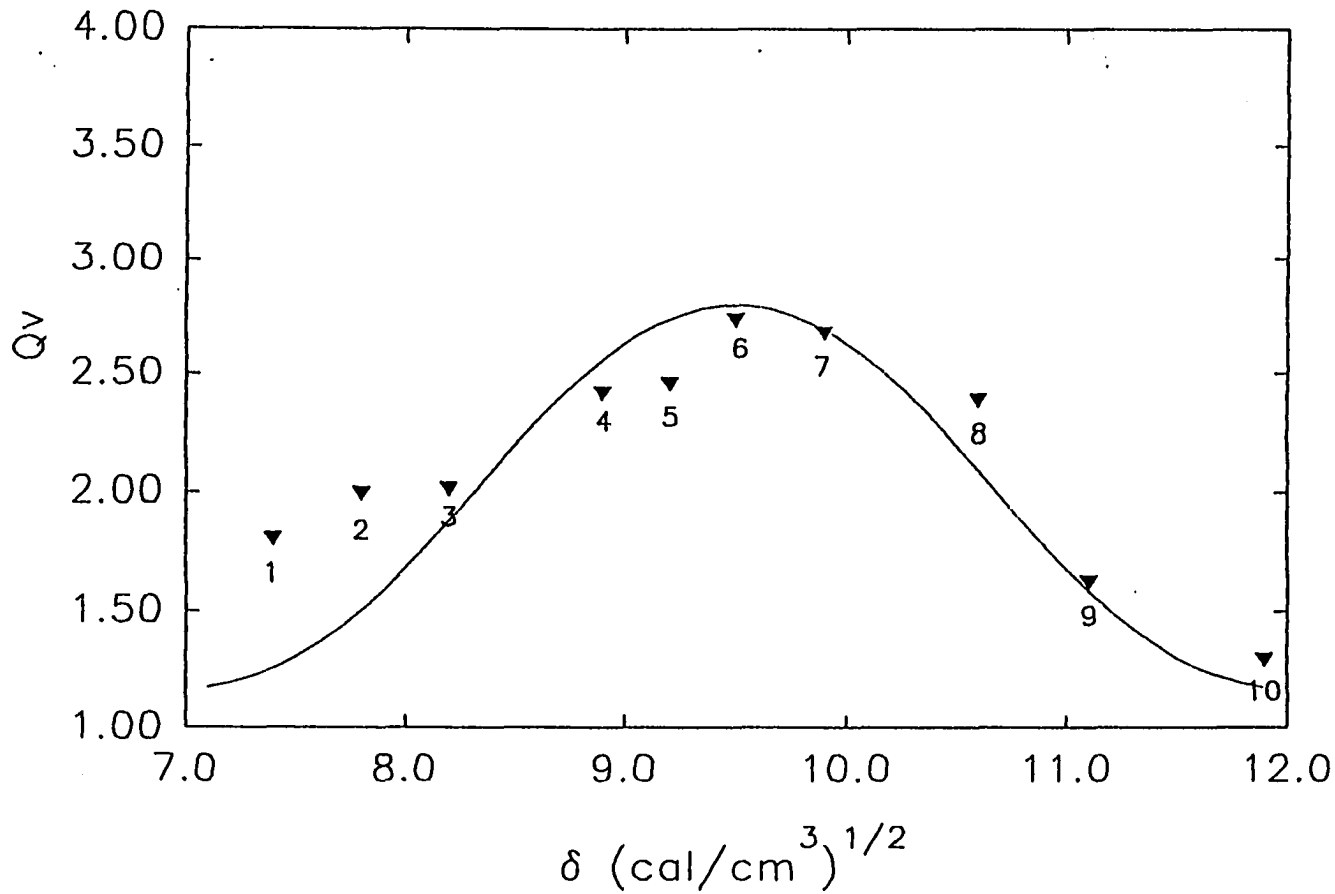

Figure 35. Swelling ratio of Brotherson 1-23B4-A kerogen (20% maturation) as a function of swelling solvent solubility parameter. The line is the theoretical prediction by Flory's model assuming $\bar{M}_c$ = 1320. See Table 17 for solvent identification.

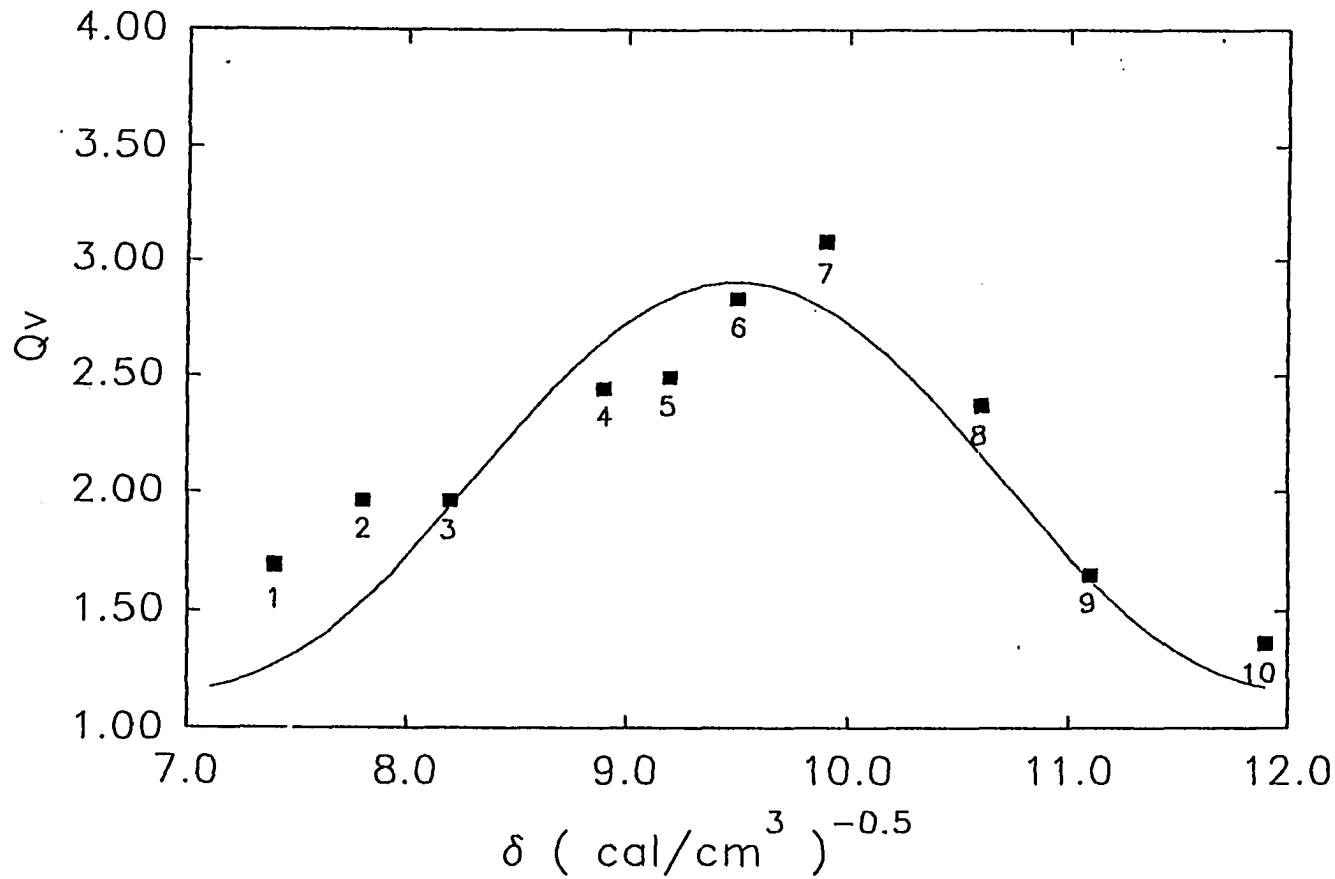

Figure 36. Swelling ratio of Brotherson 1-23B4-B kerogen (35% maturation) as a function of swelling solvent solubility parameter. The line is the theoretical prediction by Flory's model assuming $\bar{M}_c$ = 1430. See Table 17 for solvent identification.

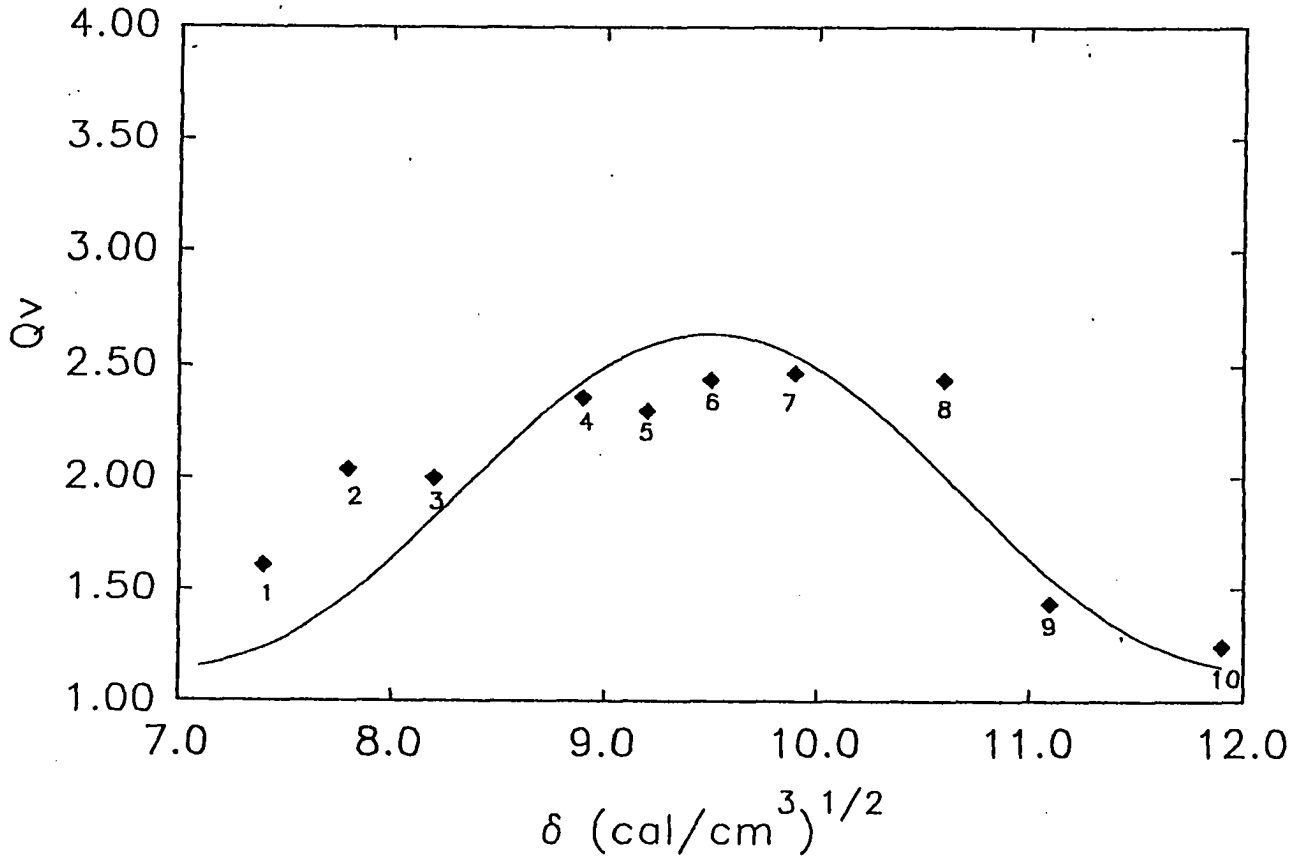

Figure 37. Swelling ratio of Brotherson 1-3B4 kerogen (80% maturation) as a function of swelling solvent solubility parameter. The line is the theoretical prediction by Flory's model assuming $\bar{M}_c$ = 1360. See Table 17 for solvent identification.

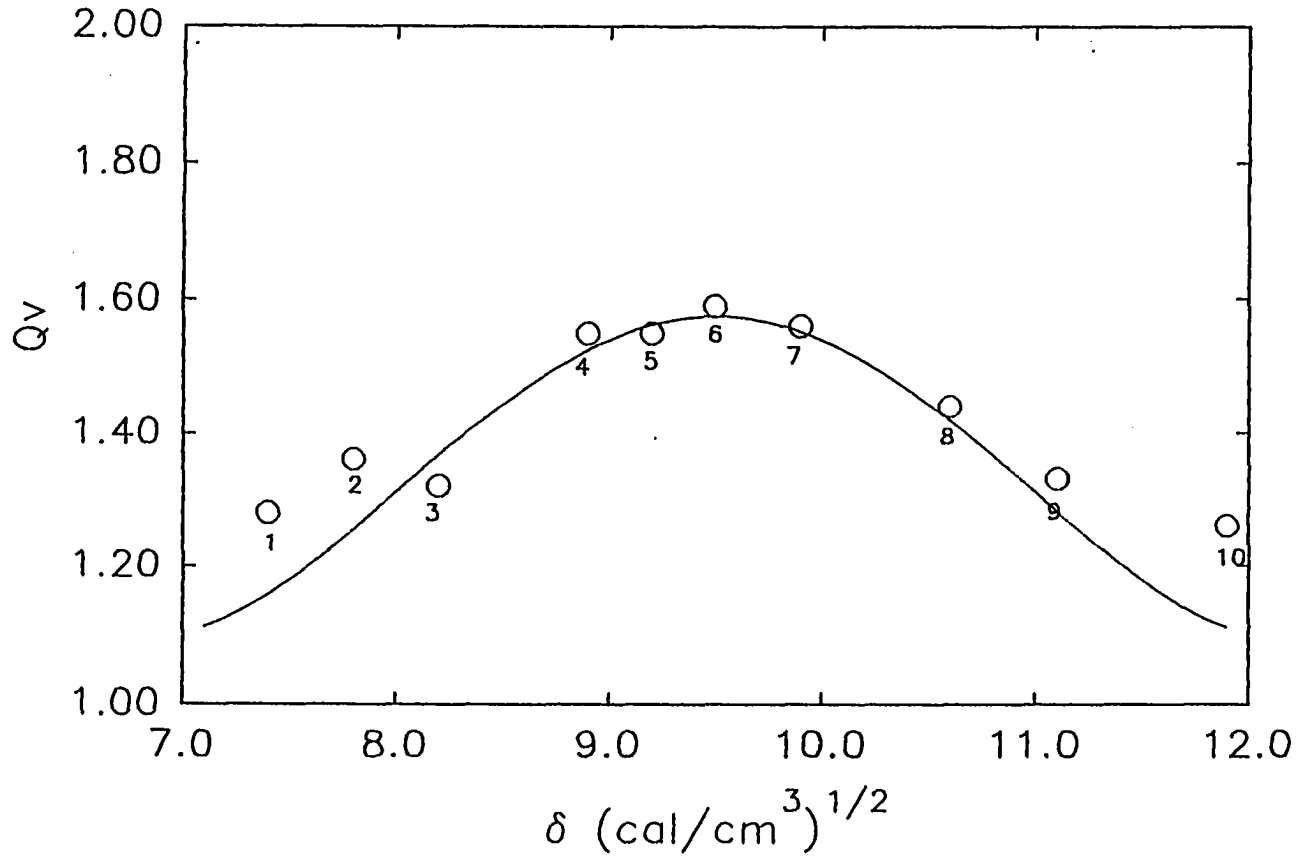

Figure 38. Swelling ratio of Christansen 1-33A5 kerogen (100% maturation) as a function of swelling solvent solubility parameter. The line is the theoretical prediction by Flory's model assuming $\bar{M}_c$ = 290. See Table 17 for solvent identification.

maturation) is different from the two less mature samples. Regular solution theory is followed. The maximum in the swelling ratio increases to ~ 10 $(cal/cm^3)^{1/2}$. The increase in the solubility parameter indicates that the chemical structure of Uinta Basin kerogen has changed. The swelling ratios of this kerogen in the swelling solvents are comparable to the 20% mature sample.

The swelling of Brotherson 1-3B4 kerogen (80% maturation) deviates from regular solution theory behavior. Compared with the three less mature samples, the swelling ratios of this kerogen in poor solvents, such as heptane, methylcyclohexane, cyclohexane, nitroethane, and acetonitrile, remain unchanged; the swelling ratios in good solvents decrease slightly. The swelling ratios of this kerogen in the set of organic solvents display a plateau between 8.9 and 10.6 $(cal/cm^3)^{1/2}$ (see Figure 37). Of the samples, only this one (80% maturation) deviates significantly from regular solution theory behavior. We will nevertheless treat it similarly to the other samples. The different swelling behavior suggests significant structural changes. The solubility parameter of this kerogen can be estimated as ~ 10 $(cal/cm^3)^{1/2}$.

The swelling of Christansen 1-33A5 kerogen (100% maturation) displays the typical behavior predicted by regular solution theory. The maximum of the swelling ratio falls back to 9.5 $(cal/cm^3)^{1/2}$. The swelling ratios of this kerogen in all solvents decreased significantly except for acetonitrile which

is unchanged.

In general, the solvent swelling of the Uinta Basin maturation series follows regular solution theory. The solubility parameter of Uinta Basin kerogen is 9.5 $(cal/cm^3)^{1/2}$ for the <5% and 20% mature samples. This value increases slightly to ~ 10 $(cal/cm^3)^{1/2}$ for the 35% and 80% mature samples and falls back to 9.5 $(cal/cm^3)^{1/2}$ for the 100% mature sample.

The different swelling behaviors of the kerogen maturation series suggest that Uinta Basin kerogen continuously changes its chemical structure with increasing maturation. Examining the van Krevelen diagram of Uinta basin kerogen (Figure 9, section V.2), the O/C ratio appears to be constant during the oil formation stage. The large decrease in H/C ratio (from 1.6 to 0.5), which corresponds to hydrocarbon formation from the kerogen, should increase this kerogen aromaticity. These changes in the chemical composition can been verified using IR spectra of Uinta basin kerogen (Figure 10, section V.2). Because aromaticity increases with maturation and the solubility parameter of aromatics are higher than aliphatics, an increase in kerogen solubility parameter is expected. We have made no investigations in the functional group distributions of the kerogen maturation series and can not rationalize why only small changes in the solubility parameter were observed.

The Flory-Rehner equation was used to calculate the ideal solvent swelling curves for Uinta Basin kerogen samples.[11] The

lines shown in Figures 34-38 are the theoretical prediction of the Flory-Rehner model assuming that (1) the solubility parameter of Uinta Basin kerogen is 9.5 $(cal/cm^3)^{1/2}$, (2) the molar volume of swelling solvent is 113 cm^3/mol, which is the average value of the 10 solvents used, and (3) the number average molecular weight between cross-links of the kerogen is the value given in each figure legend. The calculated curves fit the experimental results reasonably well.

There are few deviations from the Flory-Rehner curves. Heptane swells Uinta Basin kerogen samples greater than predicted. Biphenyl shows greater swelling for Government 33-4 and Brotherson 1-3B4 kerogen samples than expected. The molar volumes of these two solvents are 147 and 154 cm^3/mol. The Flory-Rehner curves displayed in Figures 34-38 are calculated using a smaller value, 113 cm^3/mol. These differences can cause deviations between the experimental data and the calculated curves.

It is important that Uinta Basin kerogen is generally well behaved in solvent swelling studies. The agreement of the Flory-Rehner curves and the experimental results in Figures 34-38 allows us to assign the solubility parameter of Uinta Basin kerogen a value of 9.5 $(cal/cm^3)^{1/2}$. As shown in Figures 34-38, this value varies slightly at the different maturation stages, but the changes are small and do not greatly affect the calculation of the number average molecular weight between cross-links ($\bar{M}_c$) of the kerogen. For example, using δ = 10

$(cal/cm^3)^{1/2}$ for Brotherson 1-23B4-B (35% maturation) and Brotherson 1-3B4 (80% maturation) instead of δ = 9.5 $(cal/cm^3)^{1/2}$ gives $\bar{M}_c$ = 1700 and 1600 instead of $\bar{M}_c$ = 1400 and 1400, respectively. In the following $\bar{M}_c$ calculations, the solubility parameter of Uinta Basin kerogen will be treated as a fixed value throughout maturation.

a.2 Estimation of the number average molecular weight between cross-links ($\bar{M}_c$)of Uinta basin kerogens

The Flory χ parameters were calculated using Equation 7 (section IV.3) for Uinta Basin kerogens and swelling solvent pairs and the results are listed in Table 18. A value of 0.3, which is usually used in solvent swelling of coals,[4,63] was assigned to the entropy contribution, χ_s. A choice of another value of χ_s will give different results for $\bar{M}_c$, but the changes in $\bar{M}_c$ values during kerogen maturation will follow the same pattern.

The volumetric swelling ratios of Uinta Basin kerogen samples were converted to the values on a dry mineral matter free basis using Equations 9 and 10 and the results in Tables 5 and 17. The number average molecular weights between cross-links (reciprocal of the cross-link density) of these samples were then calculated using both the Flory-Rehner and Kovac equations (Equations 3 and 4). Tables 19-23 list $\bar{M}_c$ of Uinta Basin kerogen in five good solvents with solubility parameters

Table 18. χ parameters for Uinta Basin kerogen-solvent pairs

No.	Solvent	V_s (cm^3/mol)[@]	δ $(cal/cm^3)^{1/2}$[@]	χ[#]
1	n-heptane	147.4	7.4	1.40
2	methylcyclohexane	128.3	7.8	0.93
3	cyclohexane	108.7	8.2	0.61
4	toluene	106.8	8.9	0.36
5	benzene	89.4	9.2	0.31
6	tetralin	136.0	9.5	0.30
7	1-methylnaphthalene	138.8	9.9	0.34
8	biphenyl	154.1	10.6	0.56[$]
9	nitroethane	71.5	11.1	0.61
10	acetonitrile	52.6	11.9	0.61

[@]Brandrup, J. and Immergut, E. H., *Polymer Handbook, 3rd ed.*, John Wiley & Sons, 1989.

[#]Calculated using Equation 2 assuming solubility parameter of the kerogen is 9.5$(cal/cm^3)^{1/2}$ and χ_s is 0.30.

[$]Calculated at 75 °C.

Table 19. Number average molecular weight between cross-links of the HCl/HF demineralized Government 33-4 kerogen (<5% maturation)

Solvent	$\bar{M}_c$ (Flory)	$\bar{M}_c$ (Kovac)		
		N=1	N=2	N=3
cyclohexane	2500	9400	6400	5400
toluene	1800	7100	4700	3900
benzene	1200	5000	3300	2800
tetralin	2300	9700	6400	5300
1-methylnaphthalene	2100	8300	5500	4600
average	2000	7900	5300	4400

Table 20. Number average molecular weight between cross-links of the HCl/HF demineralized Brotherson 1-23B4-A kerogen (20% maturation)

Solvent	$\bar{M}_c$ (Flory)	$\bar{M}_c$ (Kovac)		
		N=1	N=2	N=3
cyclohexane	1600	6100	4200	3600
toluene	1000	4000	2700	2300
benzene	790	3100	2100	1700
tetralin	1500	6100	4100	3400
1-methylnaphthalene	1600	6500	4400	3600
average	1300	5200	3500	2900

Table 21. Number average molecular weight between cross-links of the HCl/HF demineralized Brotherson 1-23B4-B kerogen (35% maturation)

Solvent	$\bar{M}_c$ (Flory)	$\bar{M}_c$ (Kovac)		
		N=1	N=2	N=3
cyclohexane	1400	5200	3600	3100
toluene	1000	4100	2800	2300
benzene	800	3100	2100	1800
tetralin	1600	6600	4400	3600
1-methylnaphthalene	2300	9400	6200	5200
average	1400	5700	3800	3200

Table 22. Number average molecular weight between cross-links of the HCl/HF demineralized Brotherson 1-3B4 kerogen (80% maturation)

Solvent	$\bar{M}_c$ (Flory)	$\bar{M}_c$ (Kovac)		
		N=1	N=2	N=3
cyclohexane	2000	7500	5200	4400
toluene	1100	4500	3000	2500
benzene	770	3000	2000	1700
tetralin	1300	5200	3500	2900
1-methylnaphthalene	1600	6100	4100	3500
average	1400	5300	3600	3000

Table 23. Number average molecular weight between cross-links of the HCl/HF demineralized Christansen 1-33A5 kerogen (100% maturation)

Solvent	$\bar{M}_c$ (Flory)	$\bar{M}_c$ (Kovac)		
		N=1	N=2	N=3
cyclohexane	230	850	610	540
toluene	290	1080	770	660
benzene	220	830	590	510
tetralin	360	1300	950	820
1-methylnaphthalene	370	1400	970	840
average	290	1100	780	670

between 8.2 $(cal/cm^3)^{1/2}$ and 9.9 $(cal/cm^3)^{1/2}$. The other swelling solvents used are poorer solvents and the $\bar{M}_c$ of the kerogens calculated in the these solvents are unreasonable and were discarded.

The Flory-Rehner $\bar{M}_c$ values are 2000, 1300, 1400, 1400, and 290 for the <5%, 20%, 35%, 80%, and 100% mature Uinta Basin kerogen samples, respectively. The Flory-Rehner equation yields reasonable values of $\bar{M}_c$ for the four less mature samples and a small value of $\bar{M}_c$ for the 100% mature sample. The Flory-Rehner equation assumes that the polymer network is tetrafunctionally cross-linked and that the chains are long and flexible. We have no macromolecular structural information about these samples and do not know how much their structures deviate from those assumptions. We do not know the quantitative reliability of the $\bar{M}_c$ values calculated using the Flory-Rehner equation, but have confidence in their trend of the changes in the macromolecular structure during kerogen maturation.

The Kovac equation gives a better description for the 100% mature sample because it is highly cross-linked and its $\bar{M}_c$ violates one of the key assumptions of the Flory-Rehner equation that the chain length between cross-links obey a Gaussian distribution. Quantitatively, the Kovac equation requires a correct estimated the number of the freely ratable groups (N), something impossible based on these data. The goal

of this project is to follow the changes in $\bar{M}_c$ during maturation, therefore either the Flory-Rehner or the Kovac equation can be used for this purpose.

a.3 Changes in the cross-link density of Uinta Basin kerogen during maturation

The results calculated from solvent swelling experiments (see Tables 19 - 23) provide a qualitative picture of the changes in the cross-link density of Uinta Basin kerogen during maturation. The Flory-Rehner $\bar{M}_c$ deceases at the beginning of maturation. This value remains constant (1300 ~ 1400) during 20% to 80% maturation and then plunges to a small value (290) at 100% maturation. Overall, the number average molecular weight between cross-links (reciprocal of the cross-link density) of Uinta basin kerogen appears to continuously decrease with increasing maturation. This process is slow before 80% maturation and rapidly accelerates as the kerogen matures further. The $\bar{M}_c$ obtained from the Kovac equation follows the same trend.

Type I kerogen maturation has been extensively characterized and well modelled in the literature.[83,118] Figure 39 shows the kinetic and thermal history model developed by Sweeney et al. for the basin from which our samples come.[83] The plot displays the relationship between the percent of kerogen converted (or the transformation ratio, the ratio of free hydrocarbons to the sum of free and pyrolyzable hydrocarbons

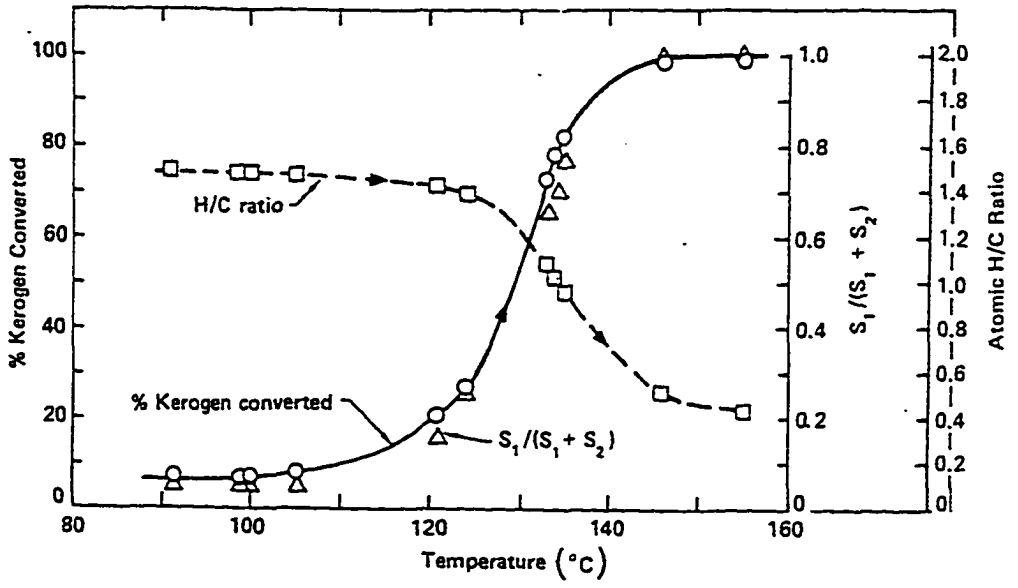

Figure 39. A kinetic and thermal history model for Type I kerogen.

Sweeney, J. J.; Burnham, A. K.; Braun, R. L. *Am. Assoc. Petro. Geol. Bull.*, **1987**, 71, 967-985.

in the oil shale, determined by Rock-Eval pyrolysis.), the kerogen H/C ratio, and the maximum burial temperature attained by Type I kerogen. This model demonstrates that the maximum rate of oil conversion of Type I kerogen occurs within a very narrow temperature window (from 120 °C to 140 °C) where the kerogen maturity increases from 20% to 80% and the H/C ratio sharply decreases from 1.4 to 0.4. A direct application of this model to Uinta Basin kerogen at different burial depths is displayed in Figure 15 (see section V.2).

Figure 40 displays the changes in Flory-Rehner $\bar{M}_c$ (reciprocal of kerogen cross-link density, see Tables 19-23) as a function of maturation on the kinetic and thermal history model (Figure 15). The plot shows a good correlation between the changes in the cross-link density and the calculated % oil generation based on Sweeny's kinetic and thermal history model. Further comparing Figures 39 and 40, the correspondence between the maturation based on the transformation ratio (determined by Rock-Eval pyrolysis) and the changes in kerogen cross-link density is clearly noticeable. Combining the results of changes in cross-link density and Sweeny's kinetic and thermal history model, we can state: (1) During 5% to 20% maturation, the kerogen is slowly converted to oil. Kerogen H/C ratio does not change (see Figure 39) and $\bar{M}_c$ decreases slightly. These indicate that kerogen fragmentation and network reconstruction slowly occur. (2) During 20% to 80% maturation, the kerogen is rapidly converted to oil. Kerogen

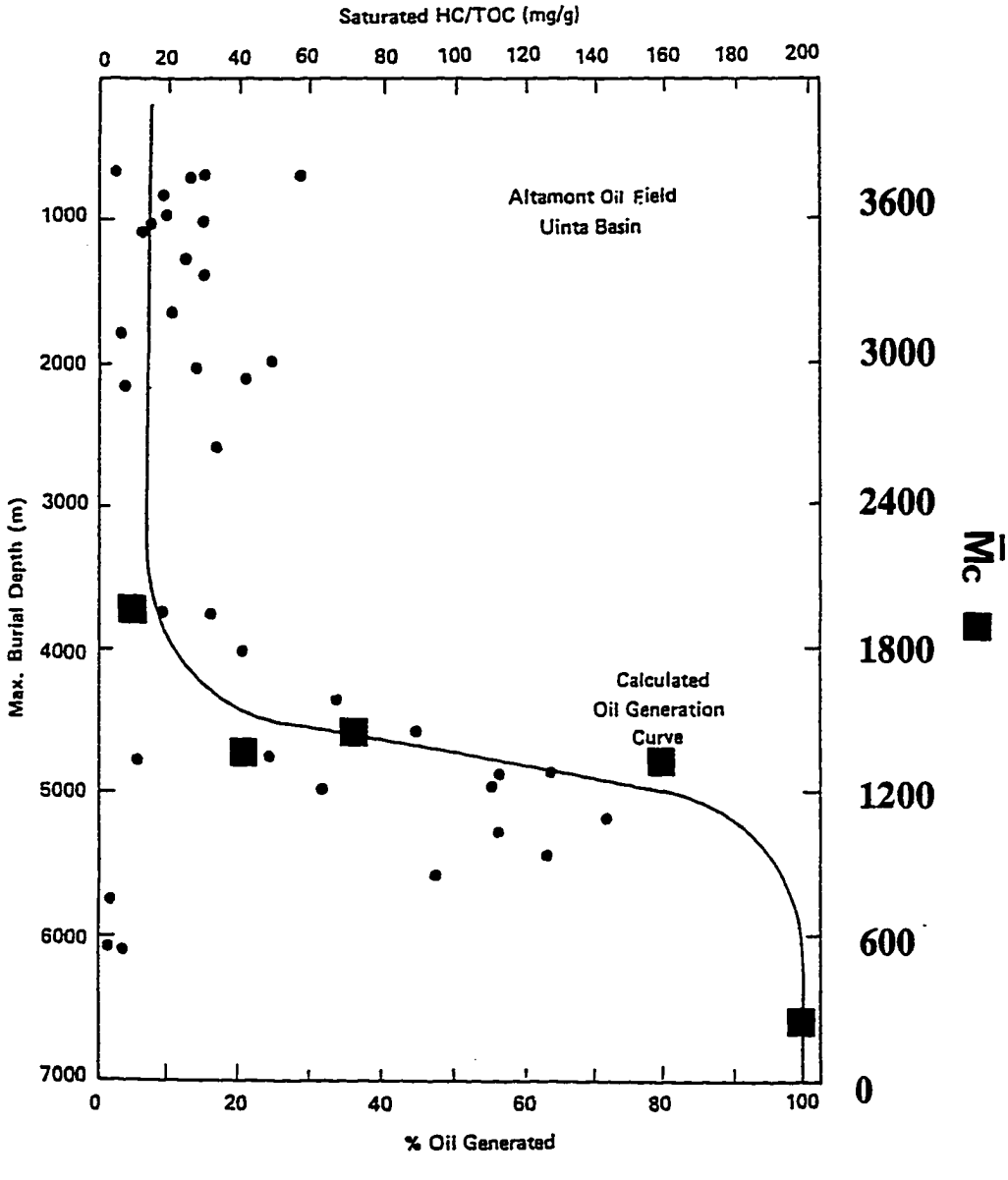

Figure 40. Changes in $\bar{M}_c$ (reciprocal of the cross-link density) of Uinta Basin kerogen and the predicted oil generation in the Uinta Basin.[@]

[@]Sweeney, J. J.; Burnham, A. K.; Braun, R. L. *Am. Assoc. Petro. Geol. Bull.*, **1987**, 71, 967-985.

H/C ratio decreases sharply from 1.4 to 0.4 (see Figure 39) and $\bar{M}_c$ remains unchanged. These indicate that the kerogen rapidly fragments and the bond cleavage does not result in significant network reconstruction. (3) During 80% to 100% maturation, oil generation is slowed down. Kerogen H/C ratio slowly decreases (see Figure 39) and $\bar{M}_c$ sharply deceases. These indicate that kerogen fragmentation becomes slow and network reconstruction rapidly accelerates.

Figure 41 shows generalized models for Type I, II, and III kerogens during maturation.[118] The changes in vitrinite reflectance for the classical kerogen types are compared under a similar thermal history. The Type I kerogen model shows that it converts to oil more quickly than Type II and III kerogens. Interestingly, the relationship between the transformation ratio of Type I kerogen and its vitrinite reflectance resembles the kinetic and thermal history model shown in Figures 39 and 15 (see section V.2).[83] The data presented in the literature show that Type I kerogen maturation has a universal pattern,[1,7,83,118] typically displayed in Figures 15, 39, and 41. We suggest that the solvent swelling technique be applied on Type I kerogen from other geological environments and results be tested against the present knowledge.

Measuring the changes in kerogen cross-link density which occur during maturation provides a new way of probing and characterizing maturation chemistry. As a tool for

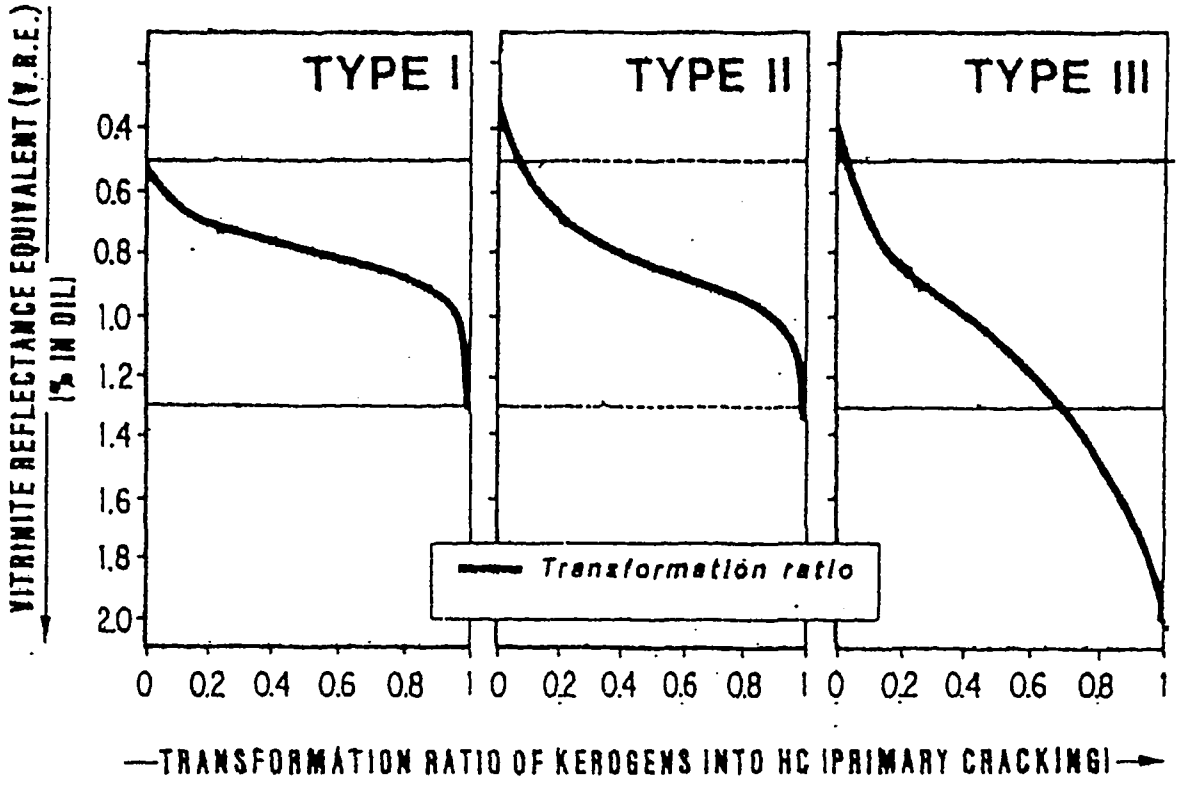

Figure 41. Generalized kerogen maturation models for the classical kerogen types under a similar thermal history.

Durand, B. *Org. Geochem.*, **1987**, 13, 445-459.

the exploration geochemist, it is independent of the techniques now being used. It has the advantage of experimental simplicity and requires small amount of samples.

One of the major difficulties in predicting oil generation is that the thermal history of a sedimentary basin cannot be directly determined.[1,54,83] Complex geological and geochemical factors which govern the sediments include sediment thermal conductivity, heat flow, surface temperature, stratigraphic movements, surface erosion, etc.[87] These factors are often too complicated to determine completely. characterizing the changes in Type I kerogen cross-link density provides a hope that a scale of thermal maturation can be established based on the changes in the macromolecular structure.

Measuring the changes in kerogen cross-link density can also provide important information for oil migration studies. "The key to predicting the quantities and compositions of hydrocarbon expelled from real source rocks lies in the proper modelling not only of hydrocarbon generation but also of primary migration."[53] Primary migration is the movement of hydrocarbons which are generated from kerogen maturation within and out of the source rock.[1,7] It is one of the most important variables for petroleum formation.

Stainforth and Reinders recently suggested that primary migration is controlled by activated diffusion processes.[53] At the molecular level, bitumen molecules and kerogen network

undergo thermal vibrations. These movements generate and redistribute free volume continuously. Bitumen molecules can move through the cross-linked kerogen network where bitumen is dissolved by thermally activated diffusion. The effective diffusion coefficient (D_i) of a bitumen species i in the kerogen network can been expressed as

$$D_i = f\lambda^2 (kT/h) \exp(-\Delta E/RT) \qquad (12)$$

where λ is the diffusion jump length, ΔE is the activation free energy of diffusion, T is the temperature, and k, h, and R are Boltzmann, Planck, and universal gas constants. f in the equation represents other factors including the diffusant size, shape, concentration, and the properties of the kerogen network, such as the cross-link density.

The results of the changes in the kerogen cross-link density provide a qualitative description for understanding the effects of kerogen maturation on the rate of the bitumen diffusion. The diffusion of bitumen molecules through the kerogen network should become more difficult as kerogen matures because (1) increasing the kerogen cross-link density increases the tortuosity of the kerogen network,[53] and (2) increasing the kerogen cross-link reduce the molecular chain motions, thus kerogen network changes to a more rigid material.[119]

Diffusion of small molecules through cross-linked rubbery polymers has been studied by Chen and Ferry.[119] Figure

42 shows log D of n-hexandecane as a function of the cross-link density for three rubbers. The plot demonstrates that Log D of the small molecule decreases with increasing the polymer cross-link density.

The results of the changes in kerogen cross-link density reveal that the cross-link density of Type I kerogen slowly decreases at the first 80% maturation and sharply decreases as the kerogen further matures. These suggest that the rapid decrease in the kerogen cross-link density during maturation may greatly reduce the diffusivity of the bitumen through the kerogen network. Oil migration is a complex process that is controlled by many parameters.[53] The kerogen cross-link density must play an active role on the molecular scale. Further testing the results of the changes in the kerogen cross-link density can provide important information for petroleum migration studies.

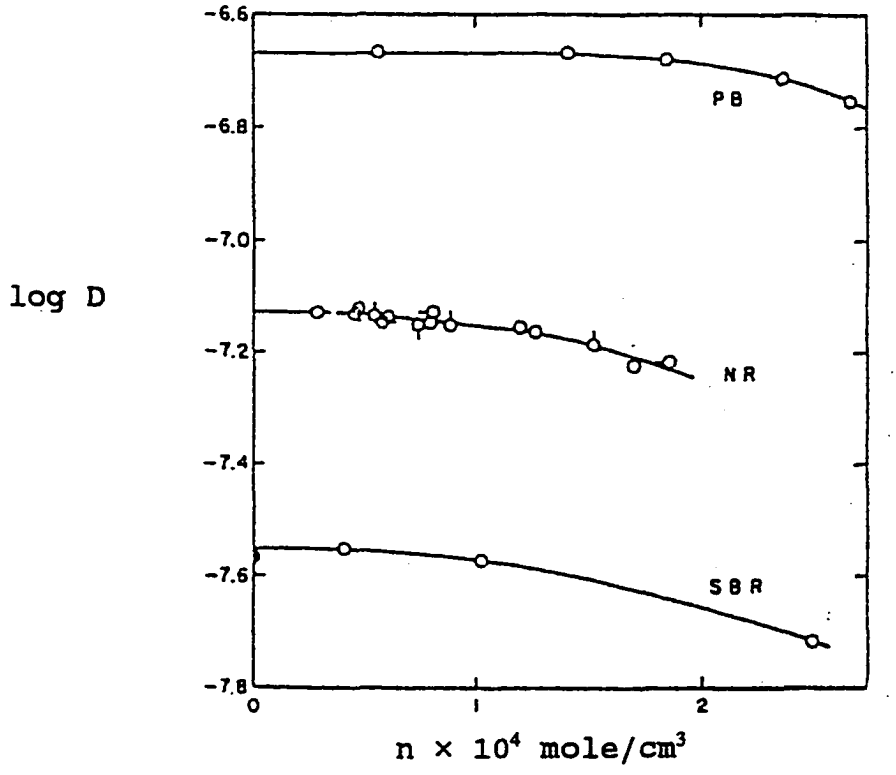

Figure 42. Log D of n-hexandecane at 25 °C plotted against the rubber cross-link density. PB: polybutadiene. NR: natural rubber. SBR: styrene-butadiene rubber.

Chen, S. P.; Ferry, J. D. *Macromol.* **1968**, 1, 270-278.

a.4 Amounts of Uinta Basin bitumen extracted

Uinta Basin bitumen samples were isolated from the kerogen concentrates by Soxhlet extraction with toluene. After the extraction, the solvent was removed using rotary evaporation followed by vacuum oven drying. Table 24 lists the amounts of bitumen extracted and the burial depths of the Uinta Basin maturation series. The amounts of bitumen are expressed as the ratios of bitumen extracted to total organic carbon. These data are based on the assumption that demineralized kerogen samples do not contain inorganic carbon (see Table 5). The maximum burial depths were estimated assuming a value of 1800 m of overburden removed for these oil shale samples.[83,84,87] Figure 43 displays the amounts of bitumen extracted from the maturation series as a function of maximum burial depth.

Tissot et al. studied 57 rock samples which cover a wide burial range in the Altamount and Redwash fields of the Uinta Basin.[84] Their results of Soxhlet extraction with chloroform are compared with the amounts of bitumen extracted from the Uinta Basin maturation series in Figure 43. The two sets of data agree well and display no obvious trend.

Determining the amount of bitumen using Soxhlet extraction is a traditional way to estimate the relative amount of oil that has been generated (or kerogen maturation).[1] The amount of bitumen produced is expected to increase with increasing the burial depth, but the

Table 24. Amounts of bitumen extracted from the Uinta Basin kerogen maturation series.

	Present burial depth (m)[@]	Maximum burial depth (m)[#]	Amount of Bitumen[$] (mg/g TOC)
Government 33-4	1630	3430	189
Brotherson 1-23B4-A	2560	4360	162
Brotherson 1-23B4-B	2780	4580	174
Brotherson 1-3B4	3260	5060	124
Christansen 1-33A5	3610	5410	175

[@]References 83, 87, and Burnham, A. K. *Personal Communication*.

[#]Estimated assuming 1800 m of erosion.[83,84]

[$]The ratio of toluene extract (mg) to total organic carbon (g).

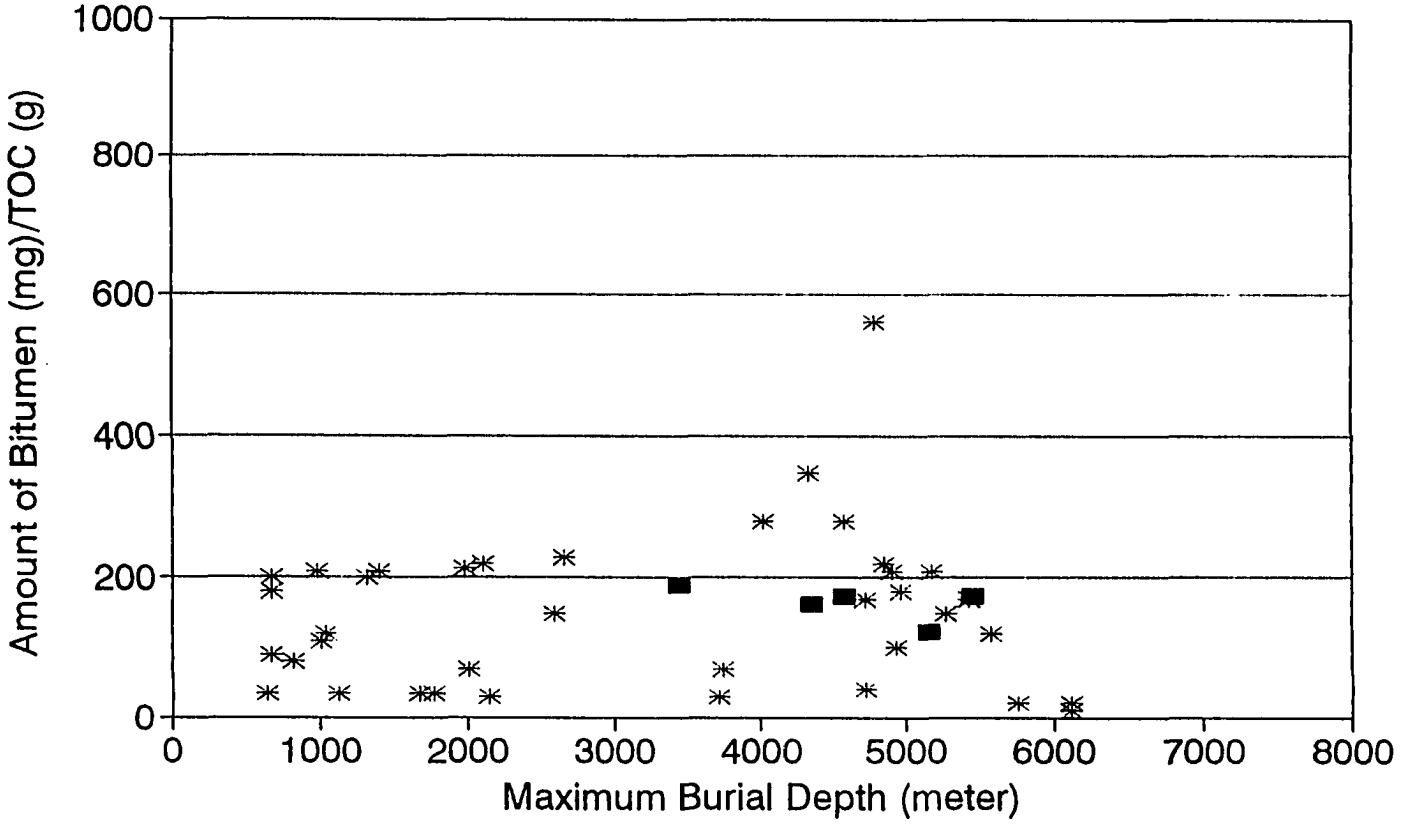

Figure 43. Amounts of Uinta Basin bitumen extracted (mg of bitumen per gram of TOC) as a function of the maximum burial depth. (■) the Uinta Basin maturation series. (*) the results published by Tissot et al.[84]

experimental results can be influenced by three factors.[1]

First, oil cracking in the rock can convert heavy components to smaller molecules and gases which migrate out from the kerogen network faster than the larger ones.[1] This will reduce the amount of bitumen remaining in an oil shale. Sweeney et al. calculated oil formation and degradation at various depths in the Uinta Basin using their thermal history model.[83] The results for 11 wells, which cover Uinta Basin kerogen from 7 to 100% maturation, are listed in Table 25. The data demonstrate that cracking oil to gas during the oil window is negligible in the Uinta Basin. Oil cracking should not affect the amounts of bitumen determined for the maturation series.

Second, oil coking condenses small bitumen molecules to larger ones, leading ultimately to an insoluble network kerogen.[1] This process increasingly incorporates heavier oil components into the kerogen and the oil remaining becomes more volatile with increasing maturation.[83] Table 25 demonstrates that 2% of bitumen is coked below 10% maturation and 30% of bitumen is coked at 100% maturation in the Uinta Basin.[83] Figure 44 illustrates how the low-boiling-point fraction increases with increasing burial depths.[83] The 7% mature sample (13 Broadhurst) has almost no fraction boiling below 200 °C and the 100% mature sample (shell Christensen) has over 60% boiling below 200 °C. The procedure which is used for determining the amount of Uinta Basin bitumen involves

Table 25. Kerogen and Bitumen fractions at selected depths in the Uinta Basin[83]

	Depth[1] (m)	T_{max} (°C)	H/C	O/C	Oil Ungenerated	Oil Coked	Oil Cracked	Liquid Oil
Energy Res. Gp. 13 Broadhurst	1,433	91	1.48	0.044	0.933	0.022	0.00	0.045
Energy Res. Gp. 13 Broadhurst	1,756	99	1.48	0.042	0.930	0.023	0.00	0.048
Davis Oil 5 Pariette Bench	927	100	1.48	0.042	0.930	0.023	0.00	0.047
Shell 1-11B4 Brotherson	2,003	105	1.47	0.041	0.925	0.024	0.00	0.051
Shell 1-11B4 Brotherson	2,643	121	1.42	0.037	0.787	0.066	0.00	0.147
Energy Res. Gp. 13 Broadhurst	2,758	124	1.39	0.036	0.670	0.101	0.00	0.229
Davis Oil 5 Pariette Bench	2,246	133	1.07	0.034	0.271	0.220	0.00	0.506
Shell 1-11B4 Brotherson	3,164	134	1.02	0.034	0.225	0.234	0.003	0.538
Gulf 1 Duchesne Co. Unit	2,747	135	0.95	0.033	0.176	0.249	0.004	0.571
Shell 1-33A5 Christensen	3,453	146	0.51	0.029	0.000	0.302	0.024	0.674
Shell 1-11B4 Brotherson	4,004	155	0.44	0.025	0.000	0.302	0.075	0.623

[1]Present-day burial depth.

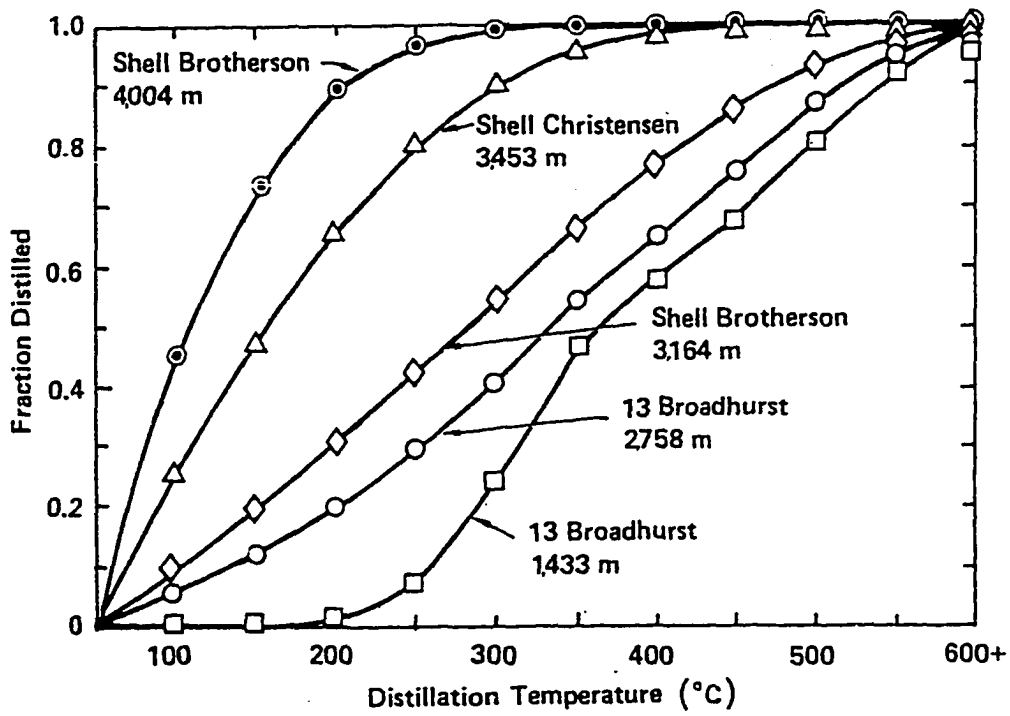

Figure 44. Bitumen boiling point distributions for selected depths in the Uinta Basin.

Sweeney, J. J.; Burnham, A. K.; Braun, R. L. *Am. Assoc. Petro. Geol. Bull.*, **1987**, 71, 967-985.

evaporating solvent from the bitumen extract solution. A certain amount of lighter bitumen molecules will be lost during this process. Table 26 shows the estimated amounts of oil coked and lost during bitumen extraction and oil migration.

Finally, oil migration removes part of bitumen from the source rock. Rock-Eval pyrolysis conducted on Uinta Basin oil shale demonstrated that serious oil migration occurred in the Altamont field when kerogen reached over 70% maturity (~ 2900 m burial depth). Approximately 60-80% of the oil in the source rock has been expelled at higher maturity.[92] Since the kerogen maturation series were collected from the same oil field, the amounts of bitumen extracted from the 80% and 100% mature samples were reduced by oil migration.

In summary, the amounts of bitumen which were isolated from the Uinta Basin maturation series agree with the literature values. However, the data cannot be trusted for estimating kerogen maturation because significant amounts of bitumen might have lost during isolation and migration.

a.5 The molecular weight distributions of Uinta Basin bitumen

Molecular weight distributions of Uinta Basin bitumen samples were determined using ^{252}Cf plasma desorption mass spectrometry (PDMS). The PDMS spectra of these samples are shown in Figures 45-49. While all the spectra display a similar shape, the distributions are slightly different. The

Table 26. Amounts of oil coked during maturation and amounts of oil lost during extraction procedures for the kerogen maturation series.

	Present burial depth (m)[@]	% of Bitumen extracted[$]	% of oil coked[#]	% of oil lost during removing solvent[•]
Government 33-4	1630	13.4	2	2
Brotherson 1-23B4-A	2560	13.2	8	10
Brotherson 1-23B4-B	2780	13.5	10	20
Brotherson 1-3B4	3260	7.8	25	30
Christansen 1-33A5	3610	10.6	30	60

[@]References 83, 92, and Burnham, A. K. *Personal Communication*.

[$]On a dry mineral matter free basis.

[#]Estimated using Table 25.

[•]Estimated using Figure 44 assuming that fractions with b.p. below 200 °C are lost.

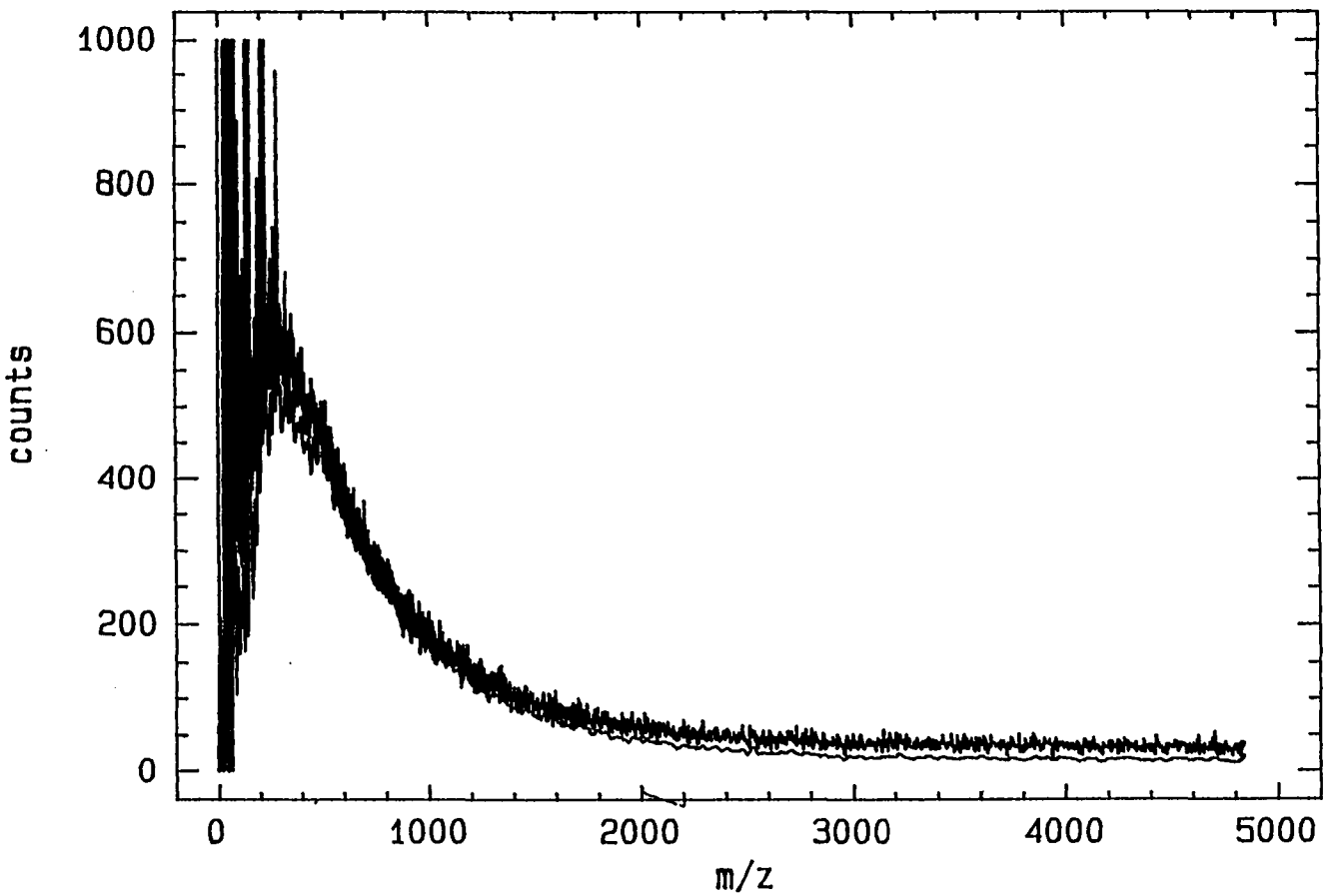

Figure 45. PDMS spectrum of Government 33-4 bitumen. Raw data (upper line) and the smoothed spectrum with the Mylar disk background subtracted (lower line).

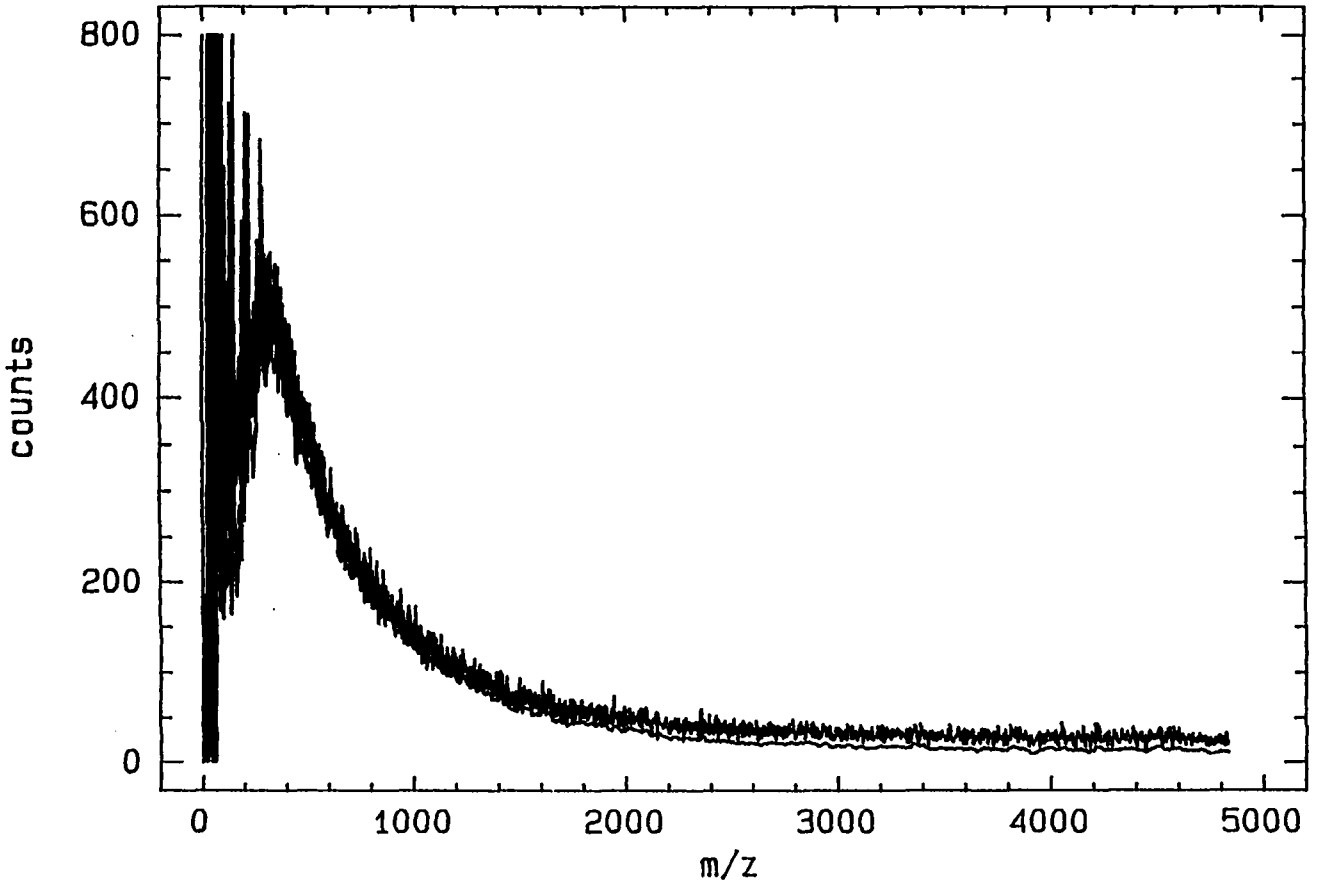

Figure 46. PDMS spectrum of Brotherson 1-23B4-A bitumen. Raw data (upper line) and the smoothed spectrum with the Mylar disk background subtracted (lower line).

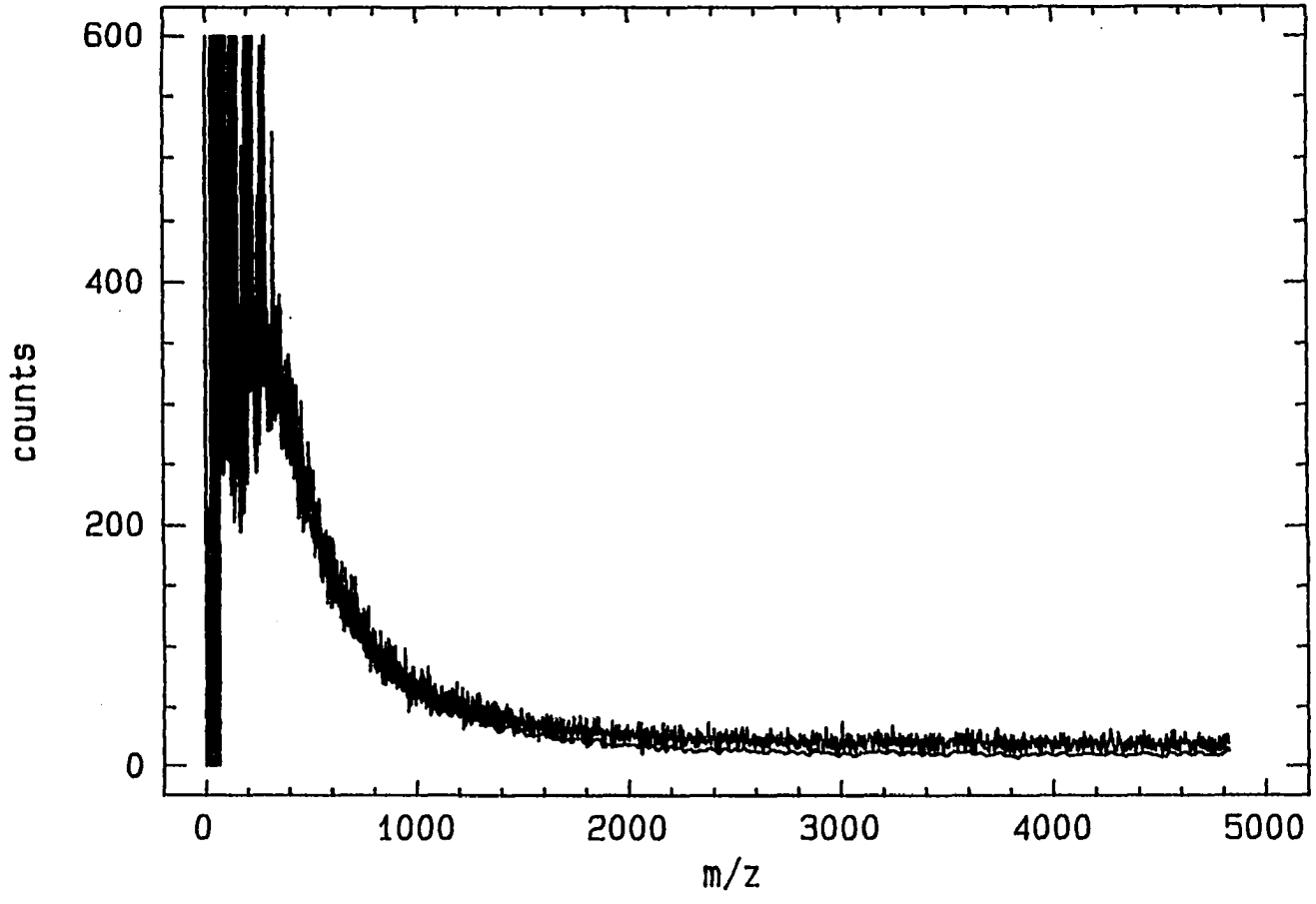

Figure 47. PDMS spectrum of Brotherson 1-23B4-B bitumen. Raw data (upper line) and the smoothed spectrum with the Mylar disk background subtracted (lower line).

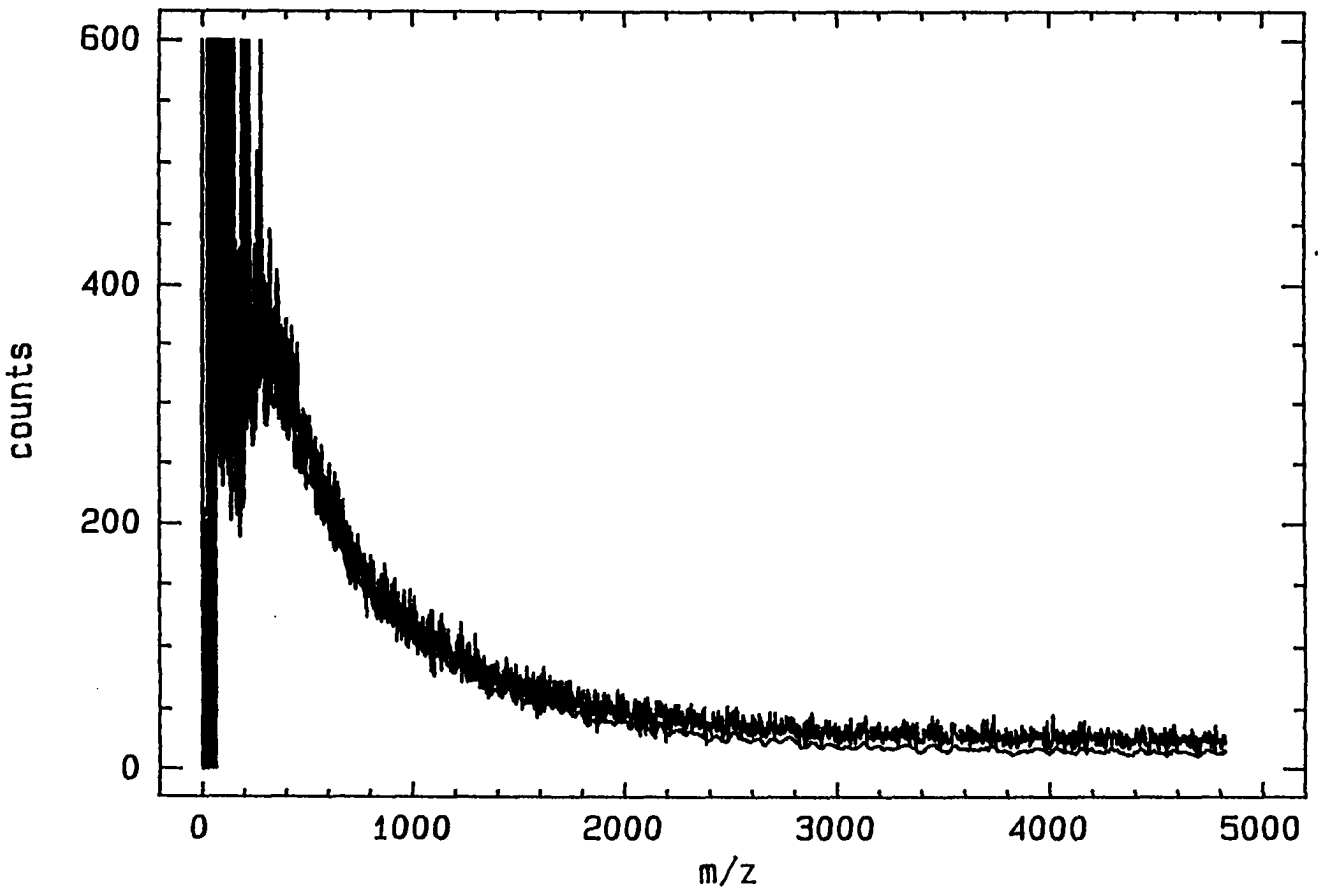

Figure 48. PDMS spectrum of Brotherson 1-3B4 bitumen. Raw data (upper line) and the smoothed spectrum with the Mylar disk background subtracted (lower line).

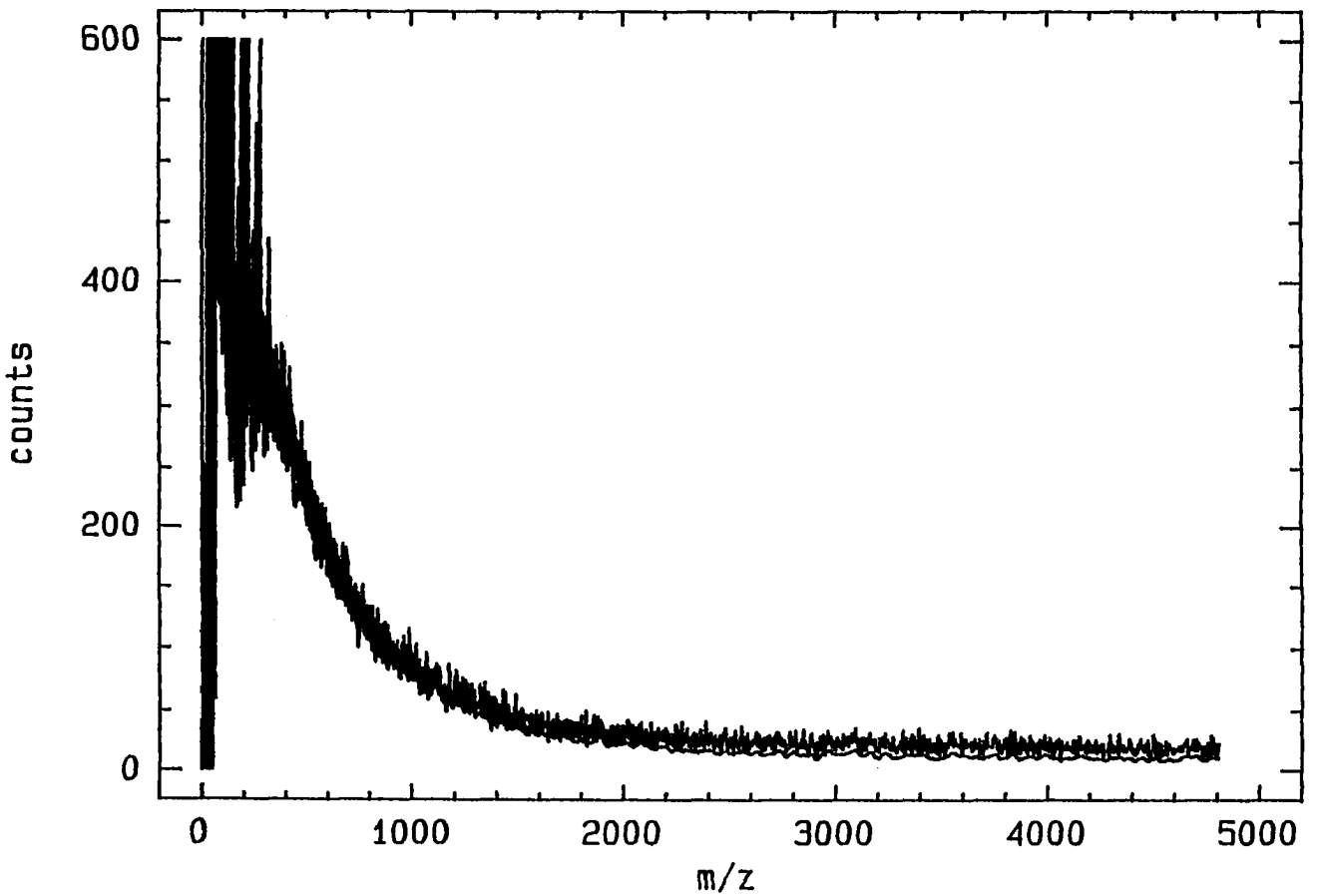

Figure 49. PDMS spectrum of Christansen 1-33A5 bitumen. Raw data (upper line) and the smoothed spectrum with the Mylar disk background subtracted (lower line).

35% mature and 100% mature samples appear to have narrower distributions than the other three samples. Number and weight average molecular weights of bitumen samples were calculated from the PDMS spectra and the results are listed on Table 27. The number average molecular weights of these samples change little and display no obvious trend with the extent of maturation.

To correlate bitumen molecular weight distribution with kerogen maturation studies, all of bitumen must be preserved in the source rock. It has been shown that oil cracking, coking, and migration influence the amount of bitumen extracted from an oil shale. These factors will also alter the bitumen molecular weight distribution during maturation. For the Uinta Basin maturation series, oil cracking does not occur within the oil window and will not be considered.[83]

The effect of oil coking on the bitumen molecular weight distribution can be predicted using the classical polycondensation theory.[11,55] The weight fractions of various molecular species in a trifunctional polycondensation are displayed in Figure 50.[11] The average molecular weights of oligomers in a polycondensation initially increase with increasing extent of reaction. After the gel point, the species in the sol decrease in average size because the larger and branched molecules are preferentially tied into the gel. For a kerogen-bitumen system, the gel is the kerogen and the sol is the bitumen. Oil coking is a polymerization process

Table 27. Average molecular weights of Uinta Basin bitumen calculated from PDMS spectra.

	% Maturation[@]	Mn[$]	Mw[$]
Government 33-4	<5	560	930
Brotherson 1-23B4-A	20	540	900
Brotherson 1-23B4-B	35	400	700
Brotherson 1-3B4	80	560	1060
Christansen 1-33A5	100	440	800

[@]Determined by thermal history model.[83]

[$]Calculated from PDMS spectra.

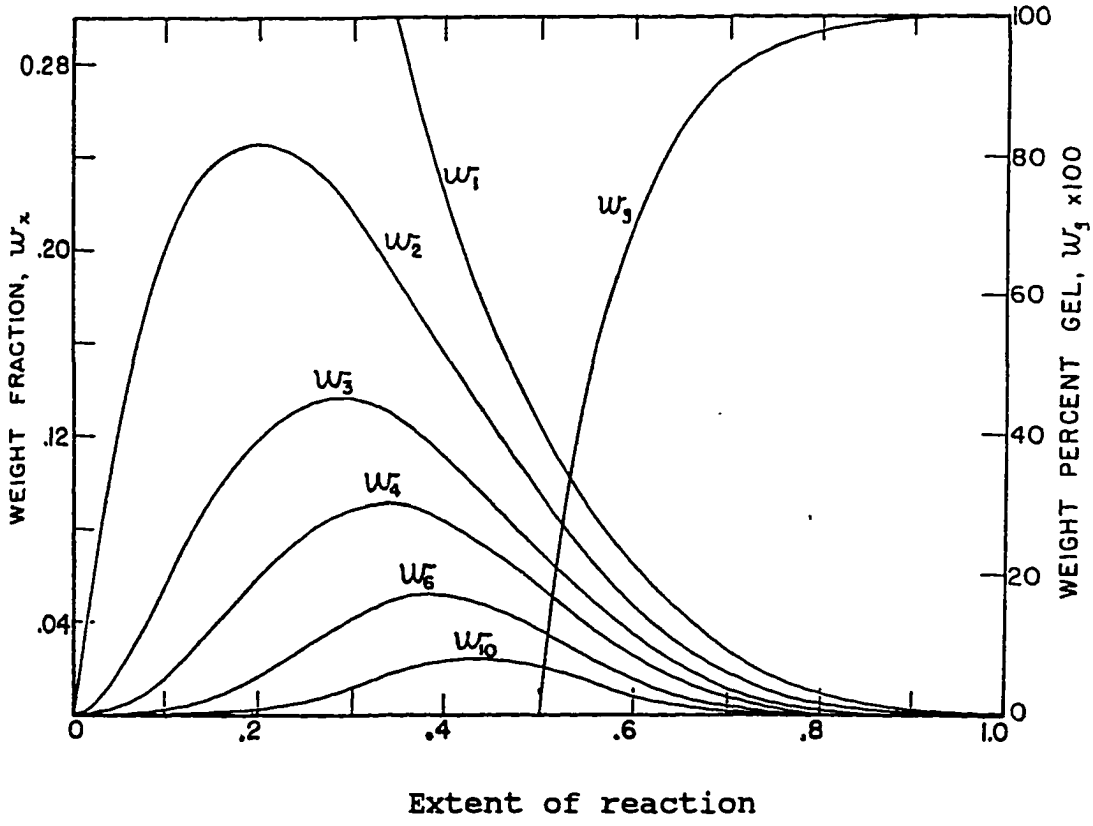

Figure 50. Weight fractions of various species in trifunctional polycondensation as a function of the extent of reaction.

Flory, P. J. *Principle of Polymer Chemistry*, Cornell University Press: Ithaca, 1953.

during which the heavier bitumen molecules are likely to be coked and to become incorporated into the kerogen network. These will narrow the bitumen molecular weight distribution and decrease the average molecular weights of bitumen.

Oil migration has a different effect to the bitumen molecular weight distributions. Because small and nopolar molecules migrate faster than large and polar molecules,[1] the shale bitumen remaining after oil migration should contain more high molecular weight species than the original bitumen, thus the average molecular weight should increase. As stated in the last section (VII a.4), serious oil migration started from 70% maturation in the Altamont field of the Uinta Basin.[92] The molecular weight distributions of the 80% and 100% mature samples were flawed due to migration.

Evolution of bitumen during maturation is more complicated than that of kerogen. Bitumen can be cracked to gas, can be coked to kerogen, and can migrate out of the source rock (see Figure 51). Determination of the amounts of bitumen and bitumen molecular weight distributions requires knowledge of cracking, coking, and migration. We cannot quantitatively estimate these factors for the Uinta Basin maturation series studied. Therefore, the results of bitumen samples will not be used to correlate with the kerogen cross-link densities measured.

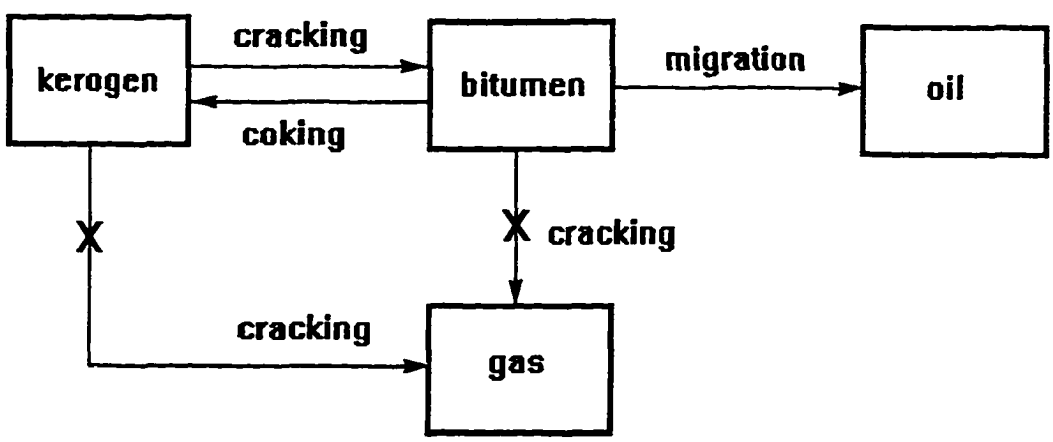

Figure 51. Evolution of Type I kerogen and bitumen during catagenesis. Cracking kerogen and bitumen to gas is neglected during the oil window.

b. Type I Kerogen Maturation Model

Two kerogen maturation models in the literature address the changes in the macromolecular structure and are displayed in Figure 52.[53,54] Both models have been used as a basis for the kinetic models. One is network depolymerization during which kerogen is thermally converted to smaller fragments. Depolymerization includes successive reactions and allows almost all the kerogen to be cracked to bitumen. As stated earlier (IV.2), this model predicts that kerogen cross-link density continuously decreases during maturation. Our experimental results shown in Figure 40 (VII a.3) against the depolymerization model and demonstrate that the overall trend of the cross-link density of Type I kerogen increases during maturation.

The other kerogen maturation model is defunctionalization during which labile bonds cleave off an inert kerogen skeleton. Defunctionalization includes parallel independent reactions and directly produces oil and gas by cracking the appended bonds from the inert core. This model predicts that the kerogen cross-linked density does not change during maturation. The defunctionalization model appears to agree with part of our experimental results, Type I kerogen cross-link density does not change during 20% to 80% maturation. But, this model can not explain the increases in the cross-link density during 5% to 20% maturation and during 80% to 100%.

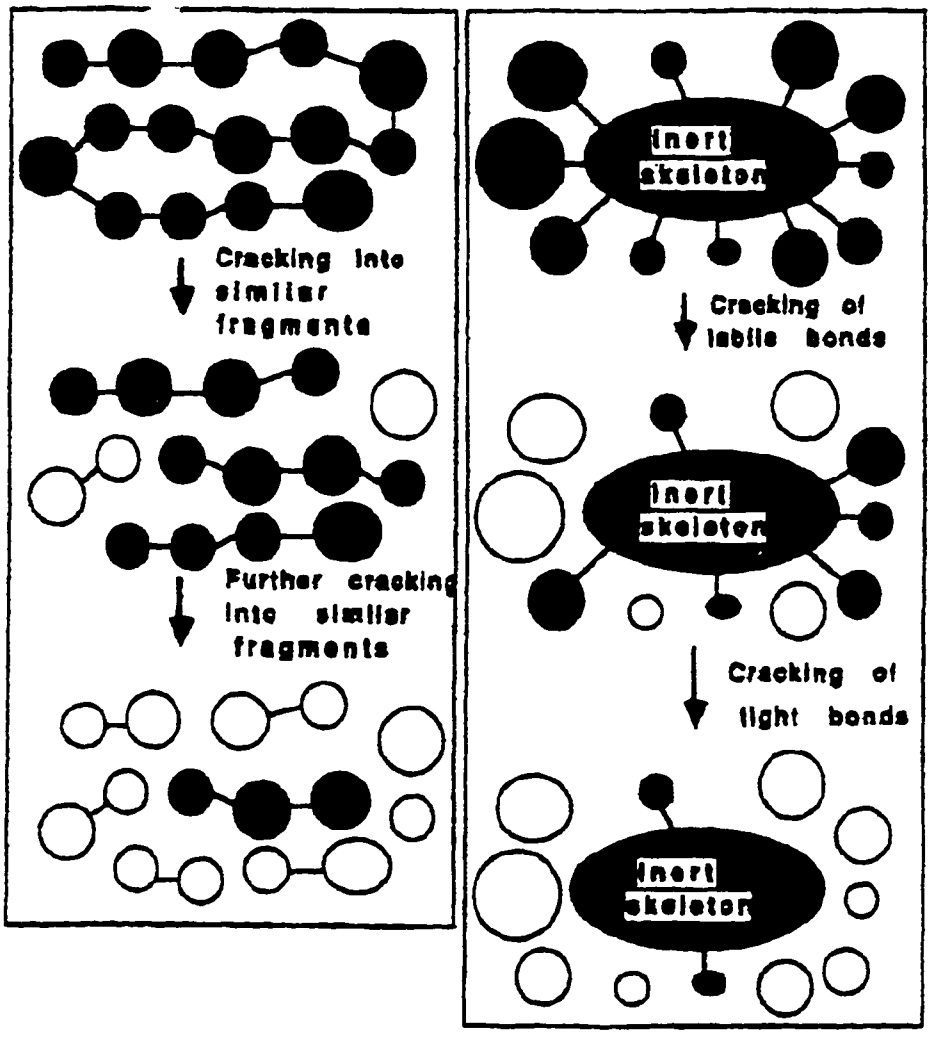

Figure 52. Depolymerization and defunctionalization models for kerogen maturation. (O) extractable, (●) non-extractable.

Stainforth, J. G.; Reinders, J. E. A. *Org. Geochem.*, **1989**, 16, 61-74.

In this thesis, we directly measured the changes in the cross-link density of Type I kerogen during the maturation process. The results reveal a very different scheme for Type I kerogen maturation. The data obtained from kerogen maturation experiments (Tables 19-23 and Figure 40) demonstrate that Type I kerogen maturation is neither a depolymerization nor a defunctionalization process. It appears to be a fragmentation accompanied by a network reconstruction process. During Type I kerogen maturation, small molecular groups cleave off from the kerogen network to form bitumen and the kerogen continuously changes to new chemical structures which slowly reconstruct to increase the cross-link density. Fragmentation reactions dominate the first 80% of maturation. As the kerogen matures further, the reconstruction rapidly accelerates and oil formation slows down. Figure 53 schematically displays this fragmentation/reconstruction model. Oil cracking, coking, and migration are not considered in the scheme.

The proposed Type I kerogen maturation model does not specify the type of fragmentation reactions occurring during oil formation. Examining Siskin's model for Green River kerogen (see Figure 5, III.3), selective bond fragmentation seems to be favored. Table 28 lists C-C bond energies for homolytic dissociation.[120] The data demonstrate that breaking C-C bonds for model compounds requires different energies. During kerogen maturation, fragmentation reactions may

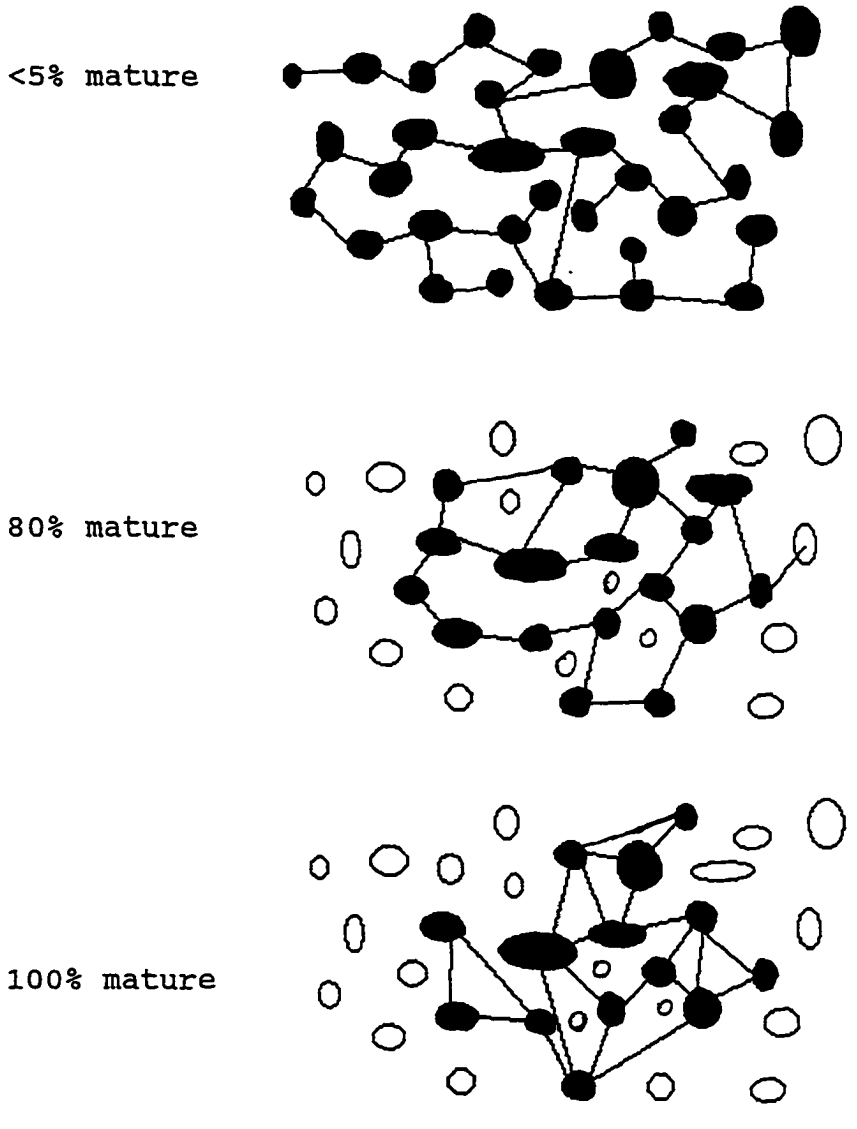

Figure 53. The fragmentation/reconstruction model for Type I kerogen maturation. The model does not consider oil cracking, coking, and migration. (O) extractable, (●) non-extractable.

Table 28. Homolytic bond dissociation energy for some C-C bonds

Bond	Energy (kcal/mol)
$CH_3-CH_2CH_3$	85
$(CH_3)_2CH-CH_3$	83
$CH_3CH_2-CH_2CH_3$	82
$CH_3CH_2-CHCH_2$	89
$CH_3-CH_2CHCH_2$	72
$CH_3CH_2-C_6H_5$	90
$CH_3-CH_2C_6H_5$	72

Carey, F. A.; Sundberg, R. J. *Advanced Organic Chemistry*, Plenum Press, New York: 1990.

selectively occur on the bonds with the lowest dissociation energies, such as C-C bonds β to double bonds or aromatics.

Both free radical and ionic mechanisms have been proposed to describe fragmentation reactions during kerogen maturation.[53] The former involves decomposition of a covalent bond into two radicals, which favors n-alkane generation from the kerogen network. The later involves clay minerals as natural catalysts and carbonium ions as intermediates, which promotes iso-alkane generation from the kerogen network. These two mechanisms may occur simultaneously in a system. When the Type I kerogen contains many long aliphatic chains,[40] the free radical mechanism may be favored during maturation, especially for the less mature kerogen. Radical substitutions which add radicals to double bonds in the network and radical transfer reactions which transfer radicals to the kerogen network can introduce more cross-links and increase the kerogen cross-link density.

Changes in the bitumen during maturation are more complicated than that of kerogen because of oil migration. Bitumen increasingly polymerizes during maturation. As a result, the oil is selectively coked to and incorporated into the kerogen. The average molecular weight of bitumen decrease with increasing maturation. Bitumen also migrates out of the source rock at a certain maturation stage. This increases the average molecule weight of bitumen remaining in the source rock. We could not quantitatively estimate coking and

migration effects for the maturation series. Evolution of bitumen during maturation deserves further testing on a maturation series. A series from which oil has not migrated out is necessary.

In this section, the changes in kerogen cross-link density, the amount of bitumen, and its molecular weight distribution were measured in a Type I kerogen maturation series. Solvent swelling technique was successfully applied to Uinta basin kerogens. As an independent tools being used, it provided macromolecular structure information of maturation chemistry. Based on the results of the changes in the cross-link density, a fragmentation/reconstruction model was proposed for Type I kerogen maturation. The model represents a schematic picture of the changes in the macromolecular structure of Type I kerogen during maturation. It provides new insight of molecular evolution of Type I kerogen maturation and is important for studying the thermal history of oil basins and petroleum migration.

Chapter VIII

Summary and Conclusions

The research presented in this dissertation is a study of the changes in the macromolecular structure of a Type I kerogen during the maturation process. The solvent swelling and PDMS molecular weight distribution techniques were first developed and these techniques were then applied to a Type I kerogen maturation series. The work can be summarized as follows.

(1) The solvent swelling technique can be used to study the macromolecular structure of Type I kerogens. Solvent swelling of Green River kerogen followed regular solution theory well and the network did not have specific interactions with polar solvents. The measured solubility parameter of Green River kerogen was about 9.7 $(cal/cm^3)^{1/2}$ using regular solution theory. The kerogen cross-link density was calculated using swelling theories. The results demonstrate that Green River kerogen is a highly cross-linked system. Solvent swelling of Rundle kerogen followed regular solution theory except that hydrogen-bonding solvents showed slightly enhanced swelling. The solubility parameter of Rundle kerogen was estimated at ~ 10 $(cal/cm^3)^{1/2}$. The solvent swelling technique of polymer science appears to be a unique tool for exploring the macromolecular structure of kerogen. The results can be directly used to reflect bond making and breaking which occur

during kerogen maturation.

(2) ^{252}Cf plasma desorption mass spectrometry (PDMS) is a fast, easy, and reliable technique to determine bitumen molecular weight distributions. PDMS molecular weight distributions of Green River, Rundle, and Athabasca bitumens were measured. The number average molecular weights (M_n) calculated from these PDMS spectra agreed with the values determined by vapor pressure osmometry (VPO). The PDMS molecular weight distribution of Athabasca bitumen showed a good agreement with its gel permeation chromatography (GPC)/VPO molecular weight distribution. The PDMS technique can reveal differences and similarities in bitumen molecular weight distributions.

(3) The changes in the macromolecular structure of a Type I kerogen (Uinta Basin) maturation series were investigated. The number average molecular weight between cross-links ($\bar{M}_c$) of the kerogen, the amounts of bitumen, and bitumen molecular weight distributions were determined using the techniques developed previously. The $\bar{M}_c$ (reciprocal of the cross-link density) slowly decreases during the first 80% maturation and rapidly decreases as the kerogen matures further. These changes display a good correlation with the kinetic and thermal history models in the literature. Characterizing the changes in kerogen cross-link density which occur during maturation provides a new way of probing maturation chemistry. The amounts of bitumen extracted from the Uinta basin

maturation series agreed with the literature value, but the data do not display increases with increasing kerogen maturation because (1) light hydrocarbons were lost during vacuum removal of the solvent, and (2) oil migration reduced some bitumen molecules from the 80% and 100% mature samples.

It was proposed that Type I kerogen maturation involves fragmentation accompanied by network reconstruction. The model can be used to describe the kerogen maturation process on a macromolecular level.

List of References

1. Tissot, B. P.; Welte, D. H. *Petroleum Formation and occurrence*, Springer-Verlag: New York, 1978.

2. Speight, J. G. *The Chemistry and Technology of Petroleum*, 2nd Ed., Marcel Dekker: New York, 1991.

3. van Krevelen, D. W. *Coal*, 3rd Ed., Elsevier: Amsterdam, 1993.

4. Larsen, J. W.; Green, T. K.; Kovac, J. *J. Org. Chem.*, **1985**, 50, 4729-4735.

5. Vandenbroucke, M. in *Kerogen*, Durand, B. Ed., Editions Technip: Paris, 1980, PP. 415-444.

6. Durand, B. in *Kerogen*, Durand, B. Ed., Editions Technic: Paris, 1980; pp. 13-34.

7. Hunt, J. M. *Petroleum Geochemistry and Geology, 2nd ed.*, W. H. Freeman: San Francisco, 1996.

8. Yen, T. F. in *Oil Shale*, Yen, T. F.; Chilingarian, G. V. Ed., Elsevier: Amsterdam, 1976; pp. 129-148.

9. Rullkotter, J.; Michaelis, W. *Org. Geochem.*, **1989**, 16, 829-852.

10. Behar, F.; Vandenbroucke, W. *Org. Geochem.*, **1987**, 11, 15-24.

11. Flory, P. J. *Principles of Polymer Chemistry*, Cornell University Press: Ithaca, 1953.

12. Siskin, M.; Katritzky, A. R. Science, **1991**, 254, 231-237.

13. Largeau, C.; Casadevall, E.; Kadouri, A.; Metzger, P. *Org. Geochem.*, **1984**, 6, 327-332.

14. Largeau, C.; Derenne, S.; Casadevall, E.; Kadouri, A.; Sellier, N. *Org. Geochem.*, **1986**, 10, 1023-1032.

15. Tegelaar, E. W., de Leeuw, J. W.; Derenne, S.; Largeau, C. *Geochim. Gosmochim. Acta*, **1989**, 53, 3103-3106.

16. Hutton, A.; Bharati, S.; Robl, T. *Energy Fuels*, **1994**, 8, 1478-1488.

17. Senftle, J.; Landis, C. R.; Mclaughlin, R. L. in *Organic Geochemistry*, Engel, M. H.; Macko, S. A. Ed, Plenum Press: New York, 1993; pp. 355-374.

18. Heroux, Y.; Chagnon, A.; Bertrand, R. *Am. Assoc. Petro. Geol. Bull.*, **1979**, 6, 2128-2144.

19. Hayes, J. M.; Kaplan, I. R.; Wedeking, K. W. in *Earth's Earliest Biosphere*: Its Origin and Evolution, Schopf, J. W. Ed., Princeton University Press: Princeton, 1983, pp. 93-134.

20. Monthioux, M., Landais, P.; Monin, J. C. *Org. Geochem.*, **1985**, 8, 275-292.

21. Kister, J,; Guiliano, M.; Largeau, C.; Derenne, S.; Casadevall, E. *Fuel*, **1990**, 69, 11-16.

22. Rouxhet, P. G.; Robin, P. L.; Nicaise, G. in *Kerogen*, Durand, B. Ed., Editions Technic: Paris, 1980; pp. 163-190.

23. Wilson, M. A. *N. M. R. Techniques and Applications in Geochemistry and Soil Chemistry*, Pergamon Press: New York, 1987.

24. Patience, R. L.; Mann, A. L.; Poplett, I. J. F. *Geochim. Gosmochim. Acta*, **1992**, 56, 2725-2742.

25. Miknis, F. P.; Netzel, D. A.; Smith, J. W. Mast, M. A.; Maciel, G. E. *Geochim. Gosmochim. Acta*, **1982**, 46, 977-984.

26. Mackenzie, A. S. in *Advances in Petroleum Geochemistry*, Vol. 1, Brooks, J., Welte, D. Ed., Academic Press, London; pp. 115-214.

27. Philp, R. P.; Oung, J.-N., *Anal. Chem.*, **1988**, 60, 887A-896A.

28. Whelan, J.; Thompson-Rizer, C. L. in *Organic Geochemistry*, Engel, M. H.; Macko, S. A. Ed., Plenum Press: New York, 1993; pp. 289-253.

29. Burnham, A. K.; Sweeney, J. J. *Geochim. Gosmochim. Acta*, **1989**, 53, 2649-2657.

30. Larter, S. R.; Horsfield, B. in *Organic Geochemistry*, Engel, M. H.; Macko, S. A. Ed., Plenum Press: New York, 1993; pp. 271-287.

31. Charpenay, S.; Serio, M. A.; Bassilakis, R.; Solomon, P. R. *Energy Fuels*, **1996**, 10, 19-25.

32. Charpenay, S.; Serio, M. A.; Bassilakis, R.; Solomon, P. R.; Landais, P. *Energy Fuels*, **1996**, 10, 26-38.

33. Durand, B.; Monin, J. C. in *Kerogen*, Durand, B. Ed., Editions Technic: Paris, 1980; pp. 113-141.

34. McCollum, J. D.; Wolff, W. F. *Energy Fuels*, **1990**, 4, 11-14.

35. Durand, B.; Nicaise, G. in *Kerogen*, Durand, B. Ed., Editions Technic: Paris, 1980; pp. 35-52.

36. Vitorovic, D. in *Kerogen*, Durand, B. Ed., Editions Technic: Paris, 1980; pp. 301-331.

37. Larsen, J. W.; Li, S. *Energy Fuels*, **1994**, *8*, 932-936.

38. Green, T.; Kovac, J.; Brenner, D.; Larsen, J. W. in *Coal structure*, Meyers, R. A. Ed., Academic Press: New York, 1982; pp. 199-280.

39. Morgans, W. T. A.; Terry, N. B. *Fuel*, **1958**, 37, 201-219.

40. Siskin, M.; Scouten, C. G.; Rose, K. D.; Aczel, T.; Colgrove, S. G.; Pabst, R. E. Jr. in *Composition, Geochemistry, and Conversion of Oil Shales*, Snape, C. Ed., Kluwer Academic Publishers, 1995; pp. 143-158.

41. Young, D. K.; Shih, S.; Yen, T. F. *Prepr. ACS Div. Fuel Chem.*, **1974**, 19, 109-114.

42. Burlingame, A. L.; Simoneit, B. R. *Nature*, **1969**, 222, 741-747.

43. Burlingame, A. L.; Haung, P. A.; Schnoes, H. K.; Simoneit, B. R. in *Avd. Org. Geochem.* Schenck, P. A.; Havenaar, I. Ed. Pergamon Press: Oxford, 1968; pp. 68-71.

44. Djuricic, M.; Murphy, R. C.; Vitorovic, D. Biemann, K. *Geochim. Gosmochim. Acta*, **1971**, 35, 1201-1207.

45. Schmidt-Collerus, J. J.; Prien, C. H. *Prepr. ACS Div. Fuel Chem.*, **1974**, 19, 100-108.

46. McGowan, C. W.; Diehl, H. *Fuel Process. Tech.*, **1985**, 10, 195-204.

47. Saxby, J. D. in *Oil Shale*, Yen, T. F.; Chilingarian, G. V. Ed., Elsevier: Amsterdam, 1976; pp. 103-127.

48. Robinson, W. E. in *Organic Geochemistry - Methods and Results*, Eglinto, G.; Murphy, M. Ed., Springer-Verlag: New York, 1969; pp. 163-190.

49. Miknis, F. P. in *Composition, Geochemistry, and Conversion of Oil Shales*, Snape, C. Ed., Kluwer Academic Publishers, 1995; pp. 69-91.

50. Robl, T. L.; Burtron, H. D. *Org. Geochem.*, **1993**, 20, 249-255.

51. Siskin, M.; Brons, G.; Payack, J. F. *Energy Fuels*, **1987**, 1, 248-256.

52. Siskin, M.; Brons, G.; Payack, J. F. *Energy Fuels*, **1989**, 3, 108-109.

53. Stainforth, J. G.; Reinders, J. E. A. *Org. Geochem.*, **1989**, 16, 61-74.

54. Ungerer, P. *Org. Geochem.*, **1989**, 16, 1-25.

55. Odian, G. *Principle of Polymer Chemistry*, John Wiley & Sons, Inc., 1991.

56. van Krevelen, D. W. *Fuels*, **1965**, 44, 229-242.

57. Larsen, J. W.; Mohammadi, M. Yiginsu, I.; Kovac, J. *Geochim. Gosmochim. Acta*, **1984**, 48, 135-141.

58. Yan, J.; Johnson, D. *J. Appl. Polym. Sci.*, **1981**, 26, 1623-1635.

59. Larsen, J. W.; Wei, Y.-C. *Energy Fuels*, **1988**, 2, 344-350.

60. Mark, J. E.; Lal, J. *Elastomers and Rubber Elasticity*, American Chemical Society, Washington, DC, 1982.

61. Kovac, J. *Macromolecules*, **1978**, 11, 362-365.

62. Barr-Howell, B. D.; Peppas, N. A. *Polymer Bulletin*, **1985**, 13, 91-96.

63. Green, T. K. Ph. D. Dissertation, U. Tennessee, 1984.

64. Hildebrand, J. H.; Scott, R. L. *The Solubility of Nonelectrolytes*, Dover Publications Inc., 1964.

65. Hildebrand, J. H.; Prausnitz, J. M.; Scott, R. L. *Regular and Related Solutions*, van Nostrand Reinhold Co., New York, 1970.

66. Blanks, R. F.; Prausnitz, J. M. *In. Eng. Chem. Fundamentals,* **1964**, 3, 1-8.

67. Grulke, E. A. in *Polymer Handbook,* 3rd ed., Brandrup, J.; Immergut, E. H. Ed., John Wiley & Sons, 1989; VII519-559.

68. Sperling, L. H. *Introduction to Physical Polymer Science, 2nd Ed.* John Wiley & Sons, Inc., 1992.

69. Painter, P.; Shenoy, S. *Energy Fuels*, **1995**, 9, 364-371.

70. Turpin, M.; Rand, B.; Ellis, B. *Fuel*, **1996**, 75, 107-113.

71. Green, T. K.; Kovac, J.; Larsen, J. W. *Fuel*, **1984**, 63, 935-938.

72. Larsen, J. W.; Cheng, J. C.; Pan, C.-S. *Energy Fuels*, **1991**, 5, 57-59.

73. Shadle, L. J.; Khan, M. R.; Zhang, G. Q.; Bajura, R. J. *Prepr. Am. Chem. Soc. Div. Petr. Chem.*, **1989**, 34(1), 55-61.

74. Brule, B. *J. Liq. Chromatogr.* **1979**, 2(2), 165-192.

75. Bartle, K. D; Mulligan, M. J.; Taylor, N.; Martin, T. G.; Snape, C. E. *Fuel*, **1984**, 63, 1556-1560.

76. Mulligan, M. J.; Thomas, K. M.; Tytko, A. P. *Fuel*, **1987**, 66, 1472-1480.

77. Champagne, P. J.; Emmanuel, M.; Ternan, M. *Fuel*, **1985**, 64, 423-425.

78. Payzant, J. D.; Rubinstein, I.; Hogg, A. M.; Straus, O. P. *Geochim. Gosmochim. Acta*, **1979**, *43*, 1187-1193.

79. McKay, J.F.; Chong, S.-L.; Gardner, G. W. *Liquid Fuels Techn.*, **1983**, 1, 259-287.

80. McKay, J.F.; Chong, S.-L. *Liquid Fuels Techn.*, **1983**, 1, 289-324.

81. Larsen, J. W.; Li, S. *Energy Fuels*, **1995**, 9, 760-764.

82. Fouch, T. D. in *Symposium on Deep Drilling Frontiers in the Central Rocky Mountains,* Bolyard, D. W. Ed., Rocky Mountain Assoc. Geol. Special Publication, 1975; pp. 163-173.

83. Sweeney, J. J.; Burnham, A. K.; Braun, R. L. *Am. Assoc. Petro. Geol. Bull.*, **1987**, 71, 967-985.

84. Tissot, B.; Deroo, G.; Hood, A. *Geochim. Gosmochim. Acta*, **1978**, 42, 1469-1486.

85. Chidsy, T. C. Jr. in *Atlas of Major Rocky Mountain Gas Reservoirs*, Robertson, J. M.; Broadhead, R. F.; Gorody, A. W.; Hjellming, C. A. Ed., 1993; pp. 83-88.

86. Bell, K. G.; Hunt, J. M. in *Organic Geochemistry*, Breger, I. A. Ed., Pergamon Press: New York, 1963; pp. 333-366.

87. Lucas, P. T.; Drexler, J. M. in *Symposium on Deep Drilling Frontiers in the Central Rocky Mountains*, Bolyard, D. W. Ed., Rocky Mountain Assoc. Geol. Special Publication, 1975; pp. 265-273.

88. Chatfield, J. in *Stratigraphic Oil and Gas Fields - Classification, Exploration Methods, and Case Histories*, King, R. E. Ed., AAPG Memoir, 1972; pp. 342-353.

89. Robinson, W. E. in *Organic Geochemistry - Methods and Results*, Murphy, M. R, J. Ed., Springer-Verlag: New York, 1969; pp. 619-637.

90. Anders, D. E.; Gerrild, P. M. in *Hydrocarbon Source Rocks of the Greater Rocky Mountain Region*, Woodward, J.; Meissner, F. F.; Clayton, J. L. Ed., Rocky Mountain Assoc. Geol., 1984; pp. 513-529.

91. Robinson, W. E. in *Oil Shale*, Yen, T. F.; Chilingarian, G. V. Ed. Elsevier: Amsterdam, 1976; 61-79.

92. Sweeney, J. J. *Org. Geochem.*, **1988**, 13, 199-205.

93. Ternan, M.; Rahimi, P. M.; Clugston, D. M. *Energy Fuels*, **1994**, 8, 518-530.

94. Larsen, J. W.; Shawver, S. *Energy Fuels*, **1990**, 4, 74-77.

95. Otake, Y.; Suuberg, E. M. *Fuel* **1989**, 68, 1609-1612.

96. Larsen, J. W.; Lapucha, A. R.; Wernett, P. C.; Anderson, W. R. *Energy Fuels*, **1994**, 8, 258-265.

97. Larsen, J. W.; Choudhury, P. *J. Org. Chem.*, **1979**, 44, 2856-2859.

98. Solomon, P. R.; Hamblen, D. G.; Carangelo, R. M. in *Coal and Coal Products: Analytical Characterization Techniques* Fuller, E. L. Ed., Washington, D.C.: ACS 1982.

99. Kowalczyk, G. M.S. Thesis, Lehigh U., 1992.

100. Resing, H. A.; Garroway, A. N.; Hazlett, R. N. *Fuel*, **1978**, 57 450-454.

101. Russell, N. J.; Wilson, M. A.; Pugmire, R. J.; Grant, D. M. *Fuel*, **1983**, 62 601-605.

102. Hildebrand, J. H.; Scott, R. L. The solubility of noelectrolytes, Dover Publications Inc., 1964.

103. Hildebrand, J. H.; Prausnitz, J. M.; Scott R. L. Regular and related solutions. van Nostrand Reinhold co.: New York, 1970.

104. Cody, G. D. Jr.; Larsen, J. W.; Siskin, M. *Energy Fuels*, **1990**, 2, 340-344.

105. Larsen, J. W.; Azik, M.; Korda, A. *Energy Fuels*, **1992**, 6, 109-110.

106. Brenner, D. *Fuel*, **1985**, 64 167-173.

107. Macfarlane, R. D.; Torgerson, D. F. *Science*, **1976**, 191, 920-925.

108. Macfarlane, R. D. *Anal. Chem.*, **1983**, 55, 1247A-1264A.

109. Juvet, R. S.; Allmaier, G. M.; Schmid, E. R. *Anal. Chim. Acta*, **1990**, 241, 241-248.

110. Barrett, D.; Sambi, T.; Sergeant, G. D.; *Fuel*, **1990**, 69, 267-269.

111. Chait, B. T. *Int. J. Mass Spectrom. Ion Processes*, **1989**, 92, 297-329.

112. Wolf, B.; Macfarlane, R. D. *J. Am. Soc. Mass Spectrom.*, **1992**, 3, 706-715.

113. Zoeller, J. H. Jr.; Zingaro, R. A.; Macfarlane, R. D. *Int. J. Mass Spectrom. Ion Processes*, **1987**, 77, 21-30.

114. van Veelen, P. A.; Tjaden, U. R.; van der Greef, J. *Int. J. Mass Spectrom. Ion Processes*, **1991**, 110, 93-101.

115. Ungerer, P.; Bessis, F.; Chenet, P. Y.; Durand, B.; Nogaret, E.; Chiarelli, A.; Oudin, J. L.; Perrin, J. F. *Am. Assoc. Petro. Geol. Memoir*, **1984**, 35, 53-57.

116. Welte, D. H.; Yukler, M. A. *Am. Assoc. Petro. Geol. Bull.*, **1981**, 65, 1387-1396.

117. Nakayama, K.; van Siclen, D. C. *Am. Assoc. Petro. Geol. Bull.*, **1981**, 65, 1230-1255.

118. Durand, B. *Org. Geochem.*, **1987**, 13, 445-459.

119. Chen, S. P.; Ferry, J. D. *Macromol.* **1968**, 1, 270-278.

120. Carey, F. A.; Sundberg, R. J. *Advanced Organic Chemistry*, Plenum Press, New York: 1990.

Vita

Shang Li, the second son of Huiru Zhang and Yong Li, was born on August 7, 1962 in Beijing, P. R. China. After graduating from Beijing No. 4 High School in June 1980, he entered Lanzhou University in Lanzhou, P. R. China and earned a B. S. in Chemistry. He attended Lehigh University in August 1992.